Imperial College London

Theoretical and computational studies of extreme-size dust in plasmas

Christos Stavrou

17th August 2016

Submitted in part fulfilment of the requirements for the degree of
Doctor of Philosophy in of Imperial College London
and the Diploma of Imperial College London

Declaration of Originality

I hereby certify that the material of this thesis, which I now submit for the award of Doctor of Philosophy, is entirely my own work unless otherwise cited or acknowledged within the body of text. The kinetic model for small dust grains, referred to in this work as DAPF, has been developed in close collaboration with Professor Umberto De Angelis, who was the originator of the idea for the model.

London, February 2016

Christos Stavrou

There are many people to whom I owe a great deal. Whatever is of worth in what you are about to read is entirely due to them.
I would like to thank my mother, Maria Stavrou. Her support and belief in me were invaluable and I could never thank her enough.
I would like to thank my father, Kyriacos Stavrou. It was him that showed me the beauty of physics; I mourn for his loss.
I would like to thank my brothers, Marinos and Anastasios for their unconditional love.
I would like to thank my BSc supervisor, Professor Walther Schwarzacher, my MSc supervisors, Professors Greg Tallents and Howard Wilson, my PhD supervisor, Dr. Michael Coppins and Professor Umberto De Angelis.
Finally, I would like to thank Rachel, for her love and patience.

Abstract

The effects of spherical particles ("dust grains") in plasmas are investigated. The importance of dust grains in plasmas is highlighted, especially with regards to fusion energy production in magnetically confined plasmas. The investigation focuses on dust grains that are at the extremes of scale compared to the Debye length. Large dust grains, i.e. dust grains much larger than the Debye length, are investigated by the use of a simple fluid model, which is similar to compressible gas dynamics. Professor John Allen was the first to draw attention to the similarity of the model to compressible fluid dynamics in his 2007 paper [1]. The equations derived, which resemble those of compressible fluid dynamics are solved numerically with the help of a code written specifically for this purpose. The results are similar to PIC code results, with some differences in the shape of the downstream disturbance; more specifically, the downstream disturbance generated by our code is more elliptical than conical, and similar to the disturbance caused by a sphere in neutral fluids at moderate Reynolds numbers. This is to be contrasted with the results in the literature which are conical in shape, especially for low values of τ ($= \frac{T_i}{T_e}$). This may be an indication that the difference in shape is due to the ion pressure or the electron inertia, both of which we are neglecting in our assumptions.

Small dust grains are investigated using a kinetic model. The model is a continuation and evolution of the model used by Filippov [2], to include plasma flow. The equations of the model are solved analytically and the results reveal the presence of upstream structures, even in the case of supersonic flow, a result not commented on before in the relevant literature.

The work also reviews relevant analytic theories, such as ABR and OML. ABR is extended by the author to include finding the geometrical width of the sheath. This extension, if confirmed, could be used for predicting the position of the sheath edge in relation to the dust grain. In addition, the work on deriving the Bohm criterion for a spherical dust grain is investigated,

using a similar approach to the one taken in the literature for a planar wall. The result indicates that there is no such limitation in the spherical case.

Contents

List of Figures

1 Introduction

1.1 Outline

> "*The average introduction to almost any book is somewhat of a bore*"
>
> William Henry Pratt

The quote [16] belongs to an actor arguably better known as Boris Karloff, the man who played Frankestein's monster in the 1931 film adaptation of Mary Shelley's novel. The actor was born in London, not too far from

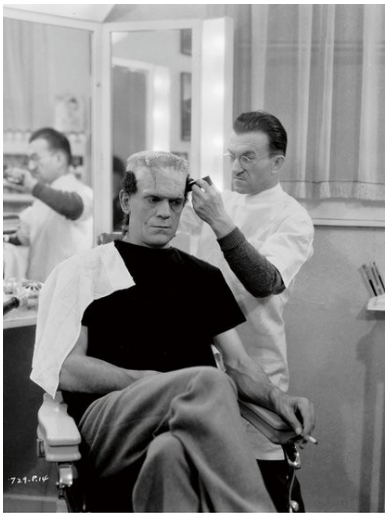

Figure 1.1: Boris Karloff became famous by playing a monster given life by lightning, the earliest form of terrestrial plasma witnessed by humans.

Imperial College, and the monster was born using lightning, the earliest form of terrestrial plasma witnessed by humans.

This work is split into 8 chapters.

Chapter 1 gives a brief outline of everything to follow and includes the aforementioned quote, by an actor born less than ten kilometres from Imperial College. It also introduces the general subject area, the topic of research that is being reported in this work, and the motivation behind it. It also defines the aim of the work and this report.

Chapter 2 provides a more technical description of plasma and dust, introducing terminology and concepts that will be useful for subsequent chapters. Chapter 3 provides a bit of background on Computational Fluid Dynamics, a method used in this work.

Chapters 4 and 7 present the methodology used in tackling the problem. Chapter 5 presents the fluid code developed to find the potential, density and fluid flow around large dust grains in a (flowing) plasma. Chapter 7 presents the kinetic model developed to find the potential, density and fluid flow around small dust grains in a flowing plasma.

Chapter 6 presents the results from the fluid code.

The work concludes with chapter 8, which summarises what was found in the course of this work, and discusses future paths to investigate.

The Bibliography provides a record of the sources used and additional material that may be of interest to the keen reader.

The topics presented in this work are inherently interesting and exciting, to me. I shall therefore endeavour to make the work presented as easily accessible to the lay-person as possible.

To the lay-person, I offer my apologies for all the cases where I have failed to do so.

To the expert, I offer my apologies for presenting material already known and for the lack of succinctness that comes with staying within expert language.

1.2 Prologue

> "*I have indeed discovered various things, but, as for immortality of my name, this should not be taken literally. A hundred years hence perhaps only a few will know who Purkyně was. But that makes no difference. For indeed we do not know who discovered the plow, and yet it serves all humanity. The cause remains the same, but not the name - and that is the important thing*"
>
> Jan Evangelista Purkyně
> [17]

It is said that when Jan Evangelista Purkyně (figure 1.2) was alive, he was

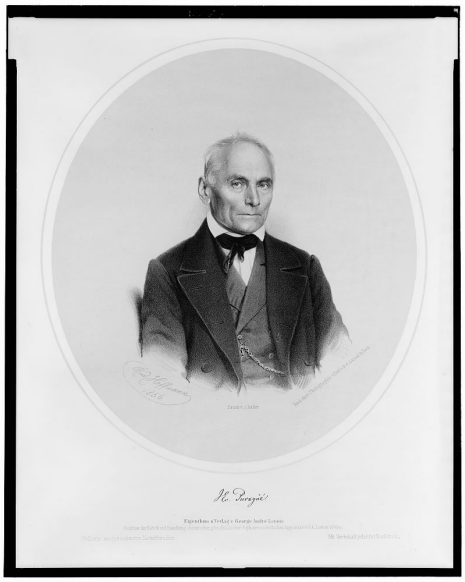

Figure 1.2: Jan Evangelista Purkyně[3]

so famous that people outside Europe could address letters to him simply as "Purkyně, Europe". Purkyně is, however, a name known to very few plasma physicists. This may at first glance appear surprising, given that he is the one that originated the term *plasma*.

Purkyně was a physiologist, not a plasma physicist, and his *plasma* referred to the liquid part of blood. In fact, he died ten years before Crookes presented his lecture on "radiant matter" to the British Association for the Advancement of Science (in 1879 [18]) and fifty-nine years before *plasma* was first used to describe an ionised gas. The term wasn't Crooke's, as his lecture was inspired by a lecture of the same title by Michael Faraday sixty-three years earlier, to which Crooke's refers [18]. Faraday called "radiant matter" matter that is "as far beyond vaporisation as that is above fluidity" [18], going as far as claiming that matter should be classified into "solid, liquid, gaseous and radiant", even though he had no proof of the existence of the fourth state [18]! The term "radiant matter" did not remain, as it was replaced by "plasma", a term first used by a man who is well known to plasma physicists, the actual godfather of "plasma" physics, Irwin Langmuir.

Langmuir had, by 1927, settled on the term *sheath* for the "region in the immediate neighbourhood of a wall or an electrode" [19] and was looking for a name for the bulk of the ionised gas. He decided to "use the name plasma to describe this region containing balanced charges of ions and electrons" [20], allegedly because it "acted as a sort of sub-stratum carrying particles... the way blood plasma carries around red and white corpuscles and germs" [19, 21].

Today, *plasma* is understood to mean *a gas that is ionised to a sufficient degree to exhibit collective effects*. This "sufficient degree" is surprisingly low; ionisation as low as one particle in ten thousand (0.01%) will transform a gas into a plasma [22]. In cases where solid or liquid particles (impurities) are present in the plasma, the plasma is called *dusty* or *complex*. The aforementioned particles are then called *dust (particles)*, a term which is, perhaps, better than *germs*.

In 1924, Langmuir gave a talk describing visual phenomena of "remarkable beauty" [23]. He was referring to effects caused by sputtering tungsten particles into his ionised gas. Thus, when the term *plasma* was born, "gas impurities" (in this case, tungsten particles) were already part of plasma [21].

Langmuir's contribution to the study of plasmas goes beyond naming them. He discovered what are now called Langmuir waves (electron density waves), invented the Langmuir probe, and his work still forms the basis for plasma fabrication techniques.

The work on plasma increased, not because of the beauty of the visual phenomena that Langmuir described, but because plasmas were interesting for two main reasons. The first reason is that plasmas suddenly appeared to be "everywhere", as research began to reveal the amount of plasma in the universe. The interest in using radio waves, for example, revealed the presence of the ionosphere in the upper atmosphere. The second reason is that plasmas could be useful. Langmuir's work, for example, was done in a lab belonging to General Electric and led to practical applications, such as plasma welding.

Langmuir won the Nobel Prize (not for his work on plasmas) in 1932, the year Lev Davidovich Landau took over the Department of Theoretical Physics at the National Scientific Centre Kharkiv Institute of Physics and Technology. Landau, like Langmuir, was another scientist with contributions in a wide range of physics topics (and a Nobel prize, also not for work done on plasmas), including major contributions to plasma physics. As a theorist, Landau predicted "Landau damping" before it was experimentally observed. Whereas Langmuir was motivated by practical applications for plasmas, it can be said that Landau's involvement in plasma physics was politically fortuitous [24]. About 18 years elapsed before Landau's 1946 paper [25] was experimentally verified by Malmerg and Wharton's 1964 "preliminary results" [26]. This was a year after the title of Hannes Alfvén, another scientist worth mentioning when talking about plasmas, was changed from "Chair of Electronics" to "Chair of Plasma Physics". The change in the title signals the importance plasmas had acquired by then. Alfvén is the only Nobel laureate to have won his prize for work relevant to plasma physics. The prize was given for the development of magnetohydrodynamics and its "fruitful" applications in plasma physics. Alfvén's interest in plasmas was different in nature to the other two scientists mentioned. Where Langmuir was looking at manipulating plasmas on earth, and Landau found them a fruitful field for theoretical work, Alfvén saw them as part of his studies in space physics.

The study of plasmas has continued to increase dramatically with time. As an indication, in August 2015 Google Scholar returned 123 pre-1924 articles relevant to plasma physics, 9430 articles for the period 1925-1970 and 263000 articles for post-1970 articles [27], a rate of increase much faster than the increase in the total number of articles (see [28]).

Research into dusty plasmas has seen a corresponding increase with dedicated experimental equipment being built, like, for example, the Magnetised Dusty Plasma eXperiment (MDPX - see [29]) and even thoughts of incorporating further dusty plasma research in the International Space Station (ISS) [30]. The ISS has already hosted some dusty plasma experiments, with PK-3 being a dedicated plasma experiment (see [31]).

There are many reasons for this increase. They can be broadly categorised in two groups - "exploration" and "progress". Plasmas are an integral part of our universe - a universe we, as a species, have always had an overwhelming desire to explore - and dust seems to be ubiquitous in plasmas: "Such (or similar) dusty or complex plasmas are ... found in astrophysics and are therefore of fundamental scientific interest" [32]. Plasmas can also be used in various ways to improve (progress) our quality of life and have found a multitude of uses. Indeed, "One of the best-known examples of basic plasma physics research triggered by applications is the complex (or dusty) plasma, since dust particles were found to influence the properties of the processing plasma and of the deposited films" [32].

I will briefly mention some from both categories later in this chapter. First, I will briefly explain why I think that research into plasmas should be moved up in the list of priorities for humans.

1.2.1 Importance of Plasmas

The most important and topical reason why plasma is important is because it is a medium in which fusion can take place. A fusion powerstation, when realised, will provide clean, secure and affordable energy and will be an integral part of our future energy portfolio. This is by no means the goal of all of plasma research, nor is this meant to detract from the important work being done for other plasma applications, nor is it meant to deny the beauty of some of the work done in discovering how plasma behaves, in nature or the laboratory. Indeed, the work, for example, done on the application of plasmas on semiconductors has a more immediate impact on society at the moment, as the owner of any modern electronic device would testify.

The importance of abundant electrical energy to quality of life cannot be overstated; the findings of Alam et al [33], for example, point to a strong correlation between life expectancy and the logarithm of per capita energy

expenditure for less developed countries, and a similar relationship to per capita energy expenditure for literacy, and physical quality of life. They also find an inverse relationship for infant mortality. It is clear that we need to increase the per capita energy expenditure of less developed countries. Ludwig Boltzmann, the same Boltzmann found in "Boltzmann distribution" or "Boltzmann constant", is quoted as saying "The struggle for existence is the struggle for available energy" [34]. The call for an increase in energy consumption in less developed countries is not controversial, even in the face of another pressing need for humanity, namely global warming.

Among the statements made in the 2014 Climate Change Report of the IPCC are that "Warming of the climate system is unequivocal, and since the 1950s, many of the observed changes are unprecedented over decades to millennia. The atmosphere and ocean have warmed, the amounts of snow and ice have diminished, and sea level has risen" [35] and "Human influence on the climate system is clear, and recent anthropogenic emissions of greenhouse gases are the highest in history. Recent climate changes have had widespread impacts on human and natural systems" [35]. It is clear that greenhouse gas emission needs to be reduced, which means fossil fuels are an unlikely candidate to solve the need for increased per capita energy consumption in developing countries. Another solution is needed.

Successive disappointments of candidate technologies seem to point to a solution that is not going to come in the form of a silver bullet; a range of technologies will be needed in a future energy portfolio. The established (fission) nuclear industry serves as an example of a "silver bullet", with the "The nuclear power industry remains as safe as a chocolate factory" quote in the March 29th 1986 edition of The Economist, four weeks before the Chernobyl catastrophe [34]. The disappointment when it comes to fusion is not inherent in itself, but is instead found in the successive delays in its realisation. This is a product of the difficulties in understanding plasmas and their behaviour and the difficulties in controlling plasma in a way that will produce a net gain in energy that will make fusion economically feasible.

The argument for fusion goes beyond environmental or humanitarian reasons. Recent studies suggest that "the availability of fusion technology can lead to savings ranging from hundreds of billions to tens of trillions of dollars" [36].

These difficulties will only be overcome with more research. "Intensive

efforts in five decades of Tokamak research has advanced the fusion product up by 10^7 times" [37][1]. Research will need to be intensified, both in terms of number of researchers and in amount of resources devoted to it, as studies have already shown that the resources committed in some areas are lacking [38]. The returns of a successful fusion research campaign are too high and the needs too pressing for us to do otherwise.

1.2.1.1 The Place for Dusty Plasma Research

Having demonstrated why I believe research into plasmas is important, it is now necessary to demonstrate why research into *dusty* plasmas is important. I will do so by showing that dust is present in tokamaks and that its presence has, or can have, negative consequences. The latter would imply that dust in tokamaks needs to be studied so that it can be understood and controlled. The importance of dust in tokamaks is not the sole reason why research into dust in plasmas is important. Indeed, we shall see in subsection 1.2.3, that the semiconductor industry has much to gain from research in dusty plasmas.

To say dust is always found in tokamak plasmas is not an exaggeration, as the scrape-off layer (SOL) and the divertor of a tokamak have similar conditions to low-temperature plasma processing devices [39]. Dust is common in such devices [39]. In fact, "significant amounts" of dust have been found in fusion devices [40]. Dust is generated at the walls, as dust particles are created at the walls whenever plasma makes contact with plasma facing components [39].

Dust has been identified as one of the problems that need attention for tokamaks [41]. For example, dust is expected to be a problem for ITER, as the amount of dust in the reactor is expected to "reach the upper limit" within a very short time after it begins operation [42] (see section 1.2.5 for more on ITER dust limits). Dust has a range of negative effects on tokamak operation, even though its "impact on the performance of current fusion devices is still not adequately understood" [40]. One effect is that dust "may potentially pose a significant safety threat due to the accumulation of rather mobile substances, which can contain toxic and radioactive materials and

[1] The "fusion product" is the product of the temperature, density and energy confinement time and is a figure of merit towards achieving self-sustaining fusion reactions.

retain tritium" [40]. Even beyond safety, dust can be a source of contamination by impurities of the core plasma [40] .

Dust, therefore, could potentially stand in the way of a successful fusion reactor. This, in turn, justifies significant research into dust, so that its effects in tokamaks can be mitigated.

1.2.1.2 The Place of This Work in Dusty Plasma Research

Specific details of the work reported here are given in 1.3. In placing this work in the greater context of dusty plasma research, suffice it to say that we will be using two different methods to look at the extremes of dust grain size. A fluid method for large dust grains and a kinetic method for small dust grains. The change in method reflects the change of the importance of the various physical parameters.

Fluid Method Fluid methods and their use in plasmas will be discussed more extensively in chapter 2. We state here the aim of this part of the work, namely to develop a self-consistent hydrodynamic model of dusty plasma that can be used to make predictions on the interaction between a large dust grain and its local plasma environment. These predictions can then be used to make other calculations, like, for example, the ion drag on the dust grain.

The aim extends to developing a computer code which will use the model to make these predictions. The program developed is called HADES (Hydrodynamic Approximation for Dust Extensible Solver) and will be discussed in more detail in chapter 5.

Kinetic Method As in the case of fluid methods, kinetic methods and their use in plasmas will be discussed more extensively in chapter 2. The aim is, again, identical to that of the fluid methods, except the application is for small dust grains. In contrast to the fluid method, however, this part of the work has been kept, where possible, analytic, limiting numerical calculations to integrals that would not yield to analytic methods.

1.2.2 Cosmic Physics

"The obvious importance of dusty plasmas in cosmic physics" [43] is easily demonstrated. Plasma comprises the vast majority of the observable universe, with figures of 95% and 99%, depending on the source, being quoted. Plasma is the material stars are made of, including the Sun, which, incidentally, contains 99.8% of the mass in the solar system. Our planet is bathed in the solar system's plasma and our solar system in interstellar plasma. Any vehicle leaving the atmosphere will likewise be bathed in plasma - a solid particle in a plasma.

Observations within the solar system provide a wealth of data for understanding plasmas. From the way plasma on the sun flows along magnetic field lines (figure 1.3) to the way planet magnetotails behave (e.g. [44]).

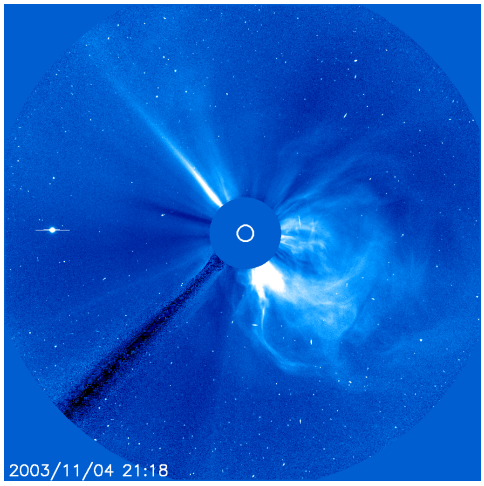

Figure 1.3: The largest solar flare measured, November 2003. [4]

Conversely, understanding plasmas helps us understand our solar system; from how the solar atmosphere behaves to how the Jovian moons interact with Jupiter ([45]) to the way the rings of Saturn behave [46].

1.2.3 Semiconductors

"Without any doubt, plasmas have been at the origin of the overwhelming success of semiconductors and their application in electronics and communications" [32]. Dust in plasmas, however, "has always been one of the main problems of materials and semiconductor technology" [42].

The semiconductor industry uses plasmas for integrated circuit fabrication, where *dust* is detrimental to yields - "Dust contamination reduces the yield and performance characteristics of fabricated devices" [47]. In industrial plasmas "The presence of dust is of critical concern...since particle contamination of semiconductor materials was estimated to account for more than 50% of device failures" [47].

The precise details of the use of plasmas in semiconductors is beyond the scope of this report; the subject is so broad that even a quick outline would be ambitious. One would have to talk of plasma etching, plasma deposition, plasma-immersion ion implantation, plasma stripping to name but a few processes. I will attempt to give a brief outline of one of these processes, namely plasma etching.

Etching refers to the removal of material from the surface of a sheet, or wafer, of semiconductor material, in an attempt to transfer the integrated circuit design onto it. Wet etching refers to the use of chemicals to remove material; plasma etching refers to the use of a plasma, which can etch either purely physically, in a sputtering process, or in a combination of physical and chemical processes.

Plasma etching replaced wet etching in the nineties, even though it had been available for around twenty years by that point [48, 49]. This is because wet etching techniques had been adequate until then. The parts of the wafer where no material is to be removed are protected by a layer of material called the mask. In wet etching, the material that is not covered by the mask is attacked chemically. The problem with wet etching is that it is isotropic, so material from below the mask is also attacked (see figure 1.4). In plasma

Figure 1.4: Chemical etching [5].

etching the material under the mask is more protected, as the plasma is accelerated vertically and mechanically attacks the wafer, allowing for the creation of a much narrower channel (see figure 1.5).

Plasma etching is negatively affected by the (inevitable) presence of dust.

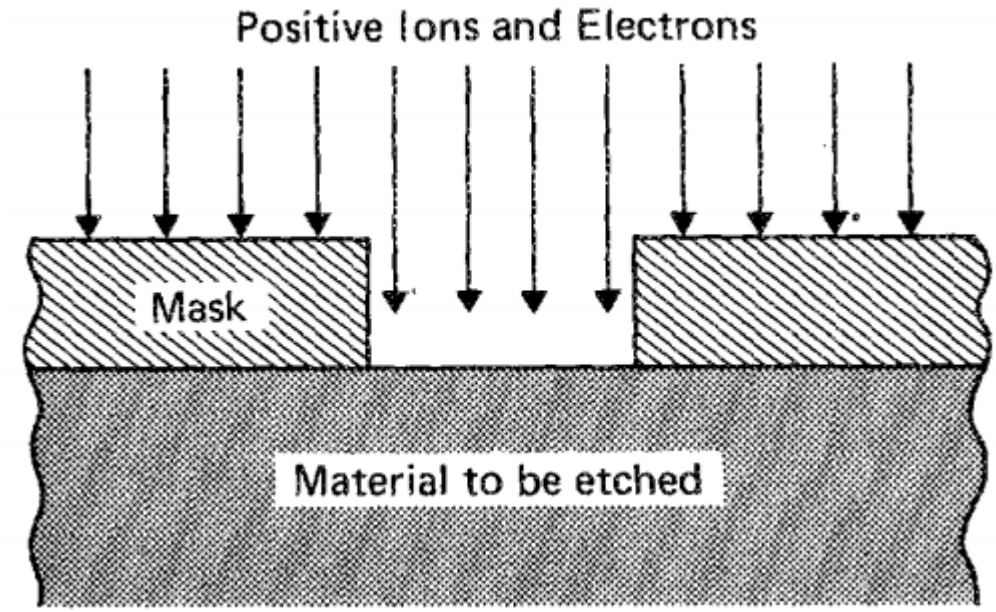

Figure 1.5: Plasma etching [6].

Dust can collide with the wafer, damaging "fine patterns on the wafer" [50]. The "presence of dust cause [sic] loss and delay in any process" [51] involved in plasma etching. This loss includes a loss of ions and electrons, that are absorbed by the dust grains, which would otherwise be part of the plasma and used in sputtering or in the calculations used to ensure accurate etching [51].

1.2.4 Crystals

Dust in plasmas can also be beneficial, as it led to "the remarkable discovery of new states of (soft) matter - the liquid and crystalline plasmas" [52] The crystal in question is a "macroscopic Coulomb crystal of solid particles in a plasma...a Coulomb solid" [7] Figure 1.6 shows one of the first images of a plasma crystal to appear in the literature. These have been used to study phase transitions at a scale visible to the unaided eye, as shown, for example in work done by Thomas et al [8] (see figure 1.7, taken from their 1996 paper).

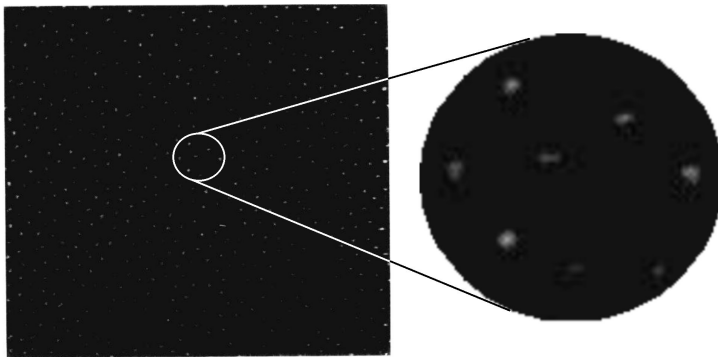

Figure 1.6: An image of a plasma crystal taken by Thomas et al.[7]

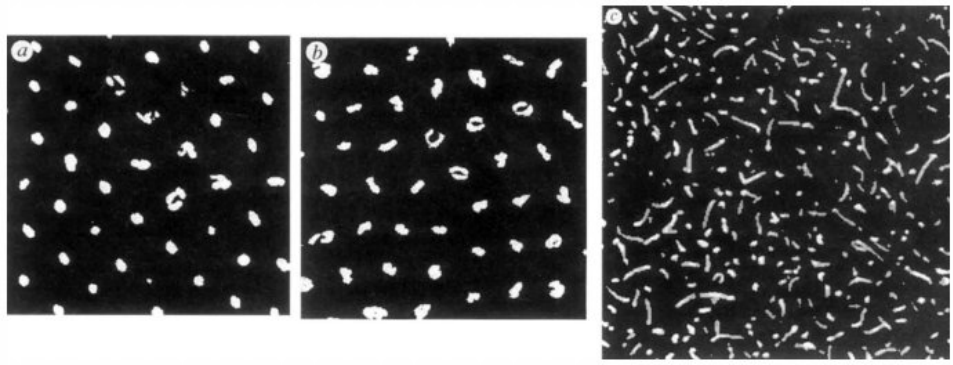

Figure 1.7: Phase transition of a plasma crystal, taken from [8]. Note the longer streaks, evidence of an increase in kinetic energy of the particles as the crystal melts, from left to right.

1.2.5 Fusion Energy

It was claimed that a fusion power station will provide clean, secure and affordable energy.

Clean, because fusion energy does not involve the release of greenhouse gases and does not produce radioactive waste in the volume that the fission industry does, and the radioactive waste that is produced has a much shorter half-life - "after a hundred years, there is no material in the permanent disposal waste category" [53].

Secure, because the fuel for fusion is deuterium and lithium, which do not suffer the same limitations in abundance or geographical location that fossil fuels do. Future fusion research will be aimed at realising deuterium-deuterium fusion, making seawater the source of enough fuel for millions of

years of consumption.

Affordable, for both of the above reasons; a cheap and abundant fuel supply and low clean-up costs. This last factor, however, is one of the hurdles remaining for commercial fusion, as capital costs and plant availability will need to be improved for fusion to be competitive.

Dust in a fusion powerstation plasma is detrimental to containment and a risk factor; "unwanted dust in plasma is also a problem in the realization of a fusion reactor" [42]. Dust can be toxic, radioactive and explosive; dust particles in fusion plasmas pose a chemical and radiological danger due to their small, hard-to-filter size and the retention of tritium [42]. The negative consequences of the presence of dust force limitations on the amount of dust that can be present in a reactor. ITER sets a limit of one tonne on the total dust that can be present in the tokamak, but a much stricter limit on the amount of dust that can be on hot surfaces. For beryllium, for example, this stricter limit is eleven kilograms, if no carbon is present, which is two orders of magnitude lower than the overall limit [54].

Dust therefore needs to be understood and controlled to minimise risk and increase the availability of the powerstation. Increased availability means reduced unit cost of energy production, making a fusion reactor a more economically feasible choice. The biggest factor for the cost-of-electricity metric used to judge the economic feasibility of fusion appears to be plant availability [55]. The accumulation of dust on hot surfaces could be a factor in reducing availability.

There are several aspects of dust that need to be understood in order to predict where dust is likely to accumulate in a tokamak. The origin and trajectory of the dust are the two main aspects. These, in turn, necessitate an understanding of the mechanisms that create dust and of the forces acting on the dust while it moves through the plasma. In this work, we concentrate on the origins of the most important force that acts on the dust grain after it has been created. This is the ion drag force [41]. Ion drag is affected by how the dust grain alters the potential, density and flow of the surrounding plasma. These three quantities are what we set out to find in this work.

Fusion powerstations have been referred to so far, with no explanation as to what exactly these would be. There are various designs that could be used. The leading contender, at the moment, is the tokamak.

1.2.5.1 Tokamaks

The word tokamak comes from a Russian acronym which stands for "toroidal chamber with magnetic coils" [56]. The idea of using thermonuclear reactions for industrial use was first proposed, in the USSR, in 1950 [56], in a letter by a soldier by the name of O A Lavrent'ev to one IV Stalin (the same idea had occured to Professor G.P. Thomson at Imperial College, in the UK, 4 years earlier [57]). The letter itself had an early concept of how to contain the plasma with electric fields [56]. The idea reached AD Sakharov (for "evaluation"), who originated the idea of holding the plasma using magnetic fields [56]. Both Lavrent'ev and Sakharov having passed a personal scrutiny by none other than LP Beriya, the idea was allowed to develop. Sakharov and IE Tamm went on to develop the design for the tokamak [56], a device that was from the start more promising than other devices (such as the Perhapsatron, a toroidal pinch device developed in Project Sherwood by Tuck and his group [58, 59]).

The tokamak encapsulates two key ideas for plasma confinement. The first is that the plasma needs to be confined by ***magnetic*** fields. The second is a natural consequence of the first, namely that the shape of the plasma needs to be able to accommodate continuous closed magnetic field lines everywhere (otherwise there would be a leak). In other words, it must accommodate a smooth vector field everywhere on its surface; this is often explained using the Hairy Ball theorem. More technically, the Euler charateristic of the shape must be 0 (which just means that there are no points on the surface that must act like sources or sinks of the vector field). The torus is one such shape (a slightly different shape, a figure-8 shape, was tried out in the Model A stellarator in Princeton [60]).

A plasma in a tokamak is not, therefore, expected to touch the walls of its container, as the containment is provided by magnetic fields. In practice, the wall and all other plasma facing components (PFC) are always hit by leaking particles (electrons and ions) as well as by the escaping radiation. This results in (physical) sputtering [11], which, along with other mechanisms, leads to the ejection of wall material, in solid or liquid form, into the plasma. This is the source of dust (see figure 1.8) in tokamaks. Areas such as the divertor (this is where the magnetic field lines outside the separatrix lead onto plasma facing components and is shown as the bottom feature in figure

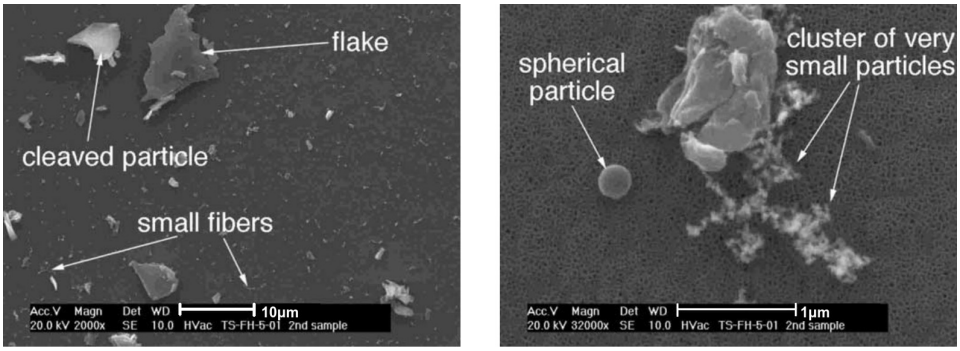

Figure 1.8: "Representative SEM micrographs demonstrating various particulate shapes of dust collected from fusion devices" [9]

1.9), especially, are particularly affected by the particle and heat flux on them.

1.2.6 Other Uses

Plasmas have been used in other types of processing, such as, for example, "the production of thin film solar cells, flat displays, architectural glass and packaging" [32]. In addition, there are "other potential plasma applications, such as the use of small, but very dense, plasmas for mechanical small-scale machining and the application of dc plasmas used in thermal plasma spraying for fast deposition of dense, thin films" [32], or even "plasma for aerodynamics and the important field of combustion and ignition" [32].

Despite the claim that dust is ubiquitous in plasmas, there are applications which are dust-free. This may be because the plasmas are too hot for solid or liquid particles to survive long enough to affect the plasma, like the centre of a tokamak or the sun, or because the time-scale is too fast for dust to have an effect, like in a plasma accelerator (although plasma accelerator research is plagued with its own problems with contaminants, especially on targets that are designed to be very thin).

There is a wide range of applications for "multi-MeV ion beams... proton imaging and deflectometry, injectors for the conventional accelerators, laser-driven stand-alone accelerators, material engineering, production of short-lived isotopes for medical diagnostics with the positron emission tomography (PET) technique, ion fast ignition in laser-induced nuclear fusion and ion sources for particle therapy" [61] to name a few. Cancer treatment,

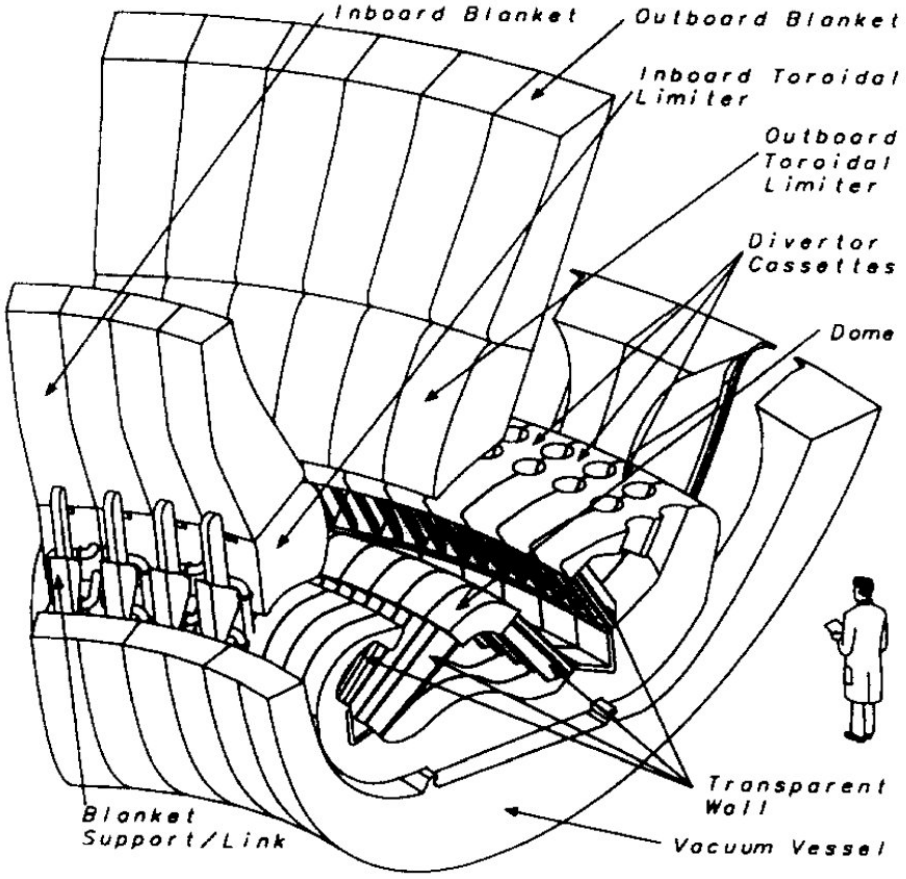

Figure 1.9: "Isometric view of ITER divertor" [10]

in particular, already uses ion beams. In fact, ion beam therapy "is now a popular treatment with conventional accelerators" [61].

1.3 Aim

The aim, or criterion for success, for this project can be summarised as follows:

> Given the plasma density, composition and flow speed and given the dust radius, we want to be able to calculate the potential, plasma velocity and plasma density around a dust grain, for dust grains of radii either much larger or much smaller than the Debye length.

In other words, we wish to understand the behaviour of dust grains in plasmas and their interaction with their local plasma environment. An interesting by-product of this work would be an understanding of the nature of dust-dust interactions in plasmas. Another would be the calculation of the ion drag force, which is of great significance for the calculation of dust grain trajectories in tokamaks.

This is something that has been attempted in the past and some suggestions of solutions do already exist. An explanation of why these suggestions were deemed insufficient for our purposes or how we improved on these methods will be given in subsequent chapters.

This work looks at dust at the two extremes of size, namely dust particles that are much smaller than the Debye length (small dust grains) or much larger than the Debye length (large dust grains). The Debye length will be introduced more formally in chapter 2; here it will suffice to say that it usually defines the (length) scales of interest in plasmas, as it is the distance over which charge screening takes place.

More specifically, this work looks at how dust particles of these two length extremes affect the plasma around them. This can be used to gain information on the ion drag on these particles. Drag forces on dust particles have a major influence on their behaviour. Indeed, in tokamaks, "the dominant force influencing its [the dust grain's] behaviour is ion drag" [62]. The importance of ion drag can be appreciated by noting that "ion drag affects (or even determines) location and configuration of the dust structures in laboratory plasma facilities" [63]. Furthermore, ion drag "is inevitable and exceptionally important in dusty (complex) plasmas" [63]. Fortov [63] lists several aspects of plasma behaviour affected by ion drag, ranging from "diffusion and mobility of dust particles" to "the properties of low-frequency waves in dusty plasmas".

The reason we are concentrating on dust particles that have radii different to the Debye length is that the problem is much harder to solve for dust particles of radius similar to the Debye length. The reason for this is the possible simplifications for the latter case are very limited.

The methodology used had to be two-pronged; a ***numerical fluid*** method was used for large dust grains and an ***analytical*** (where possible) ***kinetic*** method was used for small dust grains (the non-expert reader need not worry, as what I mean by these terms will be explained). The reason for this is

that the simplifications that can be reasonably used for each extreme of size are very different. These simplifications will be introduced in the chapters detailing each method used, namely chapters 4 and 7. Each method offers different advantages and disadvantages, which will be mentioned.

1.3.1 Solution for Large Dust Grains

The solution pathway chosen for large dust grains can be summarised as follows:

> The development of a simple fluid model (SFM) in which the plasma is assumed to be quasi-neutral, the ions are assumed to be cold and the electrons are treated by the Boltzmann law.
>
> The development of a compressible flow simulation code based on the SFM, which can calculate and output the potential, plasma velocity and plasma density around an arbitrary number of dust grains, placed arbitrarily in the chosen domain.

The reasons for this choice include a prior interest in fluid methods for dust grains within the group where this work was carried out, initiated by work done by Professor John Allen and summarised in his 2007 paper [1].

1.3.2 Solution for Small Dust Grains

The solution pathway for small dust grains can be summarised as follows:

> Develop a model based on linear theory, and using the point-sink model, with the assumption that all effects due to the dust grain only introduce a "small" perturbation in the ion distribution function.

The reasons for this choice include a prior interest of a group collaborator, Professor Umberto De Angelis, and for "educational" reasons. By "educational" we mean that the relevance of the physical parameters is made more clear in a simple, linear model. The suitability of such model is discussed in chapter 7.

2 Background on Plasma and Dust

> *"A child of five could understand this. Send someone to fetch a child of five."*
>
> Groucho Marx

In this chapter we will introduce and define some of the key concepts and terminology relevant to the work presented in later chapters. We will also present work done in the past, by other researchers, in attempting to solve similar problems.

This chapter will succeed if, by the end, the reader, and especially the non-expert reader, has an awareness and understanding of some basic plasma and dust-in-plasma concepts and ideas.

We will begin with some relevant definitions to frame the discussion in subsequent chapters. We will also talk about dust charging, as this is the dominant effect on dust grains in plasmas. We end this chapter with a discussion of how similar problems have been tackled in the past.

2.1 Plasma Definitions

Important terms in the discussion that follows, some of which have already been used in chapter 1, need to be defined in a more rigorous way.

2.1.1 Debye Length

The simplified form of the Debye length has already been introduced. The simplified form can be described, briefly, as the scale used to indicate the distance over which charges in plasmas are screened[1], or over which plasma behaviour can be observed [64].

[1] By "screened" we mean the plasma has cancelled the electric field from the charge.

A simple way to derive the Debye length, one commonly used in plasma textbooks, uses the linearised Boltzmann relation for electrons against a constant background ion density in Poisson's equation. In other words, electron density is taken as

$$n_e = n_0 e^{\frac{e\phi}{k_B T_e}} \tag{2.1}$$

$$\approx n_0 \left(1 \frac{e\phi}{k_B T_e}\right) \tag{2.2}$$

and the ion density is taken as

$$n_i = n_0 \tag{2.3}$$

which, when used in Poisson's equation, becomes

$$\nabla^2 \phi = -e \frac{n_i - n_e}{\epsilon_0} \tag{2.4}$$

$$= \frac{n_0 e^2}{\epsilon_0 k_B T_e} \phi \tag{2.5}$$

It can be seen that

$$\phi = \phi_0 e^{-\frac{n_0 e^2 |\boldsymbol{r}|}{\epsilon_0 k_B T_e}} \tag{2.6}$$

where we have the Debye length, λ_D, appearing as a scaling length.

Another way to look at the Debye length is that it is the distance below which plasma effectas cannot be observed. Assuming the typical speed of a plasma particle is its thermal speed, $v_{Th} = \sqrt{\frac{k_B T}{m}}$, then observing a particle over a distance that is smaller than $\lambda = \frac{v_{Th}}{\omega_p}$ will be too short to observe plasma oscillations (ω_p) [64]. Substituting, $\lambda = \sqrt{\frac{k_B T}{m \frac{ne^2}{\epsilon_0 m_e}}} = \sqrt{\frac{\epsilon_0 k_B T}{ne^2}}$, which is, once again, the electron Debye length.

The electrons are not the only plasma constituents to have an associated Debye length. In practice, it is often the case that electrons will be mainly responsible for the shielding, as they react much more quickly than the ions do, due to their lower inertia.

Given that, in plasmas, electrostatic interactions are the dominant form of interaction (as opposed to neutral collisions, for example), the importance of screening and, therefore, of the Debye length is obvious.

2.1.2 Plasma

A plasma is indeed *a gas that is ionised to a sufficient degree to exhibit collective effects*. A more quantitative definition of plasma is provided here.

There are three comparisons to be made when deciding whether a collection of particles constitutes a plasma.

2.1.2.1 Plasma Parameter

I have already introduced the *Debye length* (see 2.1.1), a length of great interest to plasma physicists. In its most simplified form, it is defined as

$$\lambda_{D_e} = \sqrt{\frac{\epsilon_0 k_B T_e}{n_e e^2}} \tag{2.7}$$

where the vacuum electrical permittivity, Boltzmann constant, electron temperature, electron density and elementary charge are ϵ_0, k_B, T_e, n_e, e respectively.

A sphere of radius equal to the Debye length is called a *Debye sphere* (this can be extended to other volumes, such as with a Debye cube). The (average) number of charged particles inside the Debye sphere is denoted by $N_D = \frac{4\pi n \lambda_D^3}{3}$ and is called the *plasma parameter* (strictly speaking, N_D is the *Debye number* and the argument of the Coulomb logarithm, $\Lambda = 4\pi n \lambda_D^3$ is the plasma parameter, but they are often used interchangeably).

For the purposes of this work, a collection of particles can be a plasma iff $\Lambda \gg 1$. Strictly speaking, there can exist plasmas with $\Lambda < 1$. Such plasmas are called "*strongly coupled plasmas*," and include plasmas such as the atmosphere of white dwarves; these plasmas have "more in common with a liquid" [64] (cold and dense) and will not be covered in this work. We will, instead, focus on weakly coupled plasmas, where the electrostatic interaction that dominates is between a particle and "all the particles in its Debye sphere" [64], instead of single particle-particle Coulomb collisions. At the energy densities of terrestrial plasmas, a small plasma parameter would lead to too high recombination levels, which would transform the plasma to a gas.

We shall meet the Debye length again and its importance will become apparent.

2.1.2.2 Plasma Size

As alluded to by Langmuir' distinction between the sheath and the plasma, there are differences between the bulk plasma and its edges; quasi-neutrality breaks down at the edge, for example. One such difference is that bulk plasma is ("needs to be") quasi-neutral. Typically, ion and electron speeds are different, because of the vast difference in mass. This means the initial flux onto plasma facing components (PFC) is different for ions and electrons, which means there are different rates of ion and electron loss; quasi-neutrality therefore breaks down near the edge. We need the bulk plasma to be large enough that these edge effects are negligible. As these effects are important on length scales comparable to the Debye length, this need is more formally expressed as $L \gg \lambda_D$ where L is a measure of the size of the collection of particles we are considering. This can equivalently be expressed as $\frac{\lambda_D}{L} \ll 1$.

2.1.2.3 Plasma Frequency

The behaviour of a normal gas is dictated by the collisions between its particles. The behaviour of a plasma is dictated by electrostatic interactions. For a collection of particles to be a plasma, electrostatic interactions need to be more important than collisions with neutral particles.

A metric for electrostatic interactions is the plasma frequency, defined as $\omega_p = \sqrt{\frac{n_e q_e^2}{\epsilon_0 m_e}}$, where electron density, electron charge, electrical permittivity and electron mass are n_e, q, ϵ_0, m_e, respectively.

Denoting collisions[2] by ω_c, this can be more formally expressed as $\omega_p \gg \omega_c$, or, equivalently, $\frac{\omega_c}{\omega_p} \ll 1$ [64].

We give a simple derivation of the plasma frequency here.

We begin by considering that the lightest charged particles in a plasma are electrons. In a perfectly quasi-neutral plasma, assume we move a cube of electrons slightly off its equilibrium position (see figure 2.1). Since the positive charge in the original cube position has not moved, the electrons will feel an attractive force accelerating them back to their equibrium position. The inertia of the electrons will cause them to overshoot, setting up an oscillation. This oscillation will have a characteristic frequency, which can

[2] By "collision" we mean an electrostatic interaction that scatters particles by more than 90^o.

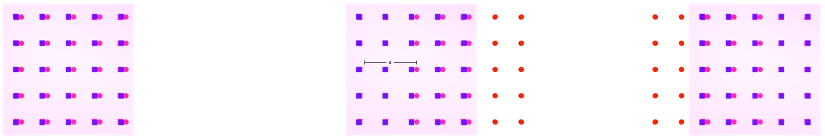

(a) Quasi-neutral cube

(b) Electrons are perturbed to the right by a distance x (shown).

(c) Electrons overshoot their equilibrium position due to their inertia.

Figure 2.1: Cartoon depicting how we can derive plasma frequency: Quasi-neutrality perturbed by moving the electrons in a cube of plasma (electrons and ions are represented by red spheres and blue cubes, respectively).

be calculated.

We limit ourselves to a simple calculation[3]: We can calculate the restoring force for a given density of electrons, and ions, and we know the inertia the electrons will have. The restoring force will be proportional to the electric field that is generated when the two positive and negative charge densities are created by the movement of the electrons (essentially creating two slabs of opposite charge).

$$\begin{aligned} F_e &= eE && (2.8)\\ &= -e\frac{\sigma}{\epsilon_0} && (2.9)\\ &= -e\frac{enx}{\epsilon_0} && (2.10) \end{aligned}$$

where σ is the charge density in the slab of charge created by this movement.

So the acceleration of the electrons is

$$\begin{aligned} \frac{\mathrm{d}^2x}{\mathrm{dt}^2} &= -e\frac{enx}{\epsilon_0 m_e} && (2.11)\\ &= -\frac{ne^2}{\epsilon_0 m_e}x && (2.12) \end{aligned}$$

which can be immediately recognised as a harmonic oscillator ($x(t) = A\cos(\omega t + \phi)$) of frequency $\omega = \sqrt{\frac{ne^2}{\epsilon_0 m_e}} = \omega_p$, the plasma frequency.

Collisions can happen between all species in a plasma. For comparison,

[3]This explanation skips over subtleties that are not important at this stage, as they do not affect the result for plasma frequency.

the ion-ion collision frequency, ω_{ii}, is

$$\omega_{ii} = \frac{\ln(\Lambda)}{\Lambda}\sqrt{\frac{n_i e^2}{\epsilon_0 m_i}} \tag{2.13}$$

where Λ is the plasma parameter [64].

2.1.2.4 Summary

A plasma is a gas that is ionised to a sufficient degree to exhibit collective effects, where $\Lambda \gg 1$, $\frac{\lambda_D}{L} \ll 1$ and $\frac{\omega_c}{\omega_p} \ll 1$.

2.1.3 Sheath

The definition for the sheath is important for understanding plasmas in general, but also for understanding dust grains immersed in plasmas.

It is also important for this work, as the fluid model we developed is only valid for a plasma, and not for a sheath, as will be made clear in this chapter.

A sheath is "a positive space-charge region" adjacent to a negative wall, "shielding the neutral plasma from the negative wall" [65]. To appreciate the importance of this, let us consider what happens when an object, be it the wall of the container holding the plasma, or a macroscopic particle immersed in the plasma, begins to interact with the plasma.

2.1.3.1 Dust Charge in a Plasma

"Normal" plasmas are made up of electrons and ions. Electrons are much lighter than even the lightest ions, so their thermal velocities will, correspondingly, be much higher. Consequently, the one-way flux of electrons on any neutral surface in the plasma, real or imaginary, will be higher than that of the ions. For a real surface, this means the accumulation of negative electric charge faster than the accumulation of positive charge[4]. A negatively charged surface repels electrons and attracts ions. This means the flux of electrons is reduced and the flux of ions is increased. This continues until the flux of electrons and ions equal each other; we say that the ion and electron currents on to the surface are equal. It is assumed that this

[4]We are assuming, here, that any charge impinging on a real surface is collected and that the ejection of charge (secondary emission) is negligible.

leads to a steady state. This argument was first presented by Langmuir in a General Electric Review article [66] in 1923 and later summarised in an article in Science [67].

This is why the charge of macroscopic particles in plasmas is normally negative.

2.1.3.2 The Positive Sheath

A charged dust grain, in a plasma, is a source of an electric field. We have already seen that electric fields are shielded in a plasma and that the Debye length determines the scale of this shielding. We expect, therefore, that the space surrounding the dust grain will have an electric field which diminishes rapidly, extending out to distances of the order of the Debye length.

A negatively charged dust grain will have a surrounding field which repels electrons. In fact, all but the most energetic electrons approaching the dust grain will be repelled. Ions, on the other hand, will be attracted. Very near the dust grain, consequently, we have a region with a diminished number of electrons. This is the "positive space-charge region" [65] that we term "the sheath."

The sheath, thus, has the surface of the dust grain as its inner boundary, and the plasma as its outer boundary[5]. The natural question, if we will treat the sheath as separate to the plasma, as indeed Irwin Langmuir, the godfather of plasma, and all subsequent authors do, is where does the plasma end and the sheath begin? This question is not a trivial one to answer; as late as 2004, 75 years after Langmuir's denominative publication and 81 years after the first explanation of the sheath, papers with titles such as "Where is the 'sheath edge'?" [68] were being authored. The difficulty in finding the sheath edge does stem, partly, in the difference on how it is defined in the literature.

For Langmuir, in his original paper [67], there does not seem to be an issue in defining what the sheath is, or where its edge is. Indeed, in his General Electric review article [66], Langmuir talks about "a layer of gas near the electrode where there are positive ions, but no electrons" [66]. In Langmuir's experiments, he was assuming monoenergetic electrons of 1 eV, however, so that the "outer edge of this sheath of ions will have a potential of

[5] We will soon see that the outer boundary is not always between the sheath and the bulk plasma.

-1" [66]. Langmuir's early definition of a sheath, then, is a region completely devoid of electrons. In a plasma with a spread of electron energies, this definition would be impractical. Langmuir, in a later paper, states that "If the initial velocities of the plasma electrons and ions could be neglected we would be justified in regarding the edge of the sheath as sharp" [69]. Tonks and Langmuir imply a different definition; they say that a point just outside the sheath would have ion and electron densities both equal to the background densities, whereas "The potential at the inside point is slightly less than in the plasma, with the result that both electron and ion densities are less there" [70]. In other words, "the sheath edge is defined as the surface at which this essential equality fails" [70]. Already, Tonks and Langmuir talk about a plasma-sheath transition region, which they describe as complicated.

For the fluid model, one of our assumptions is quasi-neutrality. In other words, the model breaks down when we reach the edge of the plasma, i.e. the sheath, according to the latter definition of the sheath. It is convenient, therefore, to adopt this definition for the sheath. This allows us to claim that the model treats the whole plasma, but breaks down in the sheath. We will quickly see that this does not make things quite that simple.

2.1.3.3 The Sheath Edge

We have decided which definition to use, so we would like now to establish where the sheath edge is. We will start with a calculation first done by Langmuir and adjusted by Bohm, which is for a non-flowing plasma and a planar wall (see chapter 3 of "Characteristics of Electrical Discharges in Magnetic Fields" [71] and Reimann [65]). This is instructive in its own right, and something of a tradition in dusty plasma textbooks. It is also, often, considered to be useful for large dust grains, as near a large dust grain, the sheath approaches a planar geometry. We will then discuss the spherical case, which is more relevant in this work.

The Sheath Edge for a Planar Wall We assume a plasma of singly charged positive ions of density n_0. We denote the ion density as n_i and electron density as n_e, so that in the bulk plasma $n_i = n_e = n_0$. We define the potential of the plasma as zero. We assume steady state conditions, so that $\frac{\partial}{\partial \mathrm{t}} = 0$. We assume an infinite planar wall present in the plasma. We choose a location near the wall, such that we are as near the wall as possible

with quasi-neutrality still approximately holding. This is how we defined the sheath edge.

We define the potential, ϕ, at this point as ϕ_0. We make no assumptions about the potential, but we assume the field at this point is negligible. In doing so, we are following the assertion by Langmuir that "it is known that in the plasma near the sheath edge the fields are so small that the potential remains close to V_0 over a distance several sheath thicknesses in extend" [71].

We look at ions and electrons inside the volume enclosed by the wall and the plane parallel to the wall at our chosen location - inside the sheath. We expect the wall to be negatively charged and, therefore, most of the electrons are repelled back from the wall. We can thus assume the electrons to be Maxwellian and their density can be found with the Boltzmann relation. This also means that it will be convenient to substitute $\phi = -\Phi$ and $\phi_0 = -\Phi_0$

$$\frac{n_e}{n_0} = e^{-\frac{e(\Phi-\Phi_0)}{k_B T_e}} \tag{2.14}$$

where k_B is Boltzmann's constant and T_e is the electron temperature.

The ions are assumed to fall to the wall with no recombination or ionisation, so the ion continuity equation is

$$n_i v \quad = \quad n_0 v_0 \tag{2.15}$$

where v is the speed of the ions and $v_0$is the speed of the ions in the plasma ("far" from the wall).

The ion conservation of energy equation is

$$\frac{1}{2} m_i v^2 - e\Phi = \frac{1}{2} m_i v_0^2 - e\Phi_0 \tag{2.16}$$

where e is the elementary charge, assuming singly ionised ions.

This means the ion speed is

$$v = \left(v_0^2 - \frac{2e}{m_i}(\Phi_0 - \Phi) \right)^{1/2} \tag{2.17}$$

For cold ions, the total kinetic energy is equal to the kinetic energy gained,

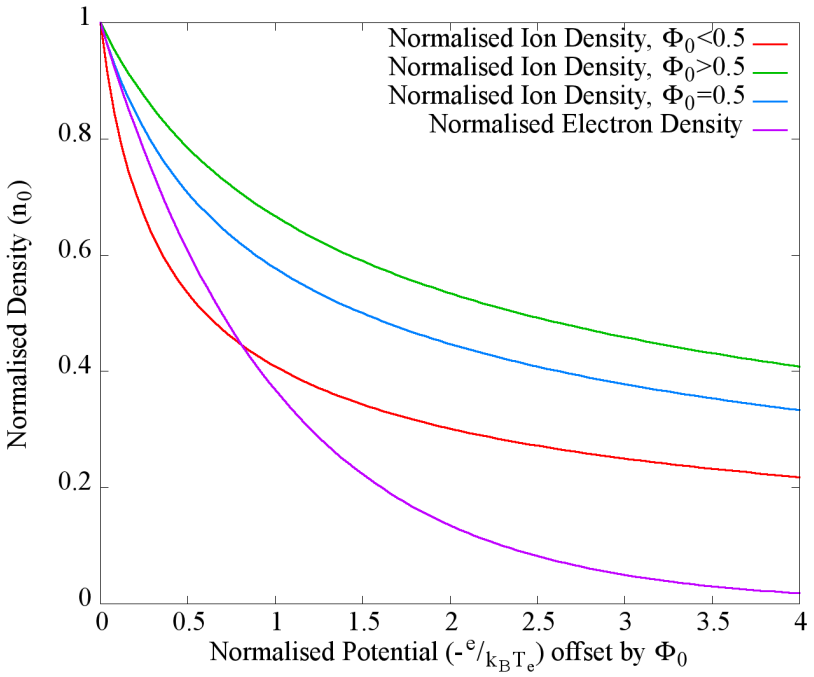

Figure 2.2: Ion and electron density in the sheath in the Bohm planar approximation.

which is equal to the potential energy lost, $\frac{1}{2}m_i v_0^2 = e\Phi_0$, so

$$v = v_0 \left(\frac{\Phi}{\Phi_0}\right)^{1/2} \tag{2.18}$$

and so

$$\frac{n_i}{n_0} = \left(\frac{\Phi}{\Phi_0}\right)^{-1/2} \tag{2.19}$$

As we get closer to a negatively charged wall, the potential is expected to become more and more negative. Plotting a graph of density change against negative potential we get figure 2.2, where we have offset each curve by Φ_0 so that all start at $\hat{\Phi}_0 = 0$.

We note that for plasmas with ions of energy corresponding to a normalised (by $-\frac{k_B T_e}{e}$) potential of $\Phi_0 < 0.5$, there is a region where the electron density is higher than the ion density, followed by the positive space charge talked about by Langmuir. It will quickly become apparent why this

is highlighted.

We can use equation 2.14 and 2.19 in Poisson's equation

$$\boldsymbol{\nabla}^2\Phi = \frac{e}{\epsilon_0}\left(n_i - n_e\right) \tag{2.20}$$

$$= \frac{en_0}{\epsilon_0}\left(\left(\frac{\Phi}{\Phi_0}\right)^{-1/2} - e^{-\frac{e(\Phi-\Phi_0)}{k_BT_e}}\right) \tag{2.21}$$

We multiply by $\nabla\Phi$ on both sides and then integrate once:

$$\frac{\left(\boldsymbol{\nabla}\Phi\right)^2}{2} = \frac{en_0}{\epsilon_0}\left(2\left(\Phi_0\Phi\right)^{1/2} + \frac{k_BT_e}{e}e^{-\frac{e(\Phi-\Phi_0)}{k_BT_e}}\right) + C \tag{2.22}$$

We use our assumption for a negligible field, $\nabla\Phi = 0$, when $\Phi = \Phi_0$, to find C, the constant of integration

$$\frac{\left(\boldsymbol{\nabla}\Phi\right)^2}{2} = \frac{en_0}{\epsilon_0}\left(2\Phi_0\left[\left(\frac{\Phi}{\Phi_0}\right)^{1/2} - 1\right] + \frac{k_BT_e}{e}\left[e^{-\frac{e(\Phi-\Phi_0)}{k_BT_e}} - 1\right]\right) \tag{2.23}$$

The left hand side of equation 2.23 is always positive. The right hand side of the equation is positive as $\Phi \to \infty$, but it is not obvious what the sign of the right hand side is as $\Phi \to \Phi_0$. We expand in $\Delta\Phi = \Phi - \Phi_0$ for $\Delta\Phi \to 0$ and find that the first two terms of the expansion[6] vanish, with the third term giving

$$\frac{\left(\boldsymbol{\nabla}\Phi\right)^2}{2} = \frac{en_0}{\epsilon_0}\frac{\Delta\Phi^2}{2}\left(\frac{e}{k_BT_e} - \frac{1}{2\Phi_0}\right) \tag{2.24}$$

We need $\left(\frac{e}{k_BT_e} - \frac{1}{2\Phi_0}\right) \geqslant 0$ so $\Phi_0 \geqslant \frac{1}{2}\frac{k_BT_e}{e}$.

This gives us a lower limit on the potential at the sheath edge. We have defined the zero of potential to be in the bulk plasma, so this analysis implies that the sheath edge cannot, at the same time, be the plasma edge.

This potential corresponds to a speed for the ions of no less than $\sqrt{\frac{k_BT_e}{m_i}}$. Bohm interpreted this to mean that the ions have to travel at a speed no smaller than $\sqrt{\frac{k_BT_e}{m_i}}$ when entering the sheath. This is the "Bohm criterion" [71, 65]. The Bohm criterion states that the ion velocity, u_i, towards the

[6] $\left(\frac{\Phi}{\Phi_0}\right)^{1/2} = \left(\frac{\Delta\Phi}{\Phi_0}+1\right)^{1/2} \to 1 + \frac{\Delta\Phi}{2\Phi_0} - \frac{\Delta\Phi^2}{8\Phi_0^2}$ and $e^{-\frac{(\Phi-\Phi_0)}{k_BT_e/e}} = e^{-\frac{\Delta\Phi}{k_BT_e/e}} \to 1 - \frac{\Delta\Phi}{k_BT_e/e} + \frac{\Delta\Phi^2}{2(k_BT_e/e)^2}$

dust grain, at the sheath edge must obey the relationship

$$u_i \geqslant u_B \tag{2.25}$$

where

$$u_B = \sqrt{\frac{k_B T_e}{m_i}} \tag{2.26}$$

It can be seen that the Bohm speed, u_B, is equal to the sound speed of the plasma.

Satisfying the Bohm criterion is a necessary prerequisite for the ions to have a sufficient density in the sheath for a positive space-charge to exist [65]. For plasmas flowing at subsonic speeds, this would imply the ions need to be accelerated to the Bohm speed. Indeed, a transition region, the "pre-sheath," is set up in the plasma (figure 2.3) , which provides the field for this acceleration [65]. Assuming the dust grain to be the source of this field would imply that the dust grain is not fully shielded. This may be an inadequate solution for some readers, as the presence of a field would imply that there is also a difference in density between the ions and electrons, i.e. the pre-sheath should be thought of as part of the sheath. In practice, this is not an issue, as it takes only differences in density of "a small fraction of 1 per cent to produce potentials of hundreds of volts" (p.199 of [71]). A plasma flowing at supersonic speeds, however, already (over)satisfies the Bohm criterion, which would imply that the dust grain is fully shielded upstream - the field is fully shielded by the sheath.

The planar wall Bohm criterion is often used for large dust grains. Thus for a plasma flowing at subsonic speeds, the surface around a dust grain at which the ions are travelling at the Bohm speed is taken to mark the edge of the sheath. For a plasma flowing at supersonic speeds, the front of the dust grain (i.e. the side of the dust grain facing the flow) would, by this definition, not need a pre-sheath. It would also mean that we cannot use the Bohm criterion for the front of a large dust grain. In such cases, where the size of the sheath is small compared to the dust radius, the sheath edge can be approximated to be at the dust grain edge.

For smaller spherical dust grains, this analysis is less relevant, as the convergence of the ions on to the dust grain provides an additional increase in density.

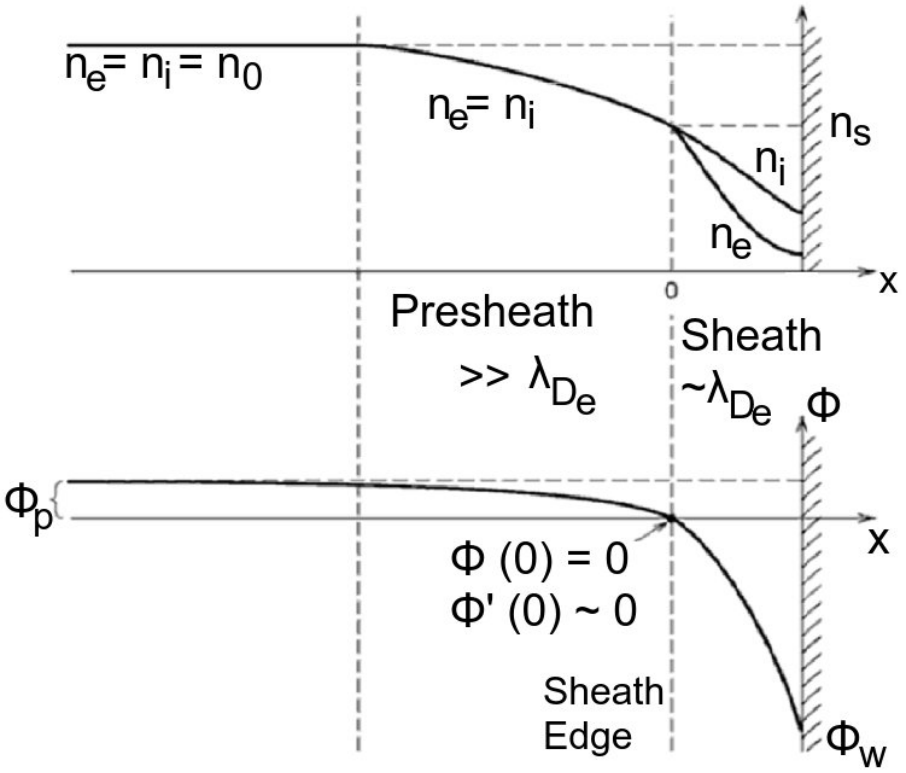

Figure 2.3: Illustration of the sheath and pre-sheath next to a planar wall. Φ_p denotes the potential difference between the background plasma and the sheath edge. Φ_w is the potential at the planar wall. [11]

This analysis implies there are 3 distinct regions that can exist: The field-free, quasi-neutral plasma, the pre-sheath, where there is an accelerating field but quasi-neutrality can still be assumed, and the sheath, where there is a field and quasi-neutrality breaks down. We can therefore have 2 distinct surfaces that are "edges". The plasma edge, which is between the plasma and the pre-sheath, and the sheath edge, which is between the sheath and the pre-sheath. In the case of supersonic flow, the pre-sheath collapses and the plasma edge must coincide with the sheath edge.

The Sheath Edge for a Spherical Dust Grain We will repeat the analysis for the planar wall, making the necessary adjustments for the spherical geometry. Whereas the analysis for the planar wall can be found in and is based on the literature, what follows is my work.

There is no change in the electron density equation, so

$$\frac{n_e}{n_0} = e^{-\frac{e(\Phi-\Phi_0)}{k_B T_e}} \tag{2.27}$$

Ion continuity needs to be modified, to reflect the convergence of the ions as they move radially inwards

$$n_i v r^2 = n_0 v_0 r_0^2 \tag{2.28}$$

$$\frac{n_i}{n_0} = \frac{v_0 r_0^2}{v r^2} \tag{2.29}$$

Conservation of energy is the same as in the planar wall case, as is our assumption of cold ions, so $v_0^2 = \frac{2e}{m}\Phi_0$ and $v = v_0 \left[\frac{\Phi}{\Phi_0}\right]^{1/2}$. We therefore have

$$\frac{n_i}{n_0} = \frac{r_0^2}{r^2}\left[\frac{\Phi}{\Phi_0}\right]^{-1/2} \tag{2.30}$$

This introduces the first additional difficulty of the spherical case, compared to the planar, namely the presence of the radius term, r. This can be overcome by using a relationship between the radius and the potential. A relationship often used in plasmas is the Debye-Hückel relationship[7], which

[7] This choice may be problematic in general for large dust grains. It does serve to demonstrate the principle of this method, however, and is valid in the high temperature limit where the Debye-Hückel relationship is valid.

does relate potential to distance:

$$\Phi = -\frac{Qe^{-\sqrt{2}\mathrm{r}/\lambda_\mathrm{D}}}{4\pi\epsilon_0 r} \tag{2.31}$$

$$r = -\frac{Qe^{-\sqrt{2}\mathrm{r}/\lambda_\mathrm{D}}}{4\pi\epsilon_0 \Phi} \tag{2.32}$$

We use this relationship in the ion density equation

$$\frac{r_0^2}{r^2} = \left(\frac{-\frac{Qe^{-\sqrt{2}\mathrm{r}_0/\lambda_\mathrm{D}}}{4\pi\epsilon_0\Phi_0}}{-\frac{Qe^{-\sqrt{2}\mathrm{r}/\lambda_\mathrm{D}}}{4\pi\epsilon_0\Phi}} \right)^2 \tag{2.33}$$

$$= \left(\frac{\frac{e^{-\sqrt{2}\mathrm{r}_0/\lambda_\mathrm{D}}}{\Phi_0}}{\frac{e^{-\sqrt{2}\mathrm{r}/\lambda_\mathrm{D}}}{\Phi}} \right)^2 \tag{2.34}$$

$$= \left(\frac{\Phi}{\Phi_0} \right)^2 e^{\frac{2\sqrt{2}}{\lambda_D}(r-r_0)} \tag{2.35}$$

For a large dust grain, the sheath width, $r - r_0$, becomes negligible compared to r and r_0, so, to make the analysis tractable, we can approximate

$$\frac{r_0^2}{r^2} \approx \left(\frac{\Phi}{\Phi_0} \right)^2 \tag{2.36}$$

We therefore have

$$\frac{n_i}{n_0} \approx \left(\frac{\Phi}{\Phi_0} \right)^2 \left[\frac{\Phi}{\Phi_0} \right]^{-1/2} \tag{2.37}$$

$$\approx \left(\frac{\Phi}{\Phi_0} \right)^{3/2} \tag{2.38}$$

We can now use these expressions in Poisson's equation

$$\nabla^2\Phi = \frac{n_0 e}{\epsilon_0} \left(\left(\frac{\Phi}{\Phi_0} \right)^{3/2} - e^{-\frac{e(\Phi-\Phi_0)}{k_B T_e}} \right) \tag{2.39}$$

As with the planar wall case, we subsequently multiply by $\nabla\Phi$ and integrate,

$$\frac{(\nabla\Phi)^2}{2} = \frac{n_0 e}{\epsilon_0} \left(\frac{2}{5}\Phi \left(\frac{\Phi}{\Phi_0} \right)^{3/2} + \frac{k_B T_e}{e} e^{-\frac{\Phi-\Phi_0}{\mathrm{k_B T_{e/e}}}} \right) + C \tag{2.40}$$

We assume fields are negligible when $\Phi = \Phi_0$

$$C = \frac{n_0 e}{\epsilon_0}\left(-\frac{2}{5}\Phi_0 - \frac{k_B T_e}{e}\right) \tag{2.41}$$

and thus

$$\frac{(\nabla\Phi)^2}{2} = \frac{n_0 e}{\epsilon_0}\left[\frac{2}{5}\Phi_0\left(\left(\frac{\Phi}{\Phi_0}\right)^{5/2} - 1\right) + \frac{k_B T_e}{e}\left(e^{-\frac{\Phi-\Phi_0}{\mathrm{k_B T_e/e}}} - 1\right)\right] \tag{2.42}$$

Similarly to the planar case, the right hand side of the equation is obviously positive for very high values of Φ, but what happens as $\Phi \to \Phi_0$ is not obvious. We expand in $\Delta\Phi = \Phi - \Phi_0$ for $\Delta\Phi \to 0$

$$\frac{(\nabla\Phi)^2}{2} = \frac{n_0 e}{\epsilon_0}\left[\left(\Delta\Phi + \frac{3}{4}\frac{\Delta\Phi^2}{\Phi_0}\right) + \left(-\Delta\Phi + \frac{\Delta\Phi^2}{2\left(\mathrm{k_B T_e/e}\right)}\right)\right] \tag{2.43}$$

$$= \frac{n_0 e}{\epsilon_0}\frac{\Delta\Phi^2}{2}\left[\frac{3}{2\Phi_0} + \frac{1}{\left(\mathrm{k_B T_e/e}\right)}\right] \tag{2.44}$$

which means we must have

$$\frac{3}{2\Phi_0} + \frac{e}{k_B T_e} \geqslant 0 \tag{2.45}$$

or

$$\Phi_0 \geqslant -\frac{3}{2}\frac{k_B T_e}{e} \tag{2.46}$$

As $\frac{3}{2}\frac{k_B T_e}{e} \geqslant 0$, this inequality is superceded by $\Phi_0 \geqslant 0$ and thus presents no limitation like in the planar case on Φ_0. In other words, the Bohm speed is not a necessary pre-requisite for the formation of a sheath in the spherical case.

This presents a problem, as the surface around a dust grain in a plasma with subsonic flow where ions achieve the sound speed cannot be used as a mark for the sheath edge.

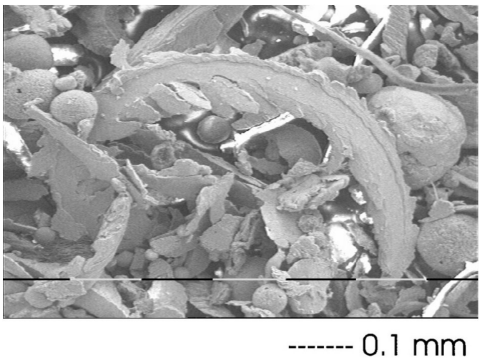

Figure 2.4: "An SEM image of the magnetic coarse fraction (see text) showing a cutting, various spheres and irregularly formed particles" from TEXTOR-94 [12].

2.2 Dust Definitions

In line with the more quantitative definition given for plasmas, a better definition is needed for dust as well. We will define "dust" as solid or liquid particles "of material of dimensions larger than that of a single ion or atom or molecule" [42]. In practice this means particles larger than about 1 nanometre. It is important to note that the charge on a dust particle is more dependent on the ambient plasma conditions (i.e. on the particle flux onto the dust particle) and less so on its own chemical composition.

Dust is routinely found in inspections of tokamaks during maintenance or upgrades and it varies in size and shape (see figure 2.4). Sharpe et al [9] report on the dust grain size distribution, for example, as shown in figure 2.5. They comment how it is similar to other devices, which they interprete to indicate similar processes are in play to create the dust particles.

In this work we only consider spherical dust grains of size either much larger or much smaller than the Debye length. The reason for this is the amount of simplifications that this allows to be used, making the work more tractable. The work remains physically relevant as dust of these sizes is found in both tokamak plasmas and other plasmas[8].

"A calculation of the charge on a particle is the starting point of every theory of dusty plasmas" [72], as the "basis of a dust physical model is

[8] A quick calculation for ASDEX-Upgrade shows the Debye length at the scrape-off layer (SOL), next to the wall, to be just under 10 μm, which indicates there are both large and small dust grains in the ASDEX-Upgrade SOL.

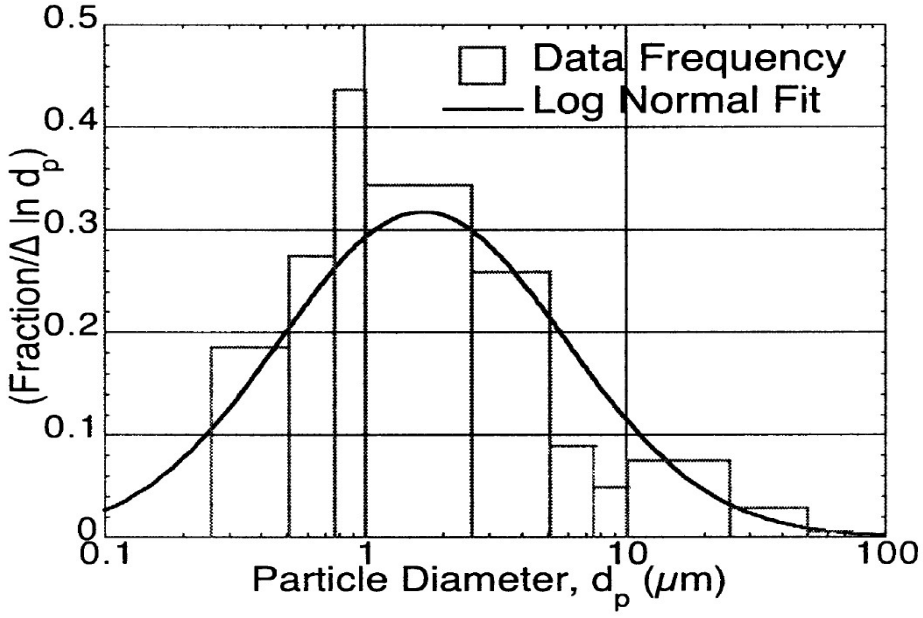

Figure 2.5: Size distribution of dust particles in ASDEX-Upgrade - taken from Sharpe et al [9].

the charging of the dust grains" [41]. In fact, "having calculated the dust grains' floating potential, it determines the flux of electrons and ions to the grain and in this way plays a major role in the determination of the forces experienced by the dust grain and the energy fluxes onto it" [41]. It is only fitting, therefore, that the way charging is calculated is briefly explained.

2.2.1 Dust Charging

"The most commonly used method of determination of the floating[9] potential of a dust particle immersed in a plasma environment is the orbital motion limited" [41]. OML is not the only charging theory, not least because it does not include all the physics of dust grain charging in a plasma, such as, for example, "additional charging mechanisms, namely, secondary electron emission and thermionic emission" [41]. Other charging theories include the full orbital motion theory (OM), and ABR (Allen, Boyd, Reynolds). Here we will quickly summarise OML, as the most often used one, and ABR, as a simple self-consistent theory which is found to be surprisingly accurate in

[9]Floating means the ion and electron currents onto the surface are equal.

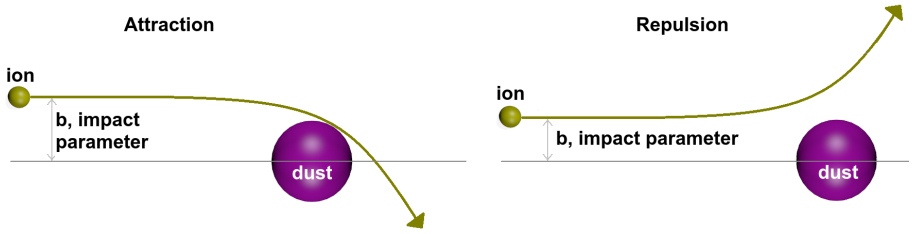

Figure 2.6: Attraction and repulsion, as used in OML.

some instances.

2.2.1.1 OML

OML stands for orbit motion limited. It was developed in 1926 by Langmuir and Mott [73] and shown not to be valid for cases of interest such as tokamaks (negatively charged dust grain, Maxwellian plasma, $T_i < T_e$) in 2000 by Allen, Annaratone and de Angelis [74]. Despite its limitations, it "remains the preferred charging model due to its simplicity" [15]. Simplicity would seem to be a poor reason for choosing a model, but most physicists, including myself, as evident by some parts of the work reported here, would be throwing stones in a glass house. In defence of this theory, "it is found experimentally that OML can be used successfully under adverse conditions" [75], even if "its validity is fortuitous" [75].

The theory calculates the charge of a dust grain by equating the currents of positive and negative charges onto the dust grain. The individual currents are calculated by considering the trajectory (orbit) of distant particles to determine whether they intersect the dust grain. The idea of a grazing orbit is used for the limiting impact parameter. The currents are a function of the dust grain potential, so equating them allows for the calculation of the potential.

More specifically, we begin by considering particles far away from the dust grain. These can either be attracted to or repelled by the dust grain, as shown in figure 2.6. In the figure we can also see the impact parameter, labelled "b". The impact parameter that will result in a grazing orbit for particle species "s", "b_{sg}", is the parameter that defines the collision cross-section for that species, $\sigma_s = \pi b_g^2$. Conservation of energy and momentum can subsequently be used to find the impact parameter for a grazing orbit,

where $v_r\,(r_d)$, the radial velocity at the surface of the dust grain, is zero. Using m, v, r_d, q, and ϕ for mass, velocity, dust radius, charge and potential respectively, and ∞, g subscripts to denote the position of the particle (initial, at infinity, and at grazing), we have:

$$m_s v_{s\infty} b_{sg} = m_s v_{sg} r_d \tag{2.47}$$

$$\frac{1}{2} m_s v_{s\infty}^2 = \frac{1}{2} m_s v_{sg}^2 + q_s \phi_d \tag{2.48}$$

which gives

$$\sigma_s = \pi r_d^2 \left(1 - \frac{2 q_s \phi_d}{m_s v_{s\infty}^2}\right) \tag{2.49}$$

The particle distribution can be used to convert this knowledge to a current to the dust grain by each species, which is just the rate at which particles reach the dust grain times their charge.

$$I_s = \int_{v_{s\infty}0}^{\infty} q_s \sigma_s\,(v_{s\infty})\, v_{s\infty} f_s\,(v_s)\,\mathrm{dv_s} \tag{2.50}$$

where $v_{s\infty} = 0$ for ions, and remembering that the cross-section will be 0 below a minimum of velocity when the dust grain repels a given species. The minimum is the velocity, $v_{s\infty m}$, below which v_{sg} becomes negative in equation 2.48. This can be incorporated more explicitly in the integral, by changing the lower limit to $\int_{v_{s\infty m}}^{\infty}$, with $v_{s\infty m} = \sqrt{\frac{2 q_s \phi_d}{m_s}}$.

The integral can be solved analytically for some cases. Remembering, for example, that we are assuming spherical symmetry, and using Maxwellian distributions, and a negatively charged dust grain, we get [15]:

$$I_{ions} = 4\pi r_d^2 n_i q_i \left(\frac{k_B T_i}{2\pi m_i}\right)^{1/2} \left(1 - \frac{q_i \phi_d}{k_B T_i}\right) \tag{2.51}$$

$$I_{electrons} = 4\pi r_d^2 n_e q_e \left(\frac{k_B T_e}{2\pi m_e}\right)^{1/2} \exp\left(\frac{q_e \phi_d}{k_B T_e}\right) \tag{2.52}$$

We assume that the charge of the dust grain will reach a steady state, at which point the negative and positive currents on to the dust grain must be equal. Equating them gives the potential at the dust grain surface for a given parameter set. We subsequently need to convert this potential to the dust charge (as explained in [76]).

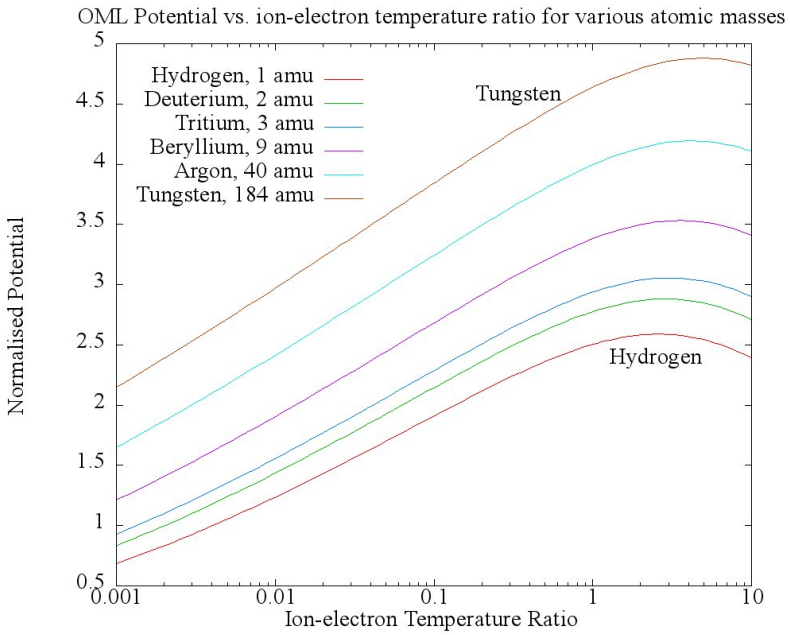

Figure 2.7: Normalised potential against ion-electron temperature ratio.

Given these assumptions, and $n_e = n_i$, $q_i = -q_e$, we then get

$$\left(\frac{T_i m_e}{T_e m_i}\right)^{1/2} \left(1 - \frac{q_i \phi_d}{k_B T_i}\right) = \exp\left(\frac{q_e \phi_d}{k_B T_e}\right) \tag{2.53}$$

We simplify our notation using $\tau = \frac{T_i}{T_e}$, $\mu = \frac{m_e}{m_i}$, and $\Phi = -\frac{q_e \phi_d}{k_B T_e}$

$$(\tau\mu)^{1/2} \left(1 + \frac{\Phi}{\tau}\right) = \exp\left(-\Phi\right) \tag{2.54}$$

We can solve for Φ

$$\Phi = -\tau + \Omega\left(\frac{\tau e^{\tau}}{\sqrt{\tau\mu}}\right) \tag{2.55}$$

where Ω is the Lambert W function.

The normalised potential then looks like figure 2.7.

For the unnormalised potential

$$-\frac{q_e\phi_d}{k_BT_e} = -\frac{T_i}{T_e} + \Omega\left(\frac{\frac{T_i}{T_e}e^{\frac{T_i}{T_e}}}{\sqrt{\frac{T_i}{T_e}\frac{m_e}{m_i}}}\right) \tag{2.56}$$

$$\phi_d = \frac{k_BT_i}{q_e} - \frac{k_BT_e}{q_e}\Omega\left(\frac{\sqrt{\frac{T_i}{T_e}}e^{\frac{T_i}{T_e}}}{\sqrt{\frac{m_e}{m_i}}}\right) \tag{2.57}$$

We can use the unnormalised potential to find the charge on the dust grain, using a method valid for small dust grains. We can use Gauss's law to approximate the charge on a dust grain, $Q = 4\pi\epsilon_0 r_d\phi_d$ (Alternatively, we can use more sophisticated methods, such as the one used in equation 38 in [76]).

$$Q = 4\pi\epsilon_0 r_d\phi_d \tag{2.58}$$

$$= 4\pi r_d\frac{\epsilon_0 k_BT_e}{e}\left(\tau - \Omega\left(\sqrt{\tau\mu}e^{\tau}\right)\right) \tag{2.59}$$

$$= 4\pi R\frac{\left(\epsilon_0 k_BT_e\right)^{3/2}}{\sqrt{n}e^2}\left(\tau - \Omega\left(\sqrt{\tau\mu}e^{\tau}\right)\right) \tag{2.60}$$

where we have normalised distances using the Debye length ($r_d = R\sqrt{\frac{\epsilon_0 k_BT_e}{ne^2}}$), masses using the mass of the electron, m_e (for example, the ion mass, m_i, becomes $m_i = M_i m_e$), and Ω is the Lambert W-function (which is the inverse of $f(x) = xe^x$). Thus, the charge on the dust grain depends on the ion and electron temperatures, the ion mass, the density (remember that $n_i = n_e$) and the dust radius. Typical values for the scrape-off layer of fusion devices are [77, 78]:

- Ion temperature: (assumed $\sim T_e$)
- Electron Temperature: 20 eV
- Ion Mass: (assumed deuterium ~ 2 amu)
- Density: $10^{19}\,m^{-3}$

Using these values, the equation reduces to

$$Q \approx 10^{-15}R \tag{2.61}$$

where Q is in coulombs and corresponds to

$$Z_{de} \approx 6 \times 10^3 R \tag{2.62}$$

where Z_{de} is the charge in elementary charge units and R is the dust radius in units of λ_D. An average-sized dust grain in ASDEX-Upgrade, for example (based on the value of $2.8\,\mu$m given by Sharpe et al [9]) would have an excess of just over 2000 electrons.

We can look at the dependence of charge on the dust radius, remembering that our vacuum capacitance assumption is only valid for small dust grains.

We will be comparing these results with the results from the fluid code and the kinetic analysis, but we note, for now, that the (normalised) potential on the dust grain surface does not depend on the dust grain radius, in contrast to the next charging theory we will discuss, namely ABR.

2.2.1.2 ABR

Allen, Boyd and Reynolds published their ABR charging theory in 1957 [79]. The theory postulates cold ions, zero fluid flow, a floating dust grain, a collisionless plasma and Boltzmann electrons with a Maxwellian velocity distribution. Cold ions and no fluid flow lead to radial ion motion. This makes conservation of energy simply

$$\frac{1}{2}mv_r^2 = -q\phi_r \tag{2.63}$$

$$v_r^2 = -\frac{2q\phi_r}{m} \tag{2.64}$$

where m, v, q and ϕ denote mass, velocity, charge and potential respectively, and the r subscript denotes the quantity at distance r from the dust grain centre. ABR solves Poisson's equation ($\nabla^2\phi = -\frac{\rho_q}{\epsilon}$, for potential, charge density and electric permittivity), which is used assuming spherical symmetry and in spherical form:

$$\frac{1}{r^2}\frac{\partial}{\partial r}\left(r^2\frac{\partial\phi}{\partial r}\right) = -\frac{e}{\epsilon_0}\left(n_i - n_e\right) \tag{2.65}$$

The theory looks at the currents on the dust grain (which must sum to zero, given the floating dust grain postulate). The ion current can be used to find the ion density. We use the expression for the ion current on a sphere

of radius r:

$$I_i = 4\pi r^2 \left(e n_{ir}\right) v_{ir} \tag{2.66}$$

$$n_{ir} = \frac{I_i}{4\pi r^2 e v_{ir}} \tag{2.67}$$

where the subscript i indicates the quantity is for ions and the subscript r indicates the quantity at a distance r from the dust grain centre.

We can use energy conservation to substitute for v_{ir}

$$n_{ir} = \frac{I_i}{4\pi r^2 e}\sqrt{-\frac{m}{2q\phi_r}} \tag{2.68}$$

We normalise $\Phi = -\frac{\phi_r e}{k_B T_e}$, $R = \frac{r}{\lambda_D}$, $J = \frac{I_i}{4\pi\lambda_D^2 e n_\infty \sqrt{\frac{2k_B T_e}{m_i}}}$ and assume singly charged ions, $q = e$, so that

$$n_{ir} = \frac{I_i}{4\pi R^2 \lambda_D^2 e}\sqrt{\frac{m_i}{2k_B T_e \Phi}} \tag{2.69}$$

$$\frac{n_{ir}}{n_\infty} = \frac{J}{R^2\sqrt{\Phi}} \tag{2.70}$$

Boltzmann electrons means

$$n_{er} = n_{e\infty} \exp\left(\frac{e\phi}{k_B T_e}\right) \tag{2.71}$$

$$\frac{n_{er}}{n_\infty} = \exp\left(-\Phi\right) \tag{2.72}$$

The electrons have a Maxwellian distribution, which is, in spherical coordinates:

$$f\left(v\right) = \left(\frac{m}{2\pi k_B T_e}\right)^{3/2} 4\pi v^2 \exp\left(-\frac{mv^2}{2k_B T_e}\right) \tag{2.73}$$

This relation is expected to break down near the dust grain, given the shielding from the dust grain, but the error is small for two reasons[10]. The first is that the dust grain will be negatively charged (a result of both the cold ion postulate, which means a higher initial flux of electrons, and the fact that the mass of electrons is much smaller than the mass of the ions), so that most electrons are reflected back from the dust grains. The second

[10] I've been made aware of another method for calculating the current onto the dust grain, which uses the one-way particle flux and arrives at the same result without approximating for this error.

is that near the dust grain the number of electrons is very small, hence the error in the asymmetry of flow is small[11]. The flux of electrons on the surface of a sphere of radius r is then

$$I_e = 4\pi r^2 e n \int_0^\infty f(v)\, v \mathrm{dv} \tag{2.74}$$

$$I_e = 4\pi r^2 e n_{e\infty} \exp(-\Phi) \int_0^\infty \left(\frac{m}{2\pi k_B T_e}\right)^{3/2} 4\pi v^2 \exp\left(-\frac{mv^2}{2k_B T_e}\right) v dv \tag{2.75}$$

$$= 4\pi r^2 e n_{e\infty} \left(\frac{k_B T_e}{2\pi m}\right)^{1/2} \exp(-\Phi) \tag{2.76}$$

Given equations for both n_i and n_e, we can substitute into Poisson's equation.

$$\frac{1}{r^2}\frac{\partial}{\partial r}\left(r^2 \frac{\partial \phi}{\partial r}\right) = -\frac{e}{\epsilon_0}(n_i - n_e) \tag{2.77}$$

and normalise r

$$\frac{1}{R^2\lambda_D^2}\frac{\partial}{\lambda_D \partial R}\left(R^2\lambda_D^2 \frac{\partial \phi}{\lambda_D \partial R}\right) = -\frac{e}{\epsilon_0}(n_i - n_e) \tag{2.78}$$

$$\frac{1}{R^2\lambda_D^2}\frac{\partial}{\partial R}\left(R^2 \frac{\partial \phi}{\partial R}\right) = -\frac{e}{\epsilon_0}(n_i - n_e) \tag{2.79}$$

We then normalise ϕ

$$\frac{1}{R^2\lambda_D^2}\frac{\partial}{\partial R}\left(R^2\left(-\frac{k_B T_e}{e}\right)\frac{\partial \Phi}{\partial R}\right) = -\frac{e}{\epsilon_0}(n_i - n_e) \tag{2.80}$$

$$\frac{1}{R^2\lambda_D^2}\frac{\partial}{\partial R}\left(R^2\left(\frac{\epsilon_0 k_B T_e}{e^2 n_\infty}\right)\frac{\partial \Phi}{\partial R}\right) = \frac{n_i}{n_\infty} - \frac{n_e}{n_\infty} \tag{2.81}$$

$$\frac{1}{R^2}\frac{\partial}{\partial R}\left(R^2 \frac{\partial \Phi}{\partial R}\right) = \frac{J}{R^2\sqrt{\Phi}} - \exp(-\Phi) \tag{2.82}$$

Solving this equation gives the potential at various positions, R, for a given normalised ion current. We are interested in finding the potential at the dust grain surface. We cannot yet do this, as we do not know what value

[11] The dust grain causes zero flow in one direction, as it shields the flow. This would be a problem if the opposite flow was large, but this is not the case, as most electrons are reflected due to electric repulsion. In this respect, the absolute error is small (2 electrons per second in one direction vs. 0 electrons per second in the opposite direction, for example).

of J to use, and we need two boundary conditions.

We find the boundary conditions first. We can consider two different solutions, namely the "vacuum solution", very near the dust grain, and the "plasma solution", far away. The former allows for the approximation that the terms on the right-hand side of the equation are negligible (as both n_i and $n_e$are very small near the dust grain), whereas the latter allows for the quasi-neutrality approximation (as $n_i \approx n_e$ in the background plasma), which means the difference between the two terms on the right-hand side can be neglected; this, in turn, implies that the left-hand side can be neglected. The equation is thus simplified as follows:

$$\frac{1}{R^2}\frac{\partial}{\partial R}\left(R^2\frac{\partial \Phi}{\partial R}\right) = 0 \tag{2.83}$$

$$\frac{2}{R}\frac{\partial \Phi}{\partial R} + \frac{\partial^2 \Phi}{\partial R^2} = 0 \tag{2.84}$$

for the vacuum solution, and

$$0 = \frac{J}{R^2\sqrt{\Phi}} - \exp\left(-\Phi\right) \tag{2.85}$$

for the plasma solution.

The vacuum solution is $\Phi = \frac{A}{R} + B$. Looking at the plasma solution, we have

$$\frac{J}{R^2\sqrt{\Phi}} = \exp\left(-\Phi\right) \tag{2.86}$$

$$R = \left(\frac{J}{\exp\left(-\Phi\right)\sqrt{\Phi}}\right)^{1/2} \tag{2.87}$$

This corresponds to figure 2.8, where the potential shown is multi-valued, but we ignore the higher values as unphysical.

The plasma solution is obviously valid for small values of Φ (as we are far from the dust grain). For low values of Φ, $\exp\left(\Phi\right)\sqrt{\Phi} \approx \sqrt{\Phi}$, which makes equation 2.87

$$R = \left(\frac{J}{\sqrt{\Phi}}\right)^{1/2} \tag{2.88}$$

$$\Phi = \frac{J^2}{R^4} \tag{2.89}$$

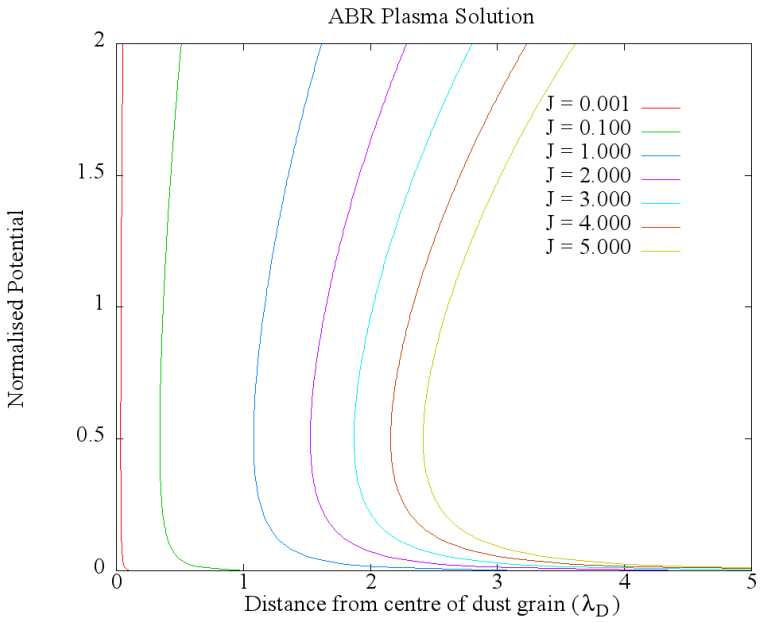

Figure 2.8: Normalised potential against normalised distance, R, for the plasma solution of ABR.

This means a $1/r$ behaviour for the vacuum solution changes to a $1/r^4$ behaviour for the plasma solution.

The plasma solution gives one boundary condition. Differentiating and taking the reciprocal we find

$$\frac{d\Phi}{dR} = \frac{4R\Phi^{3/2}\exp(-\Phi)}{J(2\Phi-1)} \tag{2.90}$$

This gives the second boundary condition when taken at a distance far away from the dust grain. "Far away" is vague, so Kennedy et al [80] provided a slightly better definition, namely

$$\frac{4\Phi(2\Phi-3)(2\Phi+1)}{(2\Phi-1)^3} \ll \frac{J}{\Phi^{1/2}}$$

[80]. To quantify this, we can convert it, as Kennedy et al do, to

$$\frac{J}{\gamma} = \frac{4\Phi^{3/2}(2\Phi-3)(2\Phi+1)}{(2\Phi-1)^3} \tag{2.91}$$

with γ is an arbitrary number, as long as $\gamma \gg 1$. This can be plotted with

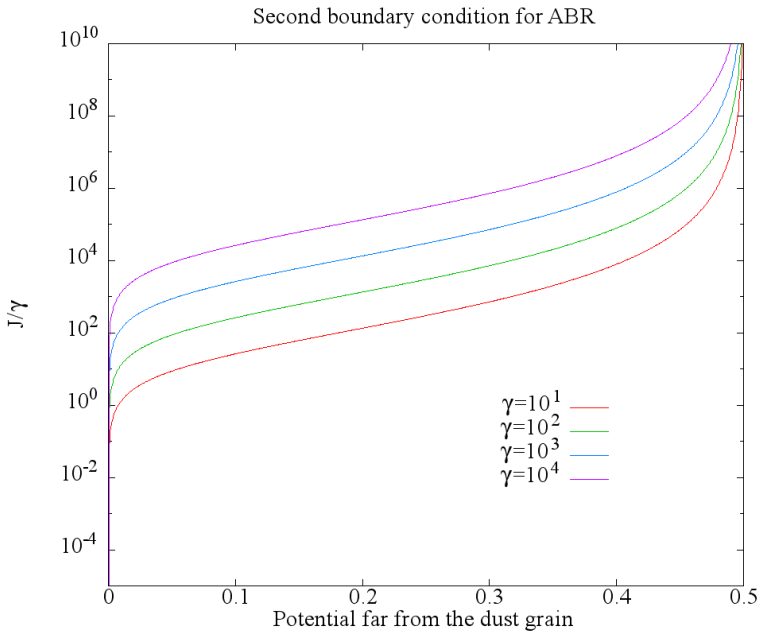

Figure 2.9: Second boundary value for the ABR solution.

a suitable choice of γ, as in figure 2.9.

This is still vague, but, as will be seen in paragraph 2.2.1.2, I have devised a method to calculate the sheath width, which gives a lower bound to what "far away" must be.

We can now solve ABR. The steps required are as follows:

1. Choose a value for J.

2. Use the chosen J to find the potential far from the dust grain, using equation 2.91.

3. Use J and the potential found from step 2 to find the distance from the dust grain, using equation 2.87.

4. Numerically integrate towards the dust grain using equation 2.82.

5. When J, as calculated by $J = \frac{R^2\sqrt{\mu}}{2\sqrt{\pi}} \exp(-\Phi)$, matches the choice made in step 1 (where R, Φ are given by the steps above and $\mu = \frac{m_i}{m_e}$ is given by the choice of ion mass, m_i), then we have reached the dust radius.

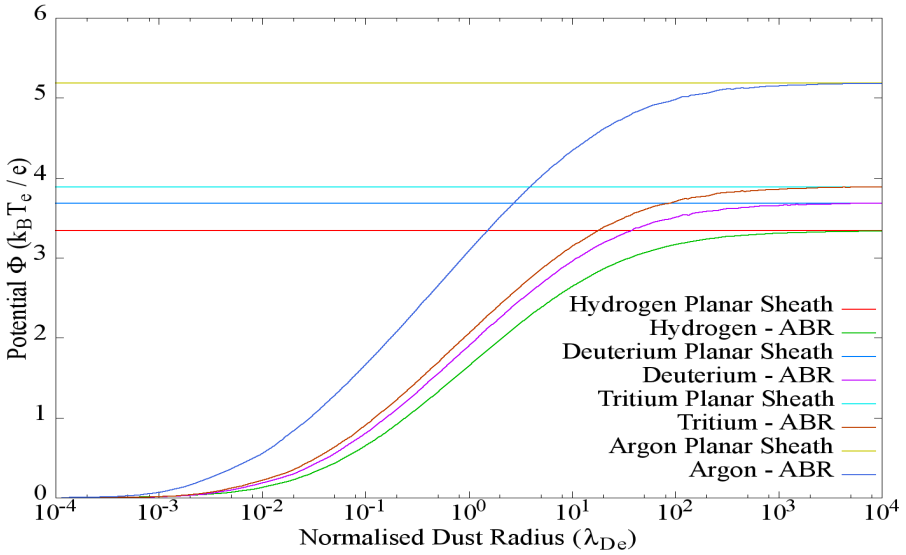

Figure 2.10: Normalised Potential against normalised dust radius for plasmas of different atomic mass, as predicted by ABR.

Given that the only parameter, other than the dust grain radius, we can change in ABR is the square root of the ion-mass-to-electron-mass ratio, we would expect this value to be the determining factor in deciding the potential at the surface of a very large dust grain. Alternatively, one can assume that as the radius of a spherical dust becomes larger, the closer its surface potential will be to that of a plane, as the surface of the dust, locally, will be more and more like a plane. These both turn out to indeed be the case. Equating the one-way electron Maxwellian flux ($\Gamma_e = \frac{n_0}{4}\left(\frac{8k_BT_e}{\pi m_e}\right)^{1/2}\exp\left(-\Phi\right)$) at the surface of the dust grain with the ion flux at the sheath edge ($\Gamma_i = n_0\exp\left(-\frac{1}{2}\right)\left(\frac{k_BT_e}{m_i}\right)^{1/2}$)[12], we get a planar normalised potential of $\Phi = -\frac{1}{2}\ln\left(2\pi\frac{m_e}{m_i}\right) + \frac{1}{2}$. The results for various dust grain radii are plotted in figure 2.10, along with the planar potential for the same ion-to-electron-mass ratios. The potential settles asymptotically to the planar sheath value as the dust radius (normalised by the Debye length) goes to infinity.

[12] $\Gamma_i = n_i v_i$, where, at the sheath edge, the ion speed is the Bohm speed. The ion density can be found by considering that all of the kinetic energy of the ions has been converted from electrical potential energy and that quasi-neutrality holds.

One can also see that as the dust radius goes to zero, the potential also goes to zero, as would be expected by the diminished collection of electrons and ions.

ABR Appraisal ABR is not used often in charging calculations, with preference given to OML. The main reason for this is the cold ion assumption, which would imply we cannot use it for warm or hot plasmas. This may turn out to be untrue, if we recast the theory in fluid terms. While it will still be true that we will not be able to use it for flowing plasmas (at least, not without modifications), the fluid picture means we are not interested in the random thermal motion of the ions, due to spherical symmetry. The Bohm criterion means the ion distribution function is truncated at the Bohm speed, which can be taken, as an approximation, to be the average speed of the ions. This means the theory needs very little modification in its fluid reincarnation. This has not been explored to its full potential, and is an appealing area for further work.

Geometrical Addition to ABR The assumption of cold ions for ABR actually allows for significant simplification, both conceptually and mathematically. The result that the ions will have fallen through a potential of $\exp(1/2)$ at the sheath edge allows us to calculate their density at that point. This along with the (small) extra step of assuming that all ions that reach the sheath edge will be collected by the dust grain, allows us to calculate the potential.

We can use ABR to find the width of the sheath. We begin with the ion current, as stated in ABR

$$\begin{aligned} I_i &= 4\pi r_s^2 n_s e v_B & (2.92)\\ &= 4\pi r_s^2 n_\infty \exp(-1/2)\, e \left(\frac{k_B T_e}{m_i}\right)^{1/2} & (2.93) \end{aligned}$$

where v_B is the Bohm speed, the speed the ions have at the sheath edge, and the subscript "s" indicates at the sheath edge.

We then quote the electron current, again, as used in ABR

$$I_e = 4\pi r_d^2 n_\infty e \left(\frac{k_B T_e}{2\pi m_e}\right)^{1/2} \exp(-\Phi) \qquad (2.94)$$

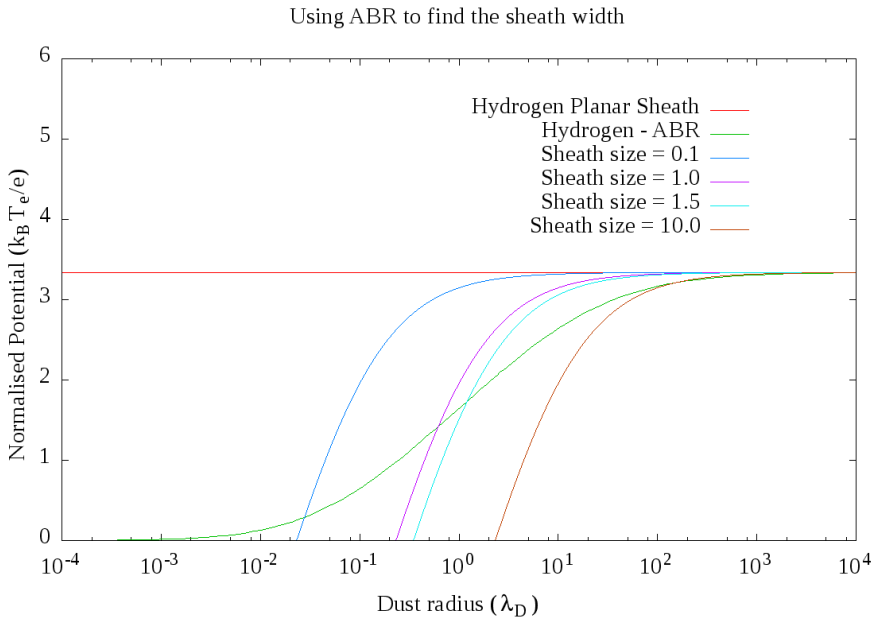

Figure 2.11: An attempt to find the sheath width by using ABR.

where the "d" subscript indicates at the dust grain surface.

We set $I_i = I_e$, so

$$\exp\left(-\Phi + 1/2\right) = \frac{r_s^2}{r_d^2}\left(\frac{2\pi m_e}{m_i}\right)^{1/2} \tag{2.95}$$

$$\Phi = -1/2 \ln\left(\left(\frac{r_s}{r_d}\right)^4 \left(\frac{2\pi m_e}{m_i}\right)\right) + 1/2 \tag{2.96}$$

This looks remarkably similar to the planar sheath equation, as expected. We convert this to add the sheath width, $r_s = r_d + \lambda_s$

$$\Phi = -1/2 \ln\left(\left(\frac{r_d + \lambda_s}{r_d}\right)^4 \left(\frac{2\pi m_e}{m_i}\right)\right) + 1/2 \tag{2.97}$$

We can now plot Φ against r_d for various sheath widths and compare with ABR. This is shown in figure 2.11. We can scan for various sheath sizes and find the corresponding dust radii. Doing so results in figure 2.12, which shows a logarithmic-like behaviour, and a larger sheath width for plasmas of higher atomic mass ions. This is essentially the same as equating the ABR solution with equation 2.97 and solving for the dust radius.

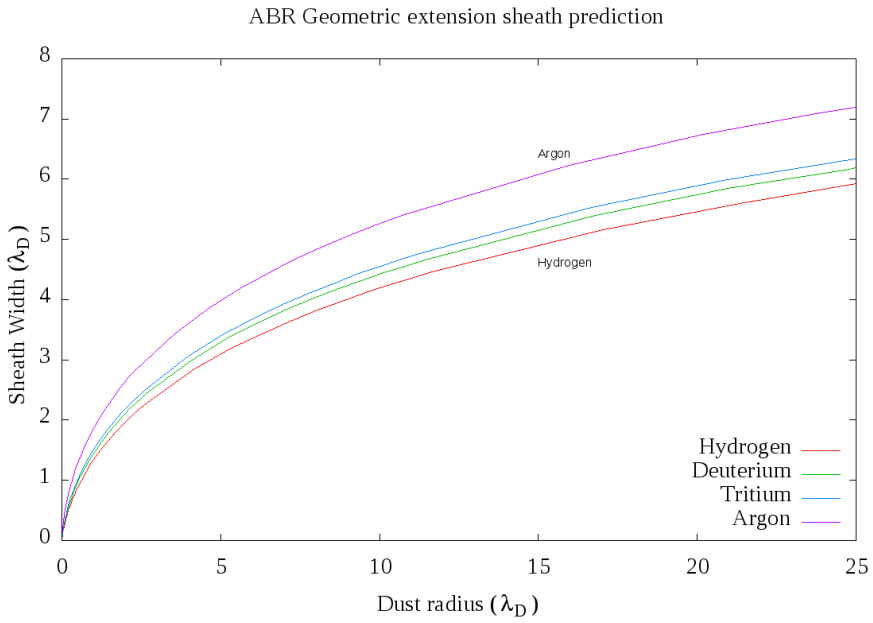

Figure 2.12: Sheath size against dust radius, as predicted by the ABR geometric extension for plasmas of singly charged ions of different atomic mass.

Does this make sense? We consider that a higher atomic mass implies a lower ion current, which would mean a lower electron current, i.e. a higher potential at the dust grain (as shown in figure 2.10). A higher potential on the dust grain would, in turn, imply a stronger effect on the surrounding plasma, which would mean the sheath would be of a bigger width.

Being able to calculate the width of the sheath can help with calculating the charge on the dust grain, as it provides a check on any potential profile assumptions that are made in calculating the charge (e.g. the often quoted charge found assuming vacuum capacitance).

2.2.1.3 Comparing ABR and OML

We could consider comparing the result from ABR with the result for OML. Before doing so, let's look at some of the key features of the results from each theory.

The potential predicted by OML does not depend on dust radius, but does depend on the ion-to-electron temperature ratio. This is shown in in equation 2.55. The potential predicted by ABR does depend on radius

(figure 2.10), but does not depend on the ion-to-electron temperature ratio (which is assumed to be zero). Both theories give results that are dependent on the ion-to-electron mass ratio. Given the different parameters that can be changed in each, however, means that we can match the two theories for a given radius or ion-to-electron temperature ratio in what would be a meaningless exercise. I will refrain from further travails down this road.

2.2.2 Ion Drag

As mentioned already, ion drag is the most important force on a dust grain, and not just in a fusion device. As such, several attempts have been made to predict the ion drag on a dust grain. The main theories pertaining to these attempts are the "pair [binary] collision approach" and the "linear kinetic approach" [81]. The way small grains are tackled in this work is related to the linear kinetic approach. The way large dust grains are tackled is related to a third approach to calculating the ion drag on a dust grain, namely the "control surface" approach, first suggested by Allen [1]. I present these three approaches, briefly, here.

2.2.2.1 Binary Collision

The use of the Binary Collision approach (BC) is one of the two standard approaches to calculating ion drag. BC has been in use long enough to be included in standard textbooks on the subject (e.g. [82]); Lord Rutherford conducted an analysis on binary collisions as far back as 1911[83]. BC is "Basically, standard Coulomb scattering theory...adapted to determine the momentum lost by those ions that are deflected by the electric field surrounding the charged dust particle" [1].

An important assumption made in the binary collision approach is the assumption of spherical symmetry [1, 82], which allows the use of potential distributions like the Coulomb or Debye-Hückel potential distributions (equations 2.98 and 2.99).

$$\phi_{Coulomb} = \frac{k_C Q}{r} \tag{2.98}$$

$$\phi_{Debye-Hückel} = \frac{k_C Q}{r} \exp\left(-\lambda_D r\right) \tag{2.99}$$

where $k_c = \frac{1}{4\pi\epsilon_0}$ is Coulomb's constant.

This assumption is an important limitation to this approach [1].

Furthermore, BC assumes that all collisions are binary, i.e. there are no n-body (n > 2) collisions, which would imply a low density. A less restrictive assumption made is the assumption that the ion mass is much smaller than the dust grain mass.

When a dust grain and an ion interact the two possible results are deflection or collection. Both entail momentum exchange, and need to be taken into account when calculating ion drag. In the case of a beam of ions interacting with a dust grain, a summation of all the binary collisions will give the overall effect on the dust grain. In the binary collision approach, it is found that in plasmas small-angle deflections dominate [82].

In a plasma, ions interacting with a dust grain can be assumed to be originating at "infinity", i.e. they are unbound. This implies that the trajectory of the ion will be hyperbolic, with the dust grain being at the focal point of the hyperbola. If the dust radius is larger than the distance between the focal point and the vertex of the hyperbola (r_{ca}) then the ion will be collected by the dust grain; if the radius is smaller, then the ion will be deflected only. This distance can be easily found, by using conservation of angular momentum.

$$L_{\infty}^2 = m^2 v_{\infty}^2 b^2 \tag{2.100}$$

$$L_{r_{ca}}^2 = m^2 r_{ca}^2 \left(v_{\infty}^2 + \frac{2 k_C Q q}{m r_{ca}} \right) \tag{2.101}$$

$$L_{r_{ca}}^2 = L_{\infty}^2 \tag{2.102}$$

$$r_{ca} = -0.5 + 0.5 \left(1 + \left(\frac{v_{\infty}^2 b m}{k_C Q q} \right)^2 \right)^{1/2} \tag{2.103}$$

where: L_{∞} is the angular momentum at infinity, $L_{r_{ca}}$ is the angular momentum at the distance of closest approach, r_{ca} is the distance of closest approach, v_{∞} is the ion speed at infinity, b is the impact parameter, m is the ion mass, and $k_C Q q$ are the Coulomb constant, dust grain and ion charge magnitudes respectively.

The equations for a hyperbola can be subsequently used to find the semi-

major axis and eccentricity for the hyperbola.

$$r_{ca} = a(\epsilon - 1) \tag{2.104}$$

$$\epsilon = \frac{\left(a^2 + b^2\right)^{1/2}}{a} \tag{2.105}$$

$$a^3 - a^2 + \left(b^2 - 2r_{ca}\right) a - r_{ca}^2 = 0 \tag{2.106}$$

where a is the semi-major axis of the hyperbola (the distance from the vertex to the "centre", or where the two asymptotes to the hyperbola meet), and ϵ is the eccentricity of the hyperbola.

The cubic equation can be used to find a (the real root) and the value of a can be used to find the eccentricity. In the case of collection, the whole of the momentum of the ion is added to the momentum of the dust grain. In the case of deflection the momentum exchange originates in the deflection of the trajectory of the ion by an angle 2θ, where $\theta = \arccos\left(\frac{1}{\epsilon}\right)$.

$$\delta p_{dz} = -\delta p_{iz} \tag{2.107}$$

$$\delta p_{iz} = m v_\infty - m v_\infty \cos\theta \tag{2.108}$$

$$= m v_\infty \left(1 - \frac{1}{\epsilon}\right) \tag{2.109}$$

$$= m v_\infty \left(1 - \frac{a}{(a^2 + b^2)^{1/2}}\right) \tag{2.110}$$

where: δp indicates a momentum change. The subscripts d and i indicate dust or ion respectively. The subscript z indicates the z direction, which is the direction of the relative velocity of the dust and the plasma, and which was chosen without loss of generality.

The momentum change from a ring of ions (figure 2.13) is entirely parallel to the direction of flow, as any perpendicular components are cancelled out by the cylindrical symmetry of the flow. The momentum change from such a ring would thus be:

$$\delta p_{dz} = -2\pi\, b\, db\, n\, m\, v_\infty^2 \left(1 - \frac{a}{(a^2 + b^2)^{1/2}}\right) \tag{2.111}$$

where db is the thickness of the ring, and n is the plasma density.

The total momentum change by deflection can be found by summing up all

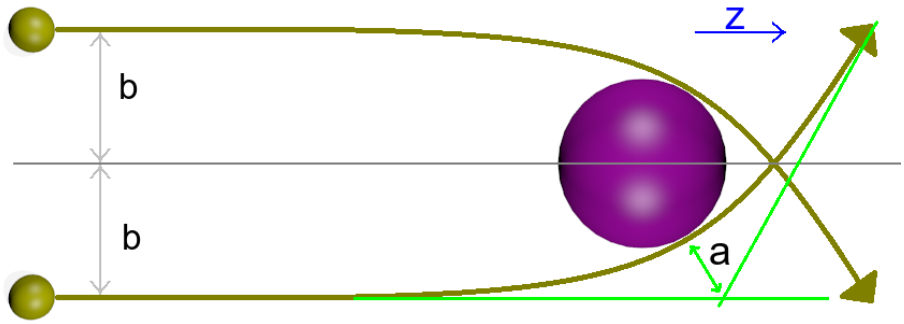

Figure 2.13: Cylindrical symmetry in flow for the binary collision approach.

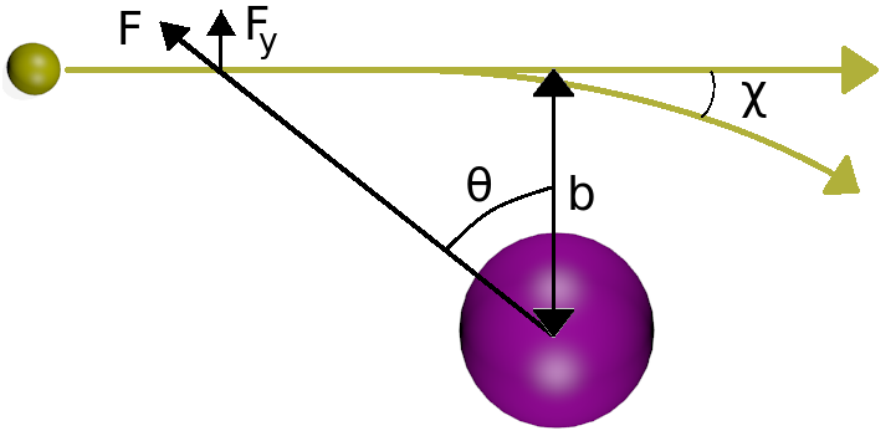

Figure 2.14: A small-angle deflection in the BC approach.

such rings from a minimum to a maximum impact parameter. A simplified expression can be found by assuming a small-angle collision, such that the ion is essentially travelling in a straight line. The force perpendicular to the direction of travel will be (referring to figure 2.14):

$$F_y = F\cos\theta \tag{2.112}$$

$$= k_C Q e^2 \frac{b}{\left(b^2 + v^2 t^2\right)^{3/2}} \tag{2.113}$$

where t is the time of travel, taking $t = 0$ to be at the point when the ion is at a distance b from the dust grain, Q is the dust grain charge and F indicates force.

Integrating along the line, from $t = -\infty$ to $t = +\infty$ we get the impulse

imparted to the ion in the perpendicular direction:

$$\delta p_{iy} = \int_{-\infty}^{\infty} k_C e^2 \frac{b}{\left(b^2 + v^2 t^2\right)^{3/2}} \mathrm{dt} \tag{2.114}$$

$$= \frac{2k_C e^2}{vb} \tag{2.115}$$

This impulse gives the ion a small deflection angle, such that $\delta p_{iy} = \delta p_{iz} \sin(\chi) \approx \delta p_{iz} \chi$, with the approximation justified for small deflection angles. The deflection angle is thus:

$$\chi = \frac{2k_C e^2}{\delta p_{iz} vb} \tag{2.116}$$

$$= \frac{2k_C e^2}{mv^2 b} \tag{2.117}$$

A Coulomb force is conservative and the collision is elastic, so, in the limit of the dust grain mass being much bigger than the ion mass, we expect the ion to have a final speed approximately equal to its original speed. The kinetic energy in the direction of motion that is perpendicular to the initial, pre-collision, motion is thus "taken from" the kinetic energy in the initial direction of motion. The new speed, w, in the initial direction of motion is thus:

$$w^2 \approx v^2 \left(1 - \chi^2\right) \tag{2.118}$$

$$w \approx v \left(1 - \chi^2\right)^{1/2} \tag{2.119}$$

$$\approx v \left(1 - \frac{\chi^2}{2}\right) \tag{2.120}$$

(where the last step expands for small χ).

It follows that the momentum loss for the ion is $mv - mw = mv\frac{\chi^2}{2}$ and that this is the momentum gain for the dust grain for each ion-dust grain interaction. Integrating for all "allowed" impact parameters, the total momentum change for the dust grain, Δp_{dz}:

$$\Delta p_{dz} = \int_{b_{min}}^{b_{max}} m_i v_i \left(1 - \frac{\chi^2}{2}\right) n_i v_i 2\pi b \mathrm{db} \tag{2.121}$$

$$= \left[2\pi m_i v_i^2 n \left(\frac{b^2}{2} - \left(\frac{2k_C e^2}{mv^2}\right)^2 \ln b\right)\right]_{b_{min}}^{b_{max}} \tag{2.122}$$

The calculation stops being valid when b_{min} is taken to be sufficiently small to produce deflection angles that cannot be considered small. The minimum impact parameter is thus often taken to be the impact parameter that would cause a deflection angle of 90^o. A problem would arise if the maximum impact parameter for collection (which would vary from the dust radius, for an uncharged dust grain, to a value larger than the dust radius for an attractive dust grain) is smaller than the minimum deflection impact parameter. A more rigorous analysis would be needed in such cases. A maximum radius for deflection needs to be used to avoid a divergent integral for the effect of deflection (see later in this section).

After the full integral is taken, the maximum and minimum impact parameters appear in a logarithm,

$$\ln \Lambda = \ln \frac{b_{max}}{b_{min}} \tag{2.123}$$

This logarithm is the Coulomb logarithm and it indicates the relative importance between large and small angle collisions [84]. The lower limit, for an attractive interaction, will be the upper limit for the collection term. In the case of a repulsive interaction (e.g. positively charged dust grain and ions), the lower limit cannot be zero, as the integral will again diverge. Instead, the impact parameter at which point the momentum change is equal twice the original momentum of the ions (as in the case of a 1D elastic collision of a light ion against a heavy dust grain) can be used. Other minimum impact parameters used in the literature are the impact parameter that would lead to 90^o collisions (b_{90}) or the de Broglie wavelength ($= \frac{\hbar}{mv}$) of the incoming ions. b_{90} can be found by setting the ion momentum change equal to the initial momentum (by conservation of energy, the final speed will be equal to the initial speed and the mass does not change, therefore the magnitude of the momentum will not change) in equation 2.115, so that $b_{90} = \frac{2k_C e^2}{mv^2}$.

The integral clearly diverges for $b_{max} = \infty$, hence b_{max}, the upper limit for the integration, is often taken to be the Debye length ($= \left(\frac{\epsilon_0 k_B T_e}{n_0 e^2}\right)^{1/2}$), as the Coulomb force is effectively shielded at this length scale in a plasma.

The analytic result makes several assumptions that are not physically justified so several authors have tried to introduce corrections to this method by, among other things, altering the integration limits (e.g. Hutchinson [85], Khrapak [86] and others).

Hutchinson introduces a correction to the limits to make the analytic result agree with the numerical results reported in his paper [85]. The limits he suggests are shown in equations 2.124 and 2.125.

$$b_{90-Hutchinson} = \frac{r_d Ze\phi}{m_i v_{eff}^2} \tag{2.124}$$

$$b_{max}^2 = \frac{\lambda_{D_e}^2}{\left(1 + \frac{r_d Ze\phi}{m_i v_{eff}^2}\right)} + r_d^2 \tag{2.125}$$

where r_d is the dust radius, Z_e is the dust charge, ϕ is the potential on the dust surface, m_i is the ion mass, v_{eff} is the effective velocity (Hutchinson provides the equation with the fitting parameters in equation 11 of his paper [85]) and λ_{D_e} is the Debye length.

The binary collision approach is the "currently accepted standard on ion drag" [41] in dusty plasmas. "The potential assumed in the current literature is a spherically symmetric Debye shielded potential" [41], shown in equation 2.99.

It is important to note, however, that its widespread use is despite the fact that the "analysis required for calculating [the total scattering cross section], using the Debye potential, is excessively complicated and it must be done numerically" [82].

Furthermore, the BC approach is a good approximation only for certain categories of plasma: "The binary collision approach for the interparticle interactions is naturally valid as long as the system is sufficiently dilute" [52]. "As the number density of microparticles grows the coupling with increasing number of neighbors becomes important" [52], which means the BC approximation becomes less accurate. Bittencourt states that using a Boltzmann collision integral that "takes into account only binary collisions limits considerably its applicability for a plasma, where each particle interacts simultaneously with a large number of neighboring charged particles" [82]. Furthermore, Bittencourt warns of the need for a quantum mechanical approach, as, if the particle density is high enough, the "quantum wave packets of the colliding particles necessarily overlap" [82]. A comparison between "the average de Broglie wavelength of each particle" and the "average interparticle separation" is therefore required[13].

[13]These vary depending on the plasma. As an example, in conditions similar to those of

Both Allen [1] and Fortov et al [63] highlight the inherent weakness of BC. Allen mentions how "the potential distribution surrounding the dust particle is 'chosen' and not deduced!" It is also assumed to be isotropic in nature, whereas it is known that interesting wake phenomena have been observed in the laboratory" [1]. Fortov et al state:

> "The binary collision approach is intrinsically inconsistent. There are the following reasons for that: (i) While the ion interacts with the charged particle, the interactions with other species (in particular— the ion–neutral collisions) are neglected. (ii) The approach presumes certain potential distribution around the test charge, although the potential is a self-consistent function of the plasma environment (e.g., ion flow velocity). (iii) The approach presumes certain distribution function for ions (usually, the shifted Maxwellian distribution)." [63]

The second (ii) point referred to by Fortov is especially important, as "The dynamics of a binary collision is [sic] governed by the interparticle force law" [82] and is reinforced when the momentum exchange analysis in [63] begins with "In this section, we assume the Debye-Hückel (Yukawa) potential around the dust particle".

It is interesting to note that Khrapak et al report that "the standard theory of Coulomb scattering usually fails for the ion-dust elastic collisions" [87].

2.2.2.2 Linear Kinetic

The Linear Dielectric method (LD) is the other standard approach to calculating ion drag [41]. According to Allen [1] a summary of this method "is to assign a permittivity to the plasma and calculate the force on the charged dust particle due to the non-uniform polarization of the surrounding plasma" [1]. Ivlev et al report that "This approach allows us to take into account ion-neutral collisions self-consistently and also to retrieve the potential distribution around the particle" [88].

---

the scrape-off layer of JET ($n \sim 10^{19} m^{-3}$ and $T_i \sim 100\,\mathrm{eV}$), the De Broglie wavelength of hydrogen ions is $\sim 10^{-12}$m and the inter-particle separation is of the order of 10^{-6}m. A density orders of magnitude higher than solid would be needed for the inter-particle distance to be comparable to the De Broglie wavelength.

Allen reports that the linear dielectric method "assumes that linear theory will suffice, whereas it is known that the underlying basic set of equations is nonlinear" [1]. Ivlev et al report that "the necessary condition for the linear approximation to be used is to have the whole range of interaction with the particle—the screening length—be much larger than the range of strong interaction—the Coulomb radius" [88]. This is because perturbations near the dust grain (closer than the Coulomb radius) are too large and the linear approximation breaks down. Essentially, this would be then the equivalent of having a large Λ in the Coulomb logarithm (introduced in the BC discussion, equation 2.123) and would thus make the LD valid when the small angle interactions are much more important than large-angle deflections (in BC terminology).

The linear dielectric method is a "kinetic approach" [63], where the ion drag is calculated by solving "the Poisson equation coupled to the kinetic equation for ions" to "obtain the self-consistent electrostatic potential around the particle" [63]. Fortov et al also state that this approach is a combination of forces originating in Landau damping and in hydrodynamic effects [63]. Normally, Landau damping refers to the exchange of energy between a wave and a particle (usually electron) distribution. In the case of ion drag, the wave is (introduced by) the movement of the dust grain through the plasma. The exchange of energy between the ions and the "dust grain wave" is what the Landau damping mentioned by Fortov refers to. Similarly, the hydrodynamic effects mentioned by the same author are brought about by the collective behaviour of the ions around the moving dust grain, much like the movement of the particles of a neutral fluid around a neutral body.

The ion drag force, F_{id}, is calculated, in the linear dielectric formalism, as simply:

$$F_{id} = -ZeE_p \tag{2.126}$$

where Ze is the charge on the dust grain and E_p is the polarisation field induced by the dust grain on the flowing plasma [63]. We can see that the linear dielectric calculations are then reduced to finding the polarisation field.

The presence of the dust grain in the flowing plasma induces polarisation [63]. The degree of polarisation depends on some of the properties of the plasma, such as electron and ion susceptibilities (which determine the

permittivity).

The degree of polarisation determines the potential distribution around the dust grain, which determines the electric field that causes the ion drag. The mathematical derivation of the full equation for the ion drag (equation 2.127) goes beyond the scope of this review, but the reader can find descriptions in articles by Ivlev et al [88] and Fortov et al [63]. It is briefly mentioned that the derivation begins with the potential around a small dust grain in a plasma (equation 2.128).

$$F_{id} = -\frac{\imath e^2 Z^2}{\pi} \int_0^{k_{max}} \frac{\mathrm{d}\boldsymbol{k}}{k} \int_{-k}^{k} \frac{k_{\|\mathrm{d}\boldsymbol{k}_\|}}{\epsilon\left(0, \boldsymbol{k}\right)} \tag{2.127}$$

where $\epsilon\left(0, \boldsymbol{k}\right)$ is the plasma permittivity and k and $k_{\|}$ are the wave numbers (in the Fourier decomposition).

The potential at $\boldsymbol{r}$ is given by:

$$\phi\left(\boldsymbol{r}\right) = \int \frac{4\pi Z \exp\left(\imath k r\right)}{k^2 \epsilon\left(-\boldsymbol{k}\boldsymbol{u}, k\right)} \frac{\mathrm{dk}}{\left(2\pi\right)^3} \tag{2.128}$$

where $\phi\left(\boldsymbol{r}\right)$ is the potential at a point located at $\boldsymbol{r}$ with respect to the centre of the dust grain and $\boldsymbol{u}$ is the relative velocity of the dust grain with respect to the plasma.

The plasma permittivity needs to be calculated to find the field. It is of interest to note that this method is not valid near the dust grain, where the linear approximation breaks down.

Allen reports, referring to both the Binary Collision and the Linear Dielectric methods, that "Neither of these two theories includes the charging of the dust particle. This is an ad hoc addition to both theories" [1]. Ivlev et al, in agreement with the comment by Allen, report that a predicted behaviour of the field is "unphysical" and that near the test charge "plasma perturbations are so strong that the linear approach is no longer valid" [88].

Another limitation reported by Ivlev et al is "the situation when $\Lambda \leqslant 1$ (e.g., relatively big particles and/or high plasma density). Then the linear dielectric response formalism is no longer applicable" [88]. The symbol Λ here is the same as in the argument of the Coulomb logarithm. Fortov et al mention that "This approach is applicable provided ions are weakly coupled to the particle" and "often the experimental conditions are such that the linear treatment is not possible" [63].

2.2.2.3 The Control Surface Approach

Allen's motivation in his 2007 paper "was to determine the drag force on a dust particle in a flowing plasma" [1]. Given the several paragraphs Allen dedicates to indicating the "deficiencies of the existing theories", one can presume that these deficiencies played a role in his decision to develop a new approach in calculating the drag force.

Allen makes "use...of a 'control surface', as employed in the subject of fluid mechanics" [1]. Briefly, the control surface approach involves using a surface surrounding the dust grain of interest to make momentum calculations. The difference in the momentum entering and leaving through the surface is used to find the force on the dust grain. The calculations are made simpler by using a surface that is far away from the dust grain, so terms in the calculation can be neglected.

The momentum calculations near the dust grain are complicated by the presence of a strong field and the non-linearities introduced in the flow. The Maxwell stress tensor (MST) is not, for example, negligible. Far away from the dust grain, the MST is negligible and the calculations are correspondingly easier. In the control surface approach, the flow far from the dust grain is used to calculate the momentum lost by the flow. It is reasoned that the lost momentum is gained by the dust grain.

Figure 2.15 illustrates the Control Surface approach. Surface S_1 is a surface very close to the dust grain surface. The momentum flux through S_1 is the same as the momentum flux onto the dust grain. Calculations to find the momentum flux through S_1 would suffer from the same complications as calculations for the dust grain surface (non-linearities and non-negligible MST). Calculations for surface S_2, a surface far from the dust grain, would be simpler, as the MST is negligible and the flow can be approximated as linear, i.e. the perturbation from the dust grain is small. It is important to note that this approximation is not relevant to the fluid model inspired by this work.

The Control Surface approach argues that, given there are no sinks or sources inside the volume between surfaces S_1 and S_2 (shaded in the figure), the momentum flux through each surface will be equal. This then allows the easier calculation for surface S_2 to suffice for finding the momentum flux onto the dust grain.

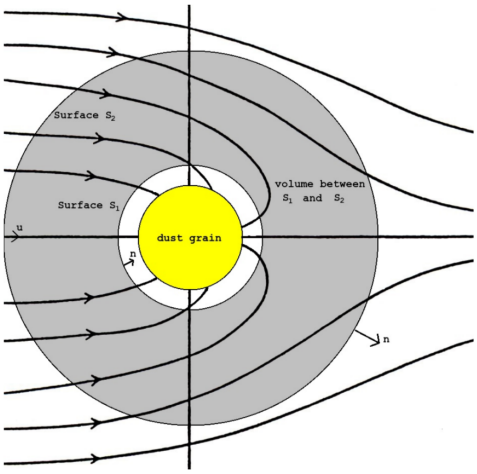

Figure 2.15: Sketch to illustrate the Control surface Approach (modified from a sketch provided by Dr. Michael Coppins).

In our treatment we will be making use of cold ion hydrodynamics. This means the ion temperature will be taken to be zero, which would mean the ion pressure is zero. Such a cold ion model was used by Allen in his control surface approach.

2.3 The Study of Plasma

2.3.1 The Need to Approximate

Plasmas of interest have particle densities ranging from $10^6 - 10^{26}\,m^{-3}$ and volumes ranging from several cubic centimetres to astronomical scales (e.g. solar wind). The Joint European Torus (JET), for example, has a volume of about $100\,m^3$ and plasma particle densities of the order of $10^{19}\,m^{-3}$.

A complete description of the plasma would involve the equation of motion of each particle, which involves finding all the forces acting on each particle due to every other particle. The number of computations scales, therefore, as N^2 (where N =number of particles); given that the number of particles could be upwards of 10^{20}, the memory and time requirements become prohibitive, both in terms of time and of computational resources. We therefore need to approximate.

To demonstrate this, let's assume the use of a "short" (2-byte) number to store the location and velocity of each particle in each direction (x-, y- and

z-) for a $1\,m^3$, $10^{20}\,m^{-3}$ plasma. We would thus need about one zettabyte (10^{21} bytes) of storage. This is of the same order of magnitude as the current capacity of the world to handle data [89]. It also compares with the total global internet traffic, which is only "expected to exceed 1.6 zettabytes" in 2018 [90]. Furthermore, assuming the number of operations to simply be N^2, we would need $= 10^{40}$ calculations for each time-step. As the "energy needed to carry out a floating point operation is in the order of 0.05 to 1 pJ/bit" [90], and assuming 16-bit operations (i.e. consistent with the 2-byte assumption), this means an energy cost of approximately 8×10^{27}J, the equivalent of approximately 100 million times the world electricity production in 2014 [91].

A typical plasma of interest will therefore have a number of particles that is too large to track, which is why we have to find ways to approximate.

This means the study of plasmas has to be limited to models which have to include various degrees of approximation. These models range from kinetic descriptions, such as models originating from the Vlasov and Fokker-Planck equations, to the ideal magnetohydrodynamic (MHD) fluid model. Each one is suitable to use for specific problems, where accuracy needs to be balanced against computational expense. The resource frugality and relative simplicity of fluid models has made them very popular in the study of plasmas. Even the relatively simple ideal MHD model has been used extensively, for example in stability studies.

2.3.1.1 PIC-code Approximation

One approximation that can reduce the number of calculations, if not the storage requirements, is the calculation of a field generated by particle concentrations and use the field instead of the direct particle-particle forces. This idea is used in particle-in-cell (PIC) codes, which are "grid-based Poisson solver[s]" [92]. Harlow introduced this concept in 1955 (see [93, 94]) for hydrodynamic calculations, and it wasn't long before Dawson (e.g. [95]) and others were using PIC codes for studying plasmas. "Particle", in this context, does not necessarily mean a physical particle, like, for example, a plasma ion. "Particle" could, instead, mean a collection of particles, a "super-particle", "each representing many charged particles" [96].

The idea of using a grid is incorporated in this work, as will be seen in

chapter 5.

2.4 Kinetic Treatment of Plasmas

I have already mentioned how, in order to accurately describe a plasma, the position and momentum of each of its constituent particles need to be provided at each moment in time. I have also mentioned how this represents an inordinate amount of information. We can start to reduce this amount of information by grouping particles together. For example, we make the reasonable assumption that all particles of each particle species in a plasma are identical and indistinguishable from each other. We can take this collection of particles into bins a step further and bin particles by position and by momentum. We can then, instead of saying "particle 1 has position $\boldsymbol{x_1}$ and momentum $\boldsymbol{p_1}$ and particle 2 has position $\boldsymbol{x_1}$ and momentum $\boldsymbol{p_1}$", say that "we have 2 particles at position $\boldsymbol{x_1}$ with momentum $\boldsymbol{p_1}$". The probability that we have a particle at an exact position with an exact momentum is 0, so we instead talk of the probability of having particles at an approximate position with an approximate momentum. "Approximate", in this context, means that the position and momentum of the particles lie within an infinitesimally small distance from the position and momentum specified.

The information in such a description is contained in the *probability density function* or the *distribution function*. This is a function that tells us how many particles within a (normally infinitesimally small) cube of physical space have a momentum that lies within a (normally infinitesimally small) cube in momentum space. JC Maxwell, of Maxwell's equations fame, was the first one to use this function in proposition IV of his 1860 paper [97]. It is this distribution function that makes a kinetic treatment so much more useful than following each particle, as it allows for analytic results to be found, despite the fact that the approximations made are miniscule. Therein, however, also lies the weakness of this treatment, namely that for distribution functions that are not easily expressed analytically, a kinetic treatment does not represent a significant improvement in the ease of describing a plasma.

The first use of these ideas were for understanding the behaviour of gases. Vlasov modified the Boltzmann equation to take into account the long-range Coulomb interactions [98], as expressed by electric and magnetic fields, and

ignored collisions. Vlasov's equation is

$$\frac{\partial \mathrm{f}}{\partial \mathrm{t}} + \boldsymbol{v} \cdot \nabla f + \frac{q}{m}\left(\boldsymbol{E} + \frac{\boldsymbol{v}}{c} \times \boldsymbol{B}\right) \cdot \frac{\partial \mathrm{f}}{\partial \boldsymbol{v}} = 0 \tag{2.129}$$

(where f is the distribution function, $\boldsymbol{v}$ is the velocity vector, Z_i is the ion charge in elementary charge units, c is the speed of light, $\boldsymbol{E}$ and $\boldsymbol{B}$ are the electric and magnetic fields respectively), and it does not contain a source or sink term. It is suitable for plasma studies, but does not account for the presence of dust. This is problematic when studying dusty plasmas.

The presence of dust can be accounted by treating the dust grain as a sink, which it, indeed, is. Plasma species incident on the dust grain will be "absorbed" on to it. The dust grain will acquire their charge and they will "disappear" from the plasma. In practice, particles incident on to the dust grain will do one of three things. They will either leave the dust grain, as in the case of very high energy particles that will go through the dust grain, or they will stay in, or on, the dust grain, or they will hit the dust grain, recombine with a particle of another species, and create a neutral. This neutral will either then stay on the dust grain, increasing its mass, or it will leave the dust grain. In the latter two cases, the dust grain has, in effect, acted like a sink, so modelling the dust grain as a sink is reasonable.

A sink can be added in the Vlasov equation by adding a sink term - a term that describes the absorption of particles in the distribution function. The sink term can take many forms, depending on the situation we want to describe.

Solutions to the full Vlasov equation are difficult to calculate, so, very often, approximate solutions are found. One common way to approximate is to linearise. Linearisation assumes that all perturbations are small, so we can ignore second order terms. For example, perturbations to the distribution function can be taken to be

$$f_0(r, v) = F(v) + f(r, v) \tag{2.130}$$

where the distribution function, $f_0(r, v)$ is taken to consist of the unperturbed distribution function, $F(v)$, and a small perturbation, $f(r, v)$, where $f(r, v) \ll F(v)$ (or, similarly, $f(r, v) \ll f_0(r, v)$). This is the approach followed for the work described in later chapters. In fact, this work builds on

the work done by Filippov et al [2].

2.4.1 Vlasov with Sink

We are interested in using kinetic theory for investigating how small dust grains affect the potential in the plasma. Small dust grains are expected to have a small effect, which would justify using linearisation. Filippov et al [2] use a delta function to indicate the presence of a very small dust grain. The "point-sink" model assumes steady-state and modifies the Vlasov equation as follows:

$$\left(\boldsymbol{v}\frac{\partial}{\partial \mathrm{r}} - \frac{e_s}{m_s}\nabla\phi\left(\boldsymbol{r}\right)\frac{\partial}{\partial \boldsymbol{v}}\right) f_s\left(\boldsymbol{r},\boldsymbol{v}\right) \quad = \quad -\delta\left(\boldsymbol{r}\right)\sigma_s\left(v\right)v f_s\left(\boldsymbol{r},\boldsymbol{v}\right) \quad (2.131)$$

where the right hand side of the equation represents the point-sink, the subscript "s" refers to the species we are considering, and σ is the cross-section of the point-sink.

Filippov et al carried through with their calculations and found a result for the potential of a dust grain in the case of no plasma flow. They found that the screening of a dust grain "is generally not described by the linearized [sic] Debye-Hückel theory" [2].

It is perhaps surprising to talk about the cross-section of a point particle. The idea of modelling the particle as a point is useful when conducting calculations involving electric forces originating from the particle. In this respect, a point particle is an acceptable approximation. In reality, the particle also collects particles that intersect its volume, hence adding a cross section actually brings the model closer to the physical reality of the situation modelled.

2.5 Plasmas as Fluids

Plasmas are fluids as they take the shape of their container, they can flow and can be continuously deformed using shear stress. Furthermore, plasmas can and do expand and contract in response to changes in pressure, so they are compressible fluids. They are different and can behave differently to the other two types of fluids, gases and liquids, due to the "collective effects" of electromagnetic forces on them. The study and modelling of plasmas as fluids was one of the first and indeed one of the most successful attempts to

understand them. Alfvén's Nobel Prize for magnetohydrodynamics (MHD), which he first published in 1942 (see [99]) is evidence of this.

Fluid models have been utilised in the study of dusty plasmas, as well, as is evident by a quick survey of the literature, e.g. earlier papers such as Verheest in 1967 [100] to more recent papers such as Shukla and Nosenko in 2011 [101]. All the papers the author found at the beginning of this work dealt with collective effects of many-dust grain systems.

The use of a fluid formalism to investigate the effects on and from an individual dust grain was found in only one paper, namely the 2007 paper by Allen [1] that inspired the pursuit of this work. Also, the models used are rarely if ever, taking into account the compressibility of the plasma. This is a reasonable omission if the plasma and the dust grain(s) within it have a low relative speed. A more accurate picture, especially in the case of relative speeds close to or higher than the speed of sound, is given by incorporating compressibility effects.

2.5.1 Fluid Treatment

To treat plasmas as fluids means we move into a continuum treatment of plasmas. We neglect the individual ions and electrons and assume we have a continuous positive and negative charge presence in space. In liquids and gases we speak of the Knudsen number, which is the ratio of the molecular mean free path (λ_c) and the scale of the volume of interest (L), like the size of a body in the fluid or the size of the domain of interest. For a substance to be treated as continuous, as a fluid, we want the Knudsen number to be much smaller than unity. In other words, we need $\frac{\lambda_c}{L} \ll 1$.

"Mean free path" is the average distance a particle travels between collisions. A small mean free path allows us to treat smaller volumes of the substance of interest as fluid. A lot of plasmas, however, are either so hot or so diffuse that the collision cross sections are very small, which means they can be treated as collisionless, $\lambda_c \to \infty$. This would imply we cannot use a fluid treatment to study these plasmas, yet MHD has been used with great success in the modelling of, for example, tokamak plasmas, which can be considered collisionless.

We will thus continue with our fluid treatment, which I will describe in chapter 4.

3 Background on Computational Fluid Dynamics

Attempting to predict the behaviour of a fluid using numerical calculations is the realm of Computational Fluid Dynamics (CFD). Toro states the definition of CFD as "the science of computing numerical solutions to partial differential or integral equations that are models for fluid flow phenomena" [102] and it is a field generally accepted to have begun in 1917 with L.F. Richardson[1], when he tried to solve partial differential equations describing the weather by hand [102]. CFD is, obviously, necessary when we cannot find analytic results to the problem we are trying to solve.

The first techniques for CFD were actually intended to be useful for human computation, such as, for example, Southwell's 1940 "Relaxation Methods in Engineering Science" [104]. By this time, the scientists that are considered today to have made critical contributions to CFD were becoming active in the field. The small list given by Toro [102] is by no means exhaustive: Von Neumann, Courant, Friedrichs, Richtmyer, Lax, Oleinik, Wendroff, Godunov, Rusanov... and I would add Harlow and his group.

Von Neumann's contribution is particularly important as his work on stability "explained and resolved the difficulties experienced by Richardson" [102] and other researchers in the field. **Stability** is one of two main themes that dominate CFD discussions, the other being **accuracy**. Hirsch [105] mentions three main themes, namely *consistency*, *stability* and *convergence*. By *consistency*, we mean that "the numerical scheme must tend to the differential equation, when time and space steps tend to zero" [105]. By *stability*, we mean ""the error ... has to remain bounded, when the number of time steps n tends to infinity " [105]. By *convergence*, we mean the numerical solution "must tend to the exact solution ... when time and space steps tend

[1] Richardson, FRS and altogether a very fascinating individual, referred to "computer" human workers in his 1922 book titled "Weather Prediction by Numerical Process" [103].

to zero" [105]. We concentrate on just stability and accuracy (consistency), as "stability is the necessary and sufficient condition for convergence" [105].

I will include, here, a short and simple introduction into numerical calculations in general. This will be useful in that it will provide a framework in which to conduct a more immediately relevant discussion later on.

I will quickly note that the basic equation we want to solve is

$$\underbrace{\frac{\partial \dot{\boldsymbol{s}}}{\partial t}}_{A} + \underbrace{\left(\dot{\mathbf{s}} \cdot \nabla\right) \dot{\boldsymbol{s}}}_{B} = \underbrace{-c_s^2 \frac{1}{\rho_n} \nabla \left[\rho_n\right]}_{C} \tag{3.1}$$

where $\boldsymbol{s}$ is the spatial vector, $\dot{\boldsymbol{s}}$ is the velocity vector, c_s is the sound speed and ρ_n is the number density (see sub-section 4.3.1).

We note that this is a quasi-linear, first-order, inhomogeneous hyperbolic equation. For the lay-person, the equation is quasi-linear because we have terms of $\dot{\boldsymbol{s}}$ multiplying a derivative of $\dot{\boldsymbol{s}}$, as in term B; first-order because we only have first derivatives; and inhomogeneous because of the presence of the right-hand side of the equation; It is harder to see that the equation is hyperbolic, but we can infer it from its origin in conservation laws; physically, it has to be hyperbolic, so that the solution involves the transfer of information at finite speed.

3.1 Discretisation

3.1.1 Discretisation - Meaning and Problems

Discretisation is the division of the domain of interest into a set of finite, discrete points. Depending on the fluid method used, these will represent "point values defined at grid points" [102] or "averages over finite volumes" [102]. Discretisation can also be temporal; time is divided into discrete points, as a system can only be evolved, numerically, in discrete time-steps.

There are various problems associated with discretisation and various schemes designed to solve them. The essence of the problems associated with discretisation is that, in jumping forward in discrete, finite steps, we lose information (this is termed a *truncation error*). This loss of information means that we end up with an approximation to the actual evolution of our system. In fact, accuracy, as mentioned earlier, is one of the main issues in a numerical calculation discussion.

Discretisation is just one source of error in using a computer to calculate the solution to a problem (others include the fact we are not using an ideal computer, which introduces errors such as the *round-off* error).

In order to demonstrate discretisation and its problems, in a simple way, we start by the simplest way we can evolve a differential equation, the "Forward Euler" scheme (FE). FE approximates the evolution of a function by assuming its derivative at the beginning of the time step remains constant.

An easy function to use for demonstrating is $\frac{dy}{dx} = -2.2y$, with $y_0 = 1$. The solution of this function is, analytically, $y = e^{-2.2x}$. A graph of this function with its Forward Euler solved approximation using various steps sizes is shown in figure 3.1. The graph demonstrates how the Forward Euler is only an approximation and how the step size affects the accuracy of the approximation quite significantly. The left side of the figure shows how a large step size will result in a function that doesn't even qualitatively resemble the correct one. A step size of 1.0, in this instance, results in an oscillating function that diverges. A step size of 0.5 also behaves differently, with the first step even leading to a negative value. Smaller step sizes (right side of the figure) behave qualitatively similarly to the correct function, but are still inaccurate.

The graph also demonstrates how accuracy is improved by reducing the step size. A small step size leads to a higher number of required steps for a given interval, which means a larger time required for calculations.

The left side of the graph also demonstrates another issue with numerical calculations, namely that of stability. It is evident that FE with a step size of 1.0 for this function is not stable. The notion of stability is one of great importance for numerical calculations, which is why I will talk more about it at various parts of this chapter and why I introduce it before I present any the various schemes.

3.1.2 Stability

This is a good place to introduce stability analysis, one area where von Neumann made significant contributions to CFD. In fact, I will only be introducing the Von Neumann stability analysis and we will look at differencing schemes (such as the Forward Euler), following subsection 20.1.1 of [106]. For this section, superscripts representing an index (spatial) will be

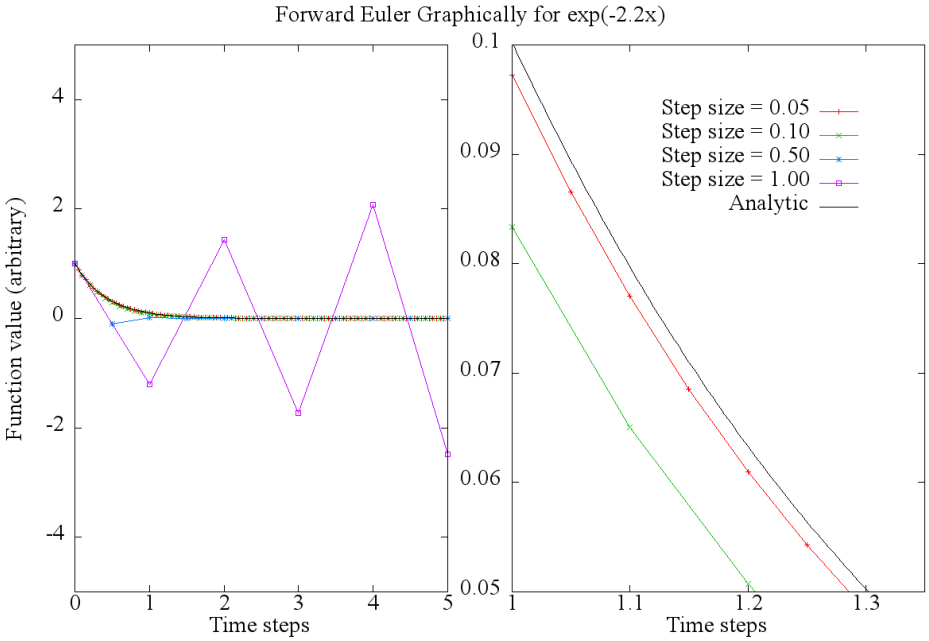

Figure 3.1: Forward Euler Approximations for $y = e^{-2.2x}$.

bracketed - non-bracketed superscripts will have the normal mathematical meaning of exponentiation.

We will be looking at a forward time centered space differencing scheme (a forward Euler scheme)

$$\frac{u_{n+1}^{(k)} - u_n^{(k)}}{\Delta t} = -v\left(\frac{u_n^{(k+1)} - u_n^{(k-1)}}{2\Delta x}\right) \tag{3.2}$$

We begin by assuming that the coefficients of the differencing scheme can be taken to be constant; von Neumann analysis is local [106]. This allows us to find solutions such that

$$u_n^{(k)} = \xi^n e^{\imath k \boldsymbol{q} \Delta x} \tag{3.3}$$

where $\boldsymbol{q}$ is the "real spatial wave number" [106] (often denoted as $\boldsymbol{k}$ in the literature) and ξ is a complex number which is a function of $\boldsymbol{q}^2$. As the successive solutions depend on a power of $\xi(\boldsymbol{q})$, we need $|\xi(\boldsymbol{q})| \leqslant 1$. Substi-

[2]The use of k and $\boldsymbol{k}$ in this context is, perhaps, an example of poor choice in symbols. Unfortunately, the use of $\boldsymbol{k}$ is the standard symbol used in the analysis, and k is often used as a spatial index. Hopefully this note will help the confused reader.

tuting in equation 3.2

$$\xi = 1 - \frac{v\Delta t}{2\Delta x}\left(e^{\imath \boldsymbol{q}\Delta x} - e^{-\imath \boldsymbol{q}\Delta x}\right) \tag{3.4}$$

$$= 1 - \imath\frac{v\Delta t}{\Delta x}\sin\left(\boldsymbol{q}\Delta x\right) \tag{3.5}$$

The magnitude of ξ is then larger than 1, so this scheme is unconditionally unstable.

This kind of analysis can be used to establish whether a numerical scheme is stable and under what conditions.

3.1.3 Forward Euler

As mentioned already, FE is the easiest scheme, but also very dependent on the step size. FE is convenient in the context of this work for introducing some more technical jargon; jargon that will be useful for describing and understanding more elaborate schemes.

Formally, FE is a *first-order explicit* scheme. A scheme is *first order* if the *global truncation error* (the total error at any given time) is proportional to the step size or the *local truncation error* (the error after one step) is proportional to the square of the step size. A scheme is *explicit* if the value at the end of the calculation depends only on already known quantities, i.e. we do not need the value of the quantity at the end of the step to calculate it.

Deriving FE will serve to demonstrate both that it is explicit and first order.

Consider a function $y\left(x\right)$ and take the Taylor expansion around x_0 (at a distance of h):

$$y\left(x_0 + h\right) = y\left(x_0\right) + hy'\left(x_0\right) + \mathcal{O}\left(h^2\right) \tag{3.6}$$

which is the Euler method. Notice that the error is proportional to the square of the step size (*local truncation error*), indicating this is a first order method. Also, notice that the right-hand side (RHS) of the equation only includes terms evaluated at x_0, indicating this is an explicit method.

FE is convenient for introducing the framework within which numerical stability can be discussed. There are various types of stabilities discussed in

a numerical context, most notable of which are *A-stability* and *L-stability*.

Let's see why (or how) FE can be unstable before discussing the two types of stability mentioned. We can use the example from figure 3.1, where we have $y'(x) = C_1 y(x)$, with $C_1 = -2.2$. Using this in equation 3.6, we get

$$\begin{aligned} y(x_0 + h) &= y(x_0) + hy'(x_0) + \mathcal{O}\left(h^2\right) \\ &= y(x_0) + hC_1 y(x_0) + \mathcal{O}\left(h^2\right) \quad (3.7) \\ &= y(x_0)[1 + hC_1] \quad (3.8) \end{aligned}$$

where we dropped the Big-O notation. For the general case, y_{n+1}, we would get

$$\begin{aligned} y_{n+1} &= y_n[1 + hC_1] \quad (3.9) \\ y_n &= y_{n-1}[1 + hC_1] \quad (3.10) \\ y_{n+1} &= y_0[1 + hC_1]^{n+1} \quad (3.11) \\ &= y_0[\phi(hC_1)]^{n+1} \quad (3.12) \\ &= y_0\phi(z)^{n+1} \quad (3.13) \end{aligned}$$

This, keeping in mind that the analytic result is $y_n = e^{C_1 x}$, will diverge for values of $|1 + hC_1| \geq 1$.

We thus have a very specific range of stability for the step size, h, depending on the value of C_1. In figure 3.1, this is indicated by the curve for step size 1.0. A numerical method that "passes" this test, i.e. it does not diverge when used for equations of the form $y' = C_1 y$, is termed to be *A-stable*. More formally, the method has to converge for all values of $hC_1 < 0$ to be termed A-stable. It can be seen that FE is not A-stable.

L-stability has even more strict criteria. A method has to be both A-stable and have $\phi(z) \to 0$ as $z \to \infty$ to be L-stable. This can better be demonstrated using the Backwards Euler scheme (BE).

Most sources in the literature that mention FE (e.g. [106]) seem to agree that FE is "not recommended for practical use", owing to what is described as low accuracy and low stability. FE is the simplest numerical scheme to implement, but suffers from stability issues.

3.1.4 Backwards Euler

BE is the "backwards" version of FE. This means it uses information from the end of the step to calculate the value at the end of the step. This makes BE an *implicit* method (contrast this with FE, which is *explicit*). BE, like FE, is first-order.

$$y(x_0 + h) = y(x_0) + hy'(x_0 + h) + \mathcal{O}\left(h^2\right) \tag{3.14}$$

$$y_{n+1} = y_n + hy'_{n+1} \tag{3.15}$$

The question naturally arises, how can information from the end of the step be used to conduct calculations during the step? Let's see how this would work with our example function, $y' = -2.2y$.

$$\begin{aligned} y_{n+1} &= y_n + hy'_{n+1} \\ &= y_n - h2.2y_{n+1} && (3.16) \\ y_{n+1} + 2.2hy_{n+1} &= y_n && (3.17) \\ y_{n+1} &= \frac{y_n}{(1 + 2.2h)} && (3.18) \end{aligned}$$

The results for various step sizes are shown in figure 3.2.

The big advantage of implicit schemes, like BE, is that they are stable. This allows for larger step sizes, although this will always be at the expense of accuracy. It is easy to see that BE is stable, as shown in figure 3.2. Even the largest step size in the figure (left side) behaves qualitatively correct, with no oscillations. It is also evident that large step sizes sacrifice accuracy.

Allowing the step size, h, to grow leads to a smaller and smaller value for y_{n+1}, i.e. $y_{n+1} \to 0$ as $h \to \infty$. As explained earlier, this makes BE an L-stable method.

The need to use information from the end of the step makes this a more computationally demanding scheme (although this is not evident in the simple example function used here), but this is often a price worth paying for the stability afforded by implicit schemes.

3.1.5 Runge-Kutta

Both FE and BE are conceptually easy methods to derive and understand. They are both, however, first-order, which means they are considered not

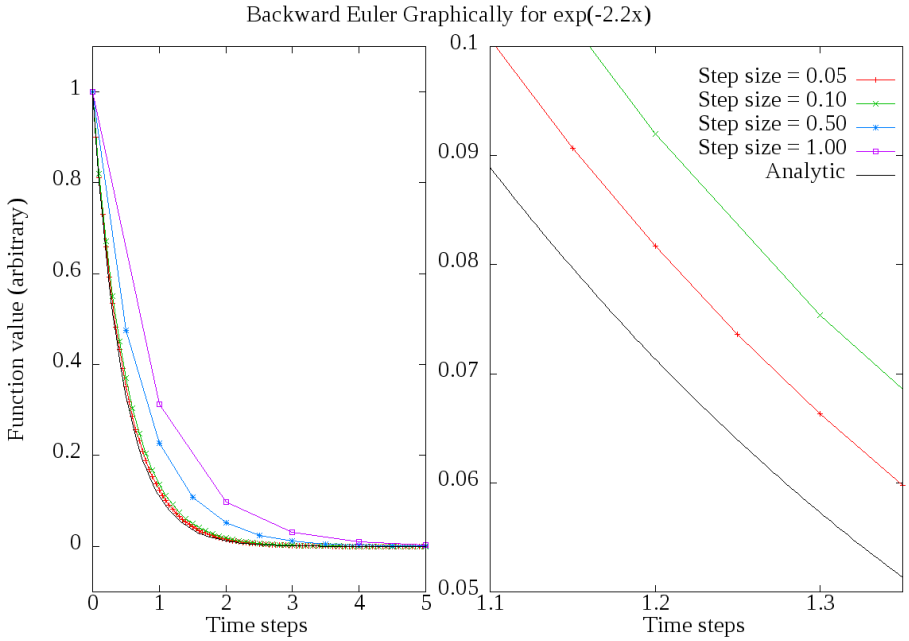

Figure 3.2: Backward Euler Approximations for $y = e^{-2.2x}$.

to be very accurate (as the error per step is proportional to the square of the step size). This is why more elaborate schemes have been devised. A family of these is the Runge-Kutta (RK) family of schemes, which include explicit and implicit methods. The "workhorse" of scientific numerical work is considered to be the RK4 scheme ([106]), which is a fourth order explicit scheme.

FE and BE are both considered to belong to the RK family. Both FE and BE are asymmetrical, in that they take the derivative of the function at the edge of the step. Higher order RK schemes try to address this asymmetry by using the derivative at points within the step. For example, the midpoint method, a second-order RK scheme, takes one trial half-step to find the derivative at the midpoint of the step. This is subsequently used instead of the derivative at the beginning (or end) of the step.

Using Taylor expansion at the middle of the step, we get the midpoint method:

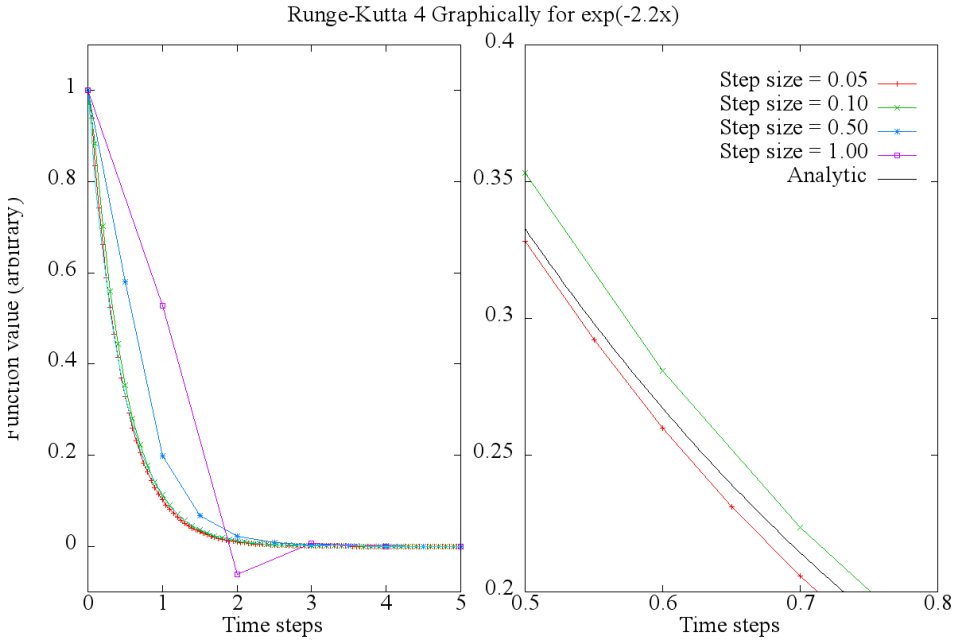

Figure 3.3: Runge-Kutta 4 approximations for $y = e^{-2.2x}$.

$$
\begin{aligned}
y\left(x_0 + h\right) &= y\left(x_0 + h/2\right) + \frac{h}{2} y'\left(x_0 + h/2\right) + \frac{h^2}{4} y''\left(x_0 + h/2\right) \\
&\quad + \mathcal{O}\left(h^3\right) && (3.19) \\
y\left(x_0\right) &= y\left(x_0 + h/2\right) - \frac{h}{2} y'\left(x_0 + h/2\right) + \frac{h^2}{4} y''\left(x_0 + h/2\right) + \\
&\quad \mathcal{O}\left(h^3\right) && (3.20) \\
y\left(x_0 + h\right) - y\left(x_0\right) &= h y'\left(x_0 + h/2\right) + \mathcal{O}\left(h^3\right) && (3.21) \\
y\left(x_0 + h\right) &= y\left(x_0\right) + h y'\left(x_0 + h/2\right) + \mathcal{O}\left(h^3\right) && (3.22)
\end{aligned}
$$

This is now a two step-method, as we need $y'\left(x_0 + h/2\right)$ which we get an estimate for using a half-step FE. The prize for the added step, however, is the increase in the order of the scheme, which, more often than not, offers greater accuracy and the ability to take larger steps.

Using combinations of different ways to calculate y' allows for error terms to cancel out, increasing the order of the scheme. RK4 uses this idea to

achieve fourth order and is calculated as follows:

$$
\begin{aligned}
y_{n+1} &= y_n + \frac{h}{6}\left(a + 2b + 2c + d\right) && (3.23)\\
a &= y'\left(x_0, y_n\right) && (3.24)\\
b &= y'\left(x_0 + \frac{h}{2}, y_n + a\frac{h}{2}\right) && (3.25)\\
c &= y'\left(x_0 + \frac{h}{2}, y_n + b\frac{h}{2}\right) && (3.26)\\
d &= y'\left(x_0 + h, y_n + ch\right) && (3.27)
\end{aligned}
$$

The results for various step sizes are shown in figure 3.3.

The main point to remember about accuracy and order is that, even though higher order does usually mean higher accuracy, this not always the case (see, for example, [106], chapter 17, which includes a highly developed horse analogy).

3.1.6 Lax and Friedrichs

This is another first order scheme, that is more stable than Euler. It becomes more stable simply by replacing the current cell values in the time derivative by the average of the cells surrounding it.

An example will clarify what is meant by this. We use an equation of the form $\frac{\partial u}{\partial t} + a\frac{\partial u}{\partial x} = 0$, for which Euler is unconditionally unstable. We will use a subscript as a time index and a superscript as a space index. The letter "n" will symbolise the current time and the letter "k" will symbolise the current position, $u_n^k = u_{time\,n}^{location\,k}$.

The Euler scheme, using a second order central approximation would then be

$$
\begin{aligned}
\frac{\partial u}{\partial t} &= -a\frac{\partial u}{\partial x} && (3.28)\\
\frac{u_{n+1}^k - u_n^k}{\Delta t} &= -a\frac{u_n^{k+1} - u_n^{k-1}}{2\Delta x} && (3.29)\\
u_{n+1}^k &= u_n^k - \Delta t a\frac{u_n^{k+1} - u_n^{k-1}}{2\Delta x} && (3.30)
\end{aligned}
$$

We use a trial solution $u_n^k = A_n \exp\left(\imath x\theta\right)$ to check the stability, as shown

by Toro in [102] (section 5.1, page 167). We substitute into 3.30

$$\begin{aligned} A^{n+1}\exp(\imath k\theta) &= A^n\exp(\imath k\theta) - \\ &\quad \Delta ta\frac{A^n\exp(\imath(k+1)\theta) - A^n\exp(\imath(k-1)\theta)}{2\Delta x} \end{aligned} \tag{3.31}$$

$$A = 1 - \Delta ta\frac{\exp(\imath\theta) - \exp(-\imath\theta)}{2\Delta x} \tag{3.32}$$

$$A = 1 - \frac{\Delta ta}{\Delta x}\imath\sin(\theta) \tag{3.33}$$

which has a magnitude of $|A| = 1 + \left(\frac{\Delta ta}{\Delta x}\sin(\theta)\right)^2 \geqslant 1$, which imply a non-converging solution, i.e. an unconditionally unstable scheme. Changing the current cell values in the time derivative, as mentioned, we have

$$u_{n+1}^k = \frac{1}{2}\left(u_n^{k+1} + u_n^{k-1}\right) - \Delta ta\frac{u_n^{k+1} - u_n^{k-1}}{2\Delta x} \tag{3.34}$$

We use the trial solution[3] as before

$$\begin{aligned} A^{n+1}\exp(\imath k\theta) &= \frac{1}{2}\left(A^n\exp(\imath(k+1)\theta) + A^n\exp(\imath(k-1)\theta)\right) - \\ &\quad \Delta ta\frac{A^n\exp(\imath(k+1)\theta) - A^n\exp(\imath(k-1)\theta)}{2\Delta x} \end{aligned} \tag{3.35}$$

$$\begin{aligned} A &= \frac{1}{2}\exp(\imath\theta)\left(1 - \frac{\Delta ta}{\Delta x}\right) + \\ &\quad \frac{1}{2}\exp(-\imath\theta)\left(1 + \frac{\Delta ta}{\Delta x}\right) \end{aligned} \tag{3.36}$$

$$= \cos(\theta) - \frac{\Delta ta}{\Delta x}\imath\sin(\theta) \tag{3.37}$$

$$|A| = \cos^2(\theta) + \left(\frac{\Delta ta}{\Delta x}\right)^2\sin^2(\theta) \tag{3.38}$$

The amplitude is then $|A| \leqslant 1$ for $0 \leqslant \frac{\Delta ta}{\Delta x} \leqslant 1$, which gives us the stability criterion for the Lax-Friedrich scheme.

Lax-Friedrichs is the method used in HADES to produce the results presented in this work (see chapter 6).

Lax-Friedrichs is a diffusive scheme, which makes this a good place to introduce the concept of numerical diffusion.

[3] Strictly speaking, we are entering a trial function for the error in the calculation. For more detail on stability analysis, see subsection 3.1.2.

3.1.6.1 Numerical Diffusion

A lot of numerical schemes introduce effects that are not present in the original model they are trying to model. One such effect often present is numerical diffusion. As the name suggests, this is diffusion that comes as a result of the numerical scheme. Looking at the example of the Lax-Friedrichs method, we have

$$u_{n+1}^k = \frac{1}{2}\left(u_n^{k+1} + u_n^{k-1}\right) - \Delta t a \frac{u_n^{k+1} - u_n^{k-1}}{2\Delta x} \tag{3.39}$$

We manipulate the left-hand side so it resembles the Euler method (forward time centered space, or FTCS)

$$\begin{aligned}
\frac{u_{n+1}^k - u_n^k}{\Delta t} &= \frac{1}{2\Delta t}\left(u_n^{k+1} + u_n^{k-1}\right) - a\frac{u_n^{k+1} - u_n^{k-1}}{2\Delta x} - \frac{u_n^k}{\Delta t} && (3.40)\\
&= -a\frac{u_n^{k+1} - u_n^{k-1}}{2\Delta x} + \frac{1}{2\Delta t}\left(u_n^{k+1} - 2u_n^k + u_n^{k-1}\right) && (3.41)\\
&= -a\frac{u_n^{k+1} - u_n^{k-1}}{2\Delta x} + \frac{1}{2\Delta t}\left[\left(u_n^{k+1} - u_n^k\right) - \left(u_n^k - u_n^{k-1}\right)\right] && (3.42)\\
&= -a\frac{u_n^{k+1} - u_n^{k-1}}{2\Delta x} + \frac{\Delta x}{2\Delta t}\left[\frac{\left(u_n^{k+1} - u_n^k\right)}{\Delta x} - \frac{\left(u_n^k - u_n^{k-1}\right)}{\Delta x}\right] && (3.43)\\
&= -a\frac{u_n^{k+1} - u_n^{k-1}}{2\Delta x} + \frac{(\Delta x)^2}{2\Delta t}\left[\frac{\frac{\left(u_n^{k+1} - u_n^k\right)}{\Delta x} - \frac{\left(u_n^k - u_n^{k-1}\right)}{\Delta x}}{\Delta x}\right] && (3.44)
\end{aligned}$$

This resembles the FTCS method for the equation

$$\frac{\partial u}{\partial t} = -a\frac{\partial u}{\partial x} + \frac{(\Delta x)^2}{2\Delta t}\frac{\partial^2 u}{\partial x^2} \tag{3.45}$$

We can see there is an extra term to the intended equation, namely $\frac{(\Delta x)^2}{2\Delta t}\frac{\partial^2 u}{\partial x^2}$, which is a diffusion term. The Lax-Friedrichs method is thus a diffusive method (it adds "numerical dissipation, or numerical viscosity" [106]).

We demonstrate this pictorially here, but delegate more rigorous treatment to the abundant literature on Stability.

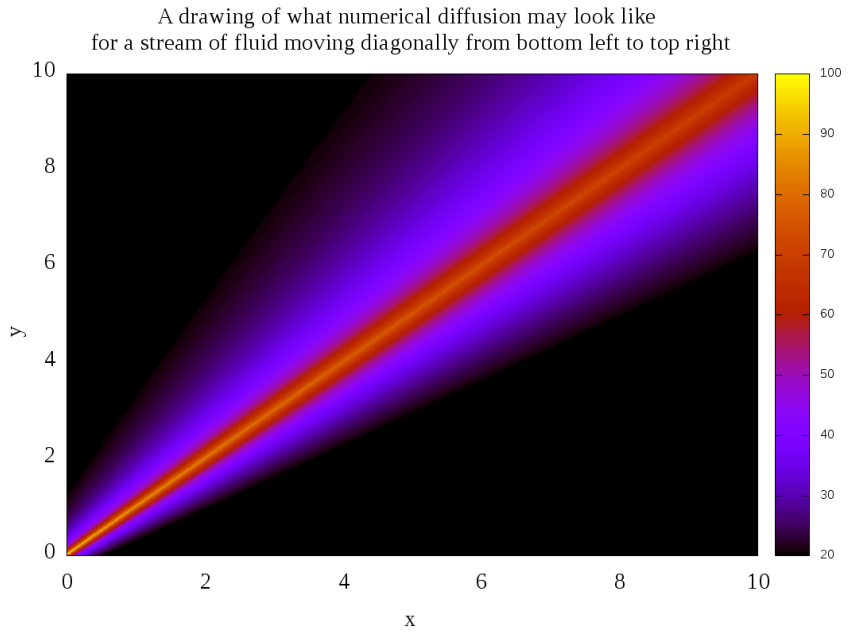

Figure 3.4: A pictoral example of numerical diffusion.

A pictorial example of numerical diffusion is shown in figure 3.4.

3.1.7 Staggered Leapfrog

This is a second-order method in both space and time. It involves calculating the time and space quantities at different index values. To clarify, in equation form we have

$$\frac{u_{n+1}^{k} - u_{n-1}^{k}}{2\Delta t} = -a\frac{u_{n}^{k+1} - u_{n}^{k-1}}{2\Delta x} \tag{3.46}$$

where we note that the differencing in time happens at position k and does not involve values from time n, whereas the differencing in space happens at time n and does not involve values from position k. This method is not stable for non-linear equations, suffering from the mesh-drifting instability, where adjacent cells decouple, creating a checker-board effect that can be overcome by adding numerical viscosity [106].

3.1.8 Crank-Nicholson

Crank-Nicholson is an unconditionally stable scheme of second order, in both time and space. It combines the explicit and implicit FTCS. The

implicit scheme is similar to the explicit scheme, but the spatial derivative is calculated at the advance time (n+1). The explicit scheme is

$$u_{n+1}^{k} = u_{n}^{k} - a\frac{\Delta t}{2\Delta x}\left(u_{n}^{k+1} - u_{n}^{k-1}\right) \tag{3.47}$$

and the implicit scheme is

$$u_{n+1}^{k} = u_{n}^{k} - a\frac{\Delta t}{2\Delta x}\left(u_{n+1}^{k+1} - u_{n+1}^{k-1}\right) \tag{3.48}$$

The Crank-Nicholson scheme combines the two, such that

$$u_{n+1}^{k} = u_{n}^{k} - \frac{a}{2}\frac{\Delta t}{2\Delta x}\left[\left(u_{n}^{k+1} - u_{n}^{k-1}\right) + \left(u_{n+1}^{k+1} - u_{n+1}^{k-1}\right)\right] \tag{3.49}$$

The implicit scheme is harder to calculate, owing to the fact that the values for the spatial derivative are not available at the start of the calculation. In the case of a non-linear problem, such as the one we are interested in, the system of equations required to be solved for the advanced time quantities becomes very expensive computationally.

Crank-Nicholson can be used for non-linear systems when it is deemed acceptable to linearise.

3.1.9 The Piecewise Parabolic Method

The Piecewise Parabolic Method (PPM) is "a standard method for compressible fluids" [107], "probably the "most influential" generalisation of Godunov's approach, the latter being "potentially [the] most powerful method" [106] for handling shocks. Godunov's approach is to simplify the problem by breaking down the function into local piecewise constant functions [108]. This basically means that we have constant functions in each cell, but a discontinuity at each cell boundary. The piecewise-constant functions and the discontinuity at cell boundaries then constitute a Reimann problem, which can be solved (locally).

This method is definitely a method to be investigated in future work, when more time is available to work with HADES, as it seems to be a preferred method in a lot of existing codes.

3.1.10 Accuracy

It is easier to discuss the accuracy of a numerical scheme by looking at what it actually solves and compare it to what it purports to solve. We call the actual solved equation the ***modified (equivalent) differential equation***.

We will demonstrate this with a simple equation of the form

$$\frac{\partial u}{\partial t} + a\frac{\partial u}{\partial x} = 0 \tag{3.50}$$

, before we apply it to equation 3.1. Let's assume a first-order-in-time, second-order-in-space discretisation such that:

$$\frac{u_{n+1}^k - u_n^k}{\Delta t} + \frac{a}{2}\frac{u_n^{k+1} - u_n^{k-1}}{\Delta x} = 0 \tag{3.51}$$

We also note that the Taylor expansions in time and space are:

$$u_{n+1}^k = u_n^k + \Delta t\frac{\partial u_n^k}{\partial t} + \frac{(\Delta t)^2}{2}\frac{\partial^2 u_n^k}{\partial t^2} + \frac{(\Delta t)^3}{6}\frac{\partial^3 u_n^k}{\partial t^3} + \mathcal{O}\left(\Delta t^4\right) \tag{3.52}$$

$$u_n^{k+1} = u_n^k + \Delta x\frac{\partial u_n^k}{\partial x} + \frac{(\Delta x)^2}{2}\frac{\partial^2 u_n^k}{\partial x^2} + \frac{(\Delta x)^3}{6}\frac{\partial^3 u_n^k}{\partial x^3} + \mathcal{O}\left(\Delta x^4\right) \tag{3.53}$$

$$u_n^{k-1} = u_n^k - \Delta x\frac{\partial u_n^k}{\partial x} + \frac{(\Delta x)^2}{2}\frac{\partial^2 u_n^k}{\partial x^2} - \frac{(\Delta x)^3}{6}\frac{\partial^3 u_n^k}{\partial x^3} + \mathcal{O}\left(\Delta x^4\right) \tag{3.54}$$

Substituting into 3.51, we get

$$\begin{aligned}\frac{u_{n+1}^k - u_n^k}{\Delta t} + \frac{a}{2}\frac{u_n^{k+1} - u_n^{k-1}}{\Delta x} &= \frac{\partial u_n^k}{\partial t} + \frac{(\Delta t)}{2}\frac{\partial^2 u_n^k}{\partial t^2} + \frac{(\Delta t)^2}{6}\frac{\partial^3 u_n^k}{\partial t^3} + \mathcal{O}\left(\Delta t^3\right) + \\ &\quad a\frac{\partial u_n^k}{\partial x} + a\frac{(\Delta x)^2}{6}\frac{\partial^3 u_n^k}{\partial x^3} + \mathcal{O}\left(\Delta x^3\right)\end{aligned} \tag{3.55}$$

$$\underbrace{\frac{u_{n+1}^k - u_n^k}{\Delta t} + \frac{a}{2}\frac{u_n^{k+1} - u_n^{k-1}}{\Delta x}}_{A} - \underbrace{\left(\frac{\partial u_n^k}{\partial t} + a\frac{\partial u_n^k}{\partial x}\right)}_{B} = \underbrace{\frac{(\Delta t)}{2}\frac{\partial^2 u_n^k}{\partial t^2} + a\frac{(\Delta x)^2}{6}\frac{\partial^3 u_n^k}{\partial x^3} + \mathcal{O}\left(\Delta t^2, \Delta x^4\right)}_{C} \tag{3.56}$$

Term B in equation 3.56 is the equation we are trying to model, however (equation 3.50), which implies that the right-hand side is the difference between our intended equation and the actual discretised result. The right-hand side is, then, the *truncation error*. We can use equation 3.50 to substitute the time derivative on the right-hand side with a space derivative.

$$\frac{\partial u}{\partial t} = -a\frac{\partial u}{\partial x} \tag{3.57}$$

$$\frac{\partial^2 u}{\partial t^2} = -a\frac{\partial}{\partial x}\left(-a\frac{\partial u}{\partial x}\right) \tag{3.58}$$

$$= a^2\frac{\partial^2 u}{\partial x^2} \tag{3.59}$$

so that we get

$$\frac{u_{n+1}^k - u_n^k}{\Delta t} + \frac{a}{2}\frac{u_n^{k+1} - u_n^{k-1}}{\Delta x} - \left(\frac{\partial u_n^k}{\partial t} + a\frac{\partial u_n^k}{\partial x}\right) = \frac{(\Delta t)}{2}a^2\frac{\partial^2 u_n^k}{\partial x^2} + a\frac{(\Delta x)^2}{6}\frac{\partial^3 u_n^k}{\partial x^3} + \mathcal{O}\left(\Delta t^2, \Delta x^4\right) \tag{3.60}$$

If we wanted to recover the original differential equation, we would need to subtract the truncation error. Alternatively, the discretised equation is modelling a differential equation that includes the truncation error, so that

$$\frac{\partial u}{\partial t} + a\frac{\partial u}{\partial x} = -\frac{(\Delta t)}{2}a^2\frac{\partial^2 u_n^k}{\partial x^2} + \mathcal{O}\left(\Delta t^2, \Delta x^2\right) \tag{3.61}$$

Equation 3.61, where we have retained only the lowest order terms, is the ***modified (equivalent) differential equation*** for equation 3.50. The right-hand side represents a numerical diffusion/viscosity term which makes this scheme unstable - "a positive viscosity is known to damp oscillations... a negative viscosity... will amplify exponentially any disturbance" [105].

4 Large Dust Grains

> *"The rabbit-hole went straight on like a tunnel for some way, and then dipped suddenly down, so suddenly that Alice had not a moment to think about stopping herself before she found herself falling down a very deep well."*
>
> Lewis Carroll, *Alice's Adventures in Wonderland*

The quote is not meant to represent an anthropomorphic view of an ion meeting a dust grain, though I expect the ion does "experience" something very similar. Instead, it is meant to represent my experience in deciding to study large dust grains in a plasma using a fluid formalism. The decision to use such a formalism and use a numerical solution led me down the rabbit hole of computational fluid dynamics, fluid solvers and discretisation. The weary reader will be relieved to know that this chapter will be less about the journey and more about the destination.

Before embarking on the details of the method, let us highlight what makes the physics of large dust grains unique and the use of a fluid model possible.

4.1 The Physics of Large Dust Grains

The meaning of "large" in the context of this work has already been introduced; "large" means (much) larger than the Debye length, i.e. $L \gg \lambda_D$. At the scale lengths of a large dust radius, the sheath that is formed around the dust grain is well defined; the sheath is a volume where quasi-neutrality breaks down, so it will be of the order of the shielding length of the plasma, i.e. of the order of the Debye length.

Understanding the dust grain behaviour hinges on understanding the ion and electron currents onto it. We need to calculate, in other words, the ion and electron currents onto the dust grain, originating from the bulk

plasma and travelling through the sheath. Trying to model the plasma and the sheath is extremely difficult, as they are quite different: their scale lengths are very different (at a ratio of the order of $\frac{\lambda_D}{L} \ll 1$) and the physics dominating their structure is very different, as one is quasineutral, with small electric fields, and the other is not quasi-neutral and has strong electric fields. Calculating the trajectory of ions and establishing whether they intersect the dust grain, and are therefore collected, is thus very challenging.

For large dust grains, the sheath is small, compared with the dust grain, like a thin shell around the dust grain. This is not a trivial point. A thin shell allows us to use approximations that lead to significant simplifications in our modelling. The most powerful simplification, and one that introduces a very small approximation, is to assume that any ions entering the sheath will hit the dust grain surface. This allows us to simplify the problem by allowing us to ignore the physics inside the sheath. This approximation allows us to say that the ion and electron currents onto the sheath are the same as the ion and electron currents onto the dust grain, ignoring what happens in the sheath.

A thin, well-defined sheath allows us, therefore, to concentrate on modelling just the quasi-neutral part of the fluid, simultaneously doing away with the sheath scale lengths. In the words of Langmuir "We shall use the name plasma to describe this region containing balanced charges of ions and electrons" [20]. It is the goal, here, then, to develop a model for the quasi-neutral plasma; a model simple enough to have tractable and solvable equations. The model will not be complicated enough to be applicable in the sheath, but this is fine for studying large dust grains in a plasma, as the dust grain edge can be approximated to be at the sheath edge.

4.2 Fluid Formalism

We will not be interested in the microscopic details of the fluid, the motion of individual ions and electrons; instead we will be looking at the macroscopic quantities and how they evolve. Using this method is evidently unsuitable for studying phenomena which happen on the microscopic scale.

The model we will be using is not applicable to studying small dust grains in a plasma. A small dust grain resides within a Debye sphere, where its immediate environment is no longer a plasma, as it is no longer quasi-neutral.

Its sheath is large compared to its radius and a significant number of ions entering the sheath are not necessarily collected by the dust grain. A model that does not include the sheath will therefore not be able to make predictions on the ion and electron currents onto the dust grain.

A large dust grain, however, has a well-developed sheath which is smaller than its radius. The dust grain and its "sheath shell" are surrounded by a quasi-neutral pre-sheath that accelerates ions towards the ion-sheath system. Because we are considering large dust grains, it is a very good approximation that any ions entering the sheath will impact the dust grain. It is possible, then, to treat the sheath edge as the dust grain edge, when we are calculating the current on to the dust grain.

This makes a quasi-neutral fluid approach for a large dust grain possible, as the fluid approach would be valid in the quasi-neutral plasma, but would break down in the sheath.

The model we will be using is simplified further, using what were deemed to be reasonable assumptions for the cases we want to use the model for.

4.2.1 The Model

We will treat the ions and the electrons as separate fluids with some simplifying assumptions regarding their properties. These will be reasonable approximations, keeping the relevance of the model to real plasmas. Some key assumptions are as follows.

We will assume cold ions, which means we are ignoring the thermal speed of the ions. There are a lot of plasmas where the thermal speed of the ions can be ignored, even though it is not zero, like for example arc discharges. This allows us to ignore the ion pressure term, as will be seen shortly, which is one ingredient that allows for a beautiful union of the two fluids (the ion and the electron fluids) into one set of equations. This approximation does lead to significant simplifications, but comes at a significant cost, as to the applicability of the model to real-world plasmas. This is one simplification that can be eliminated in future work.

We will assume isothermal electrons, which means we are interested in effects that are long compared to electron time scales (i.e. electrons have time to come to thermal equilibrium). As we are looking at effects that involve ions, this is not a very restrictive approximation. It does allow us to

eliminate temperature changes from any pressure calculations, which makes the calculations simpler. Crucially, it also allows us to use the Boltzmann relation to calculate the potential from the density.

We assume that there are no external magnetic fields. Magnetic fields would introduce an extra factor in calculating the electromagnetic forces on the fluids and are an unnecessary complication for this first version of the model.

4.2.1.1 A Complete List of the Assumptions for the Model

Our assumptions are:

1. The first assumption, which has already been stated, is that of a thin sheath, i.e. we can treat the sheath edge as the dust grain edge. The main effect of this, as explained, is that we need only worry about the quasi-neutral part of the domain. We can thus assume quasi-neutrality. Further, we will concentrate on plasmas where the ions are singly-charged, so that

$$n_i = n_e \tag{4.1}$$

   This does not limit us to hydrogen plasmas, as plasmas of other elements are usually singly charged as well.
   As explained, this assumption makes our model only applicable in the quasi-neutral plasma, and by extension, only useful in the study of large dust grains. This is fine, as large dust grains do occur and are of importance in most plasmas of interest.

2. We will concentrate on plasmas with just one ion species and treat the ions and the electrons as fluids.

   a) The equation for the conservation of momentum for each fluid is

$$\frac{\partial \left([n_s m_s \dot{\boldsymbol{s}}] \right)}{\partial t} + \nabla \cdot \left([n_s m_s \dot{\boldsymbol{s}}] \, \dot{\boldsymbol{s}} \right) = \boldsymbol{F}_{total} \tag{4.2}$$

   where $\boldsymbol{F}_{total}$ is the total force, m_s is the mass of a particle in each species, n_s is the particle density for the species and $\dot{\boldsymbol{s}}$ is the velocity.

b) The equation for the conservation of mass for each fluid is

$$\frac{\partial\left([n_s m_s]\right)}{\partial t} + \nabla \cdot \left([n_s m_s]\,\dot{\boldsymbol{s}}\right) = 0 \tag{4.3}$$

c) The forces on each fluid particle are

$$\boldsymbol{F}_{total} = \boldsymbol{F}_{collisions} + \boldsymbol{F}_{pressure} + \boldsymbol{F}_{electromagnetic} \tag{4.4}$$

3. Ions are cold, i.e. $T_i = 0$. This means that:

   a) There is no ion pressure, as $p_i = n_i k_B T_i$ (where p_i is the ion pressure, n_i is the ion density, k_B is Boltzmann's constant). Hence, for ions, $F_{pressure} = 0$.

   b) We can ignore viscosity. Viscosity is mainly due to ions (because they carry most of the momentum) and their diffusion. Cold ions will not diffuse between fluid layers, which means viscosity is zero.

4. The electron fluid is isothermal ($T_e = constant$). In other words, we are only interested in time-scales larger than the the time it takes for electrons to come to thermal equilibrium. By extension, electron pressure changes only occur when the electron density changes, $\nabla p_e = k_B T_e \nabla n_e$. This allows us to use the electron density in the Boltzmann relation for the potential, Φ

$$\Phi = -\frac{k_B T_e}{e} \ln\left(\frac{n}{n_0}\right) \tag{4.5}$$

   Electron pressure, unlike ion pressure, is thus not assumed to be zero.

5. No magnetic fields. This simplifies the Lorentz factor when calculating the forces acting on the fluid, i.e. $F_{electromagnetic} = F_{electric} = neE$

6. The plasma is collisionless, so $F_{collisions} = 0$. This can be explained by the cold ions assumption.

7. The mass of the electrons is negligible compared to the mass of the ions. We can thus ignore electron inertia and approximate the plasma velocity with the ion fluid velocity.

4.2.2 Model Validity

The set of assumptions we make dictate where the model will be valid.

In practice, cold ions means ions much colder than the electrons. Arc or glow discharges are two examples of plasmas with ions much colder than electrons, as are fluorescent lamps. These are plasmas that can be considered non-collisional, as well, indicating that our model would be valid in, at least, these two types of plasmas.

The model begins to become less valid in plasmas where our assumptions cannot be justified. For plasmas, for example, where the ion temnperature cannot be neglected,the ion pressure cannot be neglected and hence would need to be added to the model. Magnetic fields would similarly need to be taken into account, as they would affect the isotropy of the problem and would introduce a Lorentz force. The assumption of isothermal electrons would be invalid for effects that are fast compared to the time for temperature equilibrium to be achieved. A significant reformulation of the model would be needed, for example, to model shocks in a plasma.

4.3 Mathematical Formulation

We now incorporate the assumptions we make in the equations for the conservation of mass and momentum.

For ions, the equation of conservation of momentum becomes

$$\frac{\partial\left(\left[n_s m_s \dot{\boldsymbol{s}}\right]\right)}{\partial t} + \nabla \cdot \left(\left[n_s m_s \dot{\boldsymbol{s}}\right] \dot{\boldsymbol{s}}\right) = neE \tag{4.6}$$

and the equation for conservation of mass remains unchanged.

For electrons, the equation of conservation of momentum becomes

$$0 = -\nabla p_e - neE \tag{4.7}$$

Integrating and using our assumption of isothermal electrons, we get the Boltzmann relation

$$n = n_0 e^{-\mathrm{e}\Phi/\mathrm{k_B T_e}} \tag{4.8}$$

The electric field, E, is the same for the ions and the electrons, hence we

can substitute for neE in the ion conservation of momentum with

$$neE = -\nabla p_e \tag{4.9}$$

such that

$$\begin{aligned}
\frac{\partial\left([nm_i\dot{\boldsymbol{s}}]\right)}{\partial t} + \nabla\cdot\left([nm_i\dot{\boldsymbol{s}}]\,\dot{\boldsymbol{s}}\right) &= -\nabla p_e && (4.10)\\
\frac{\partial\left([nm_i\dot{\boldsymbol{s}}]\right)}{\partial t} + \nabla\cdot\left([nm_i\dot{\boldsymbol{s}}]\,\dot{\boldsymbol{s}}\right) &= -k_B T_e\nabla n && (4.11)\\
\frac{\partial\left([n\dot{\boldsymbol{s}}]\right)}{\partial t} + \nabla\cdot\left([n\dot{\boldsymbol{s}}]\,\dot{\boldsymbol{s}}\right) &= -\frac{k_B T_e}{m_i}\nabla n && (4.12)
\end{aligned}$$

The last step introduces the sound speed on the right-hand side, $c_s = \sqrt{\frac{k_B T_e}{m_i}}$. We note that the sound speed has no T_i dependence and does not include the ratio of specific heats (see 4.3.1.3).

$$\frac{\partial\left(n\dot{\boldsymbol{s}}\right)}{\partial t} + \nabla\cdot\left([n\dot{\boldsymbol{s}}]\,\dot{\boldsymbol{s}}\right) = -c_s^2\nabla n \tag{4.13}$$

We remind ourselves of the assumption that the electron mass can be ignored, which means the equation of conservation of mass for the ions can be used for the equation of conservation of mass for the whole plasma

$$\begin{aligned}
\frac{\partial\left([nm_i]\right)}{\partial t} + \nabla\cdot\left([nm_i]\,\dot{\boldsymbol{s}}\right) &= 0 && (4.14)\\
\frac{\partial\left([n]\right)}{\partial t} + \nabla\cdot\left([n]\,\dot{\boldsymbol{s}}\right) &= 0 && (4.15)
\end{aligned}$$

The two fluid model has thus been reduced to one compressible fluid, with the key equations being

$$\frac{\partial\left(n\dot{\boldsymbol{s}}\right)}{\partial t} + \nabla\cdot\left([n\dot{\boldsymbol{s}}]\,\dot{\boldsymbol{s}}\right) = -c_s^2\nabla n \tag{4.16}$$

and

$$\frac{\partial\left([n]\right)}{\partial t} + \nabla\cdot\left([n]\,\dot{\boldsymbol{s}}\right) = 0 \tag{4.17}$$

We are interested in the evolution of density and velocity of the plasma, so we expand accordingly.

4.3.1 Equations for Density and Velocity

We expand the equation of conservation of momentum, such that

$$\begin{aligned}[n]\frac{\partial([\dot{\boldsymbol{s}}])}{\partial t}+[\dot{\boldsymbol{s}}]\frac{\partial([n])}{\partial t}+\\ [\dot{\boldsymbol{s}}]\nabla\cdot(n\dot{\boldsymbol{s}})+([n]\,\dot{\boldsymbol{s}}\cdot\nabla)([\dot{\boldsymbol{s}}]) &= -c_s^2\nabla n \end{aligned} \tag{4.18}$$

We subsequently substitute using the equation of conservation of mass, $\frac{\partial([n])}{\partial t}=-\nabla\cdot([n]\,\dot{\boldsymbol{s}})$, so

$$\begin{aligned}[n]\frac{\partial([\dot{\boldsymbol{s}}])}{\partial t}-[\dot{\boldsymbol{s}}]\nabla\cdot([n]\,\dot{\boldsymbol{s}})+\\ [\dot{\boldsymbol{s}}]\nabla\cdot([n]\,\dot{\boldsymbol{s}})+[n]\,(\dot{\boldsymbol{s}}\cdot\nabla)([\dot{\boldsymbol{s}}]) &= -c_s^2\nabla n \end{aligned} \tag{4.19}$$

which gives

$$[n]\frac{\partial([\dot{\boldsymbol{s}}])}{\partial t}+[n]\,(\dot{\boldsymbol{s}}\cdot\nabla)([\dot{\boldsymbol{s}}]) = -c_s^2\nabla n \tag{4.20}$$

$$[n]\frac{\partial([\dot{\boldsymbol{s}}])}{\partial t} = -c_s^2\nabla n-[n]\,(\dot{\boldsymbol{s}}\cdot\nabla)([\dot{\boldsymbol{s}}]) \tag{4.21}$$

Dividing by the density

$$\frac{\partial([\dot{\boldsymbol{s}}])}{\partial t} = -\frac{c_s^2}{n}\nabla n-(\dot{\boldsymbol{s}}\cdot\nabla)([\dot{\boldsymbol{s}}]) \tag{4.22}$$

This means that the equations we need to solve are

The equation for velocity

$$\frac{\partial(\dot{\boldsymbol{s}})}{\partial t}=-\frac{c_s^2}{n}\nabla n-(\dot{\boldsymbol{s}}\cdot\nabla)(\dot{\boldsymbol{s}}) \tag{4.23}$$

and the equation for density

$$\frac{\partial(n)}{\partial t}=-n\nabla\cdot\dot{\boldsymbol{s}}-(\dot{\boldsymbol{s}}\cdot\nabla)\,n \tag{4.24}$$

4.3.1.1 Comments

The equations derived are interesting. For example, we note that density only appears as a ratio with density gradient, indicating that the absolute density does not affect the evolution of the velocity. We expect to have identical graphs when plotting for plasmas of different densities for otherwise

identical situations. This is indeed what we see, as shown in chapter 6.

4.3.1.2 Novelty

This model is novel. Treating the plasma as continuous has been done before, as has been studying plasmas by treating them as single fluids. The union of the two fluid into one to study the details of the interaction of dust grains with their surrounding plasma is, however, relatively new. This model builds on the work of Allen [1], who mentioned this fluid approach first. The model changes the focus, however, to the quasi-neutral assumption and the ability to model the plasma all the way up to the sheath edge, which is taken to be the same as the dust edge.

The model allows for the calculation of the evolution of macroscopic quantities, such as density and flow velocity, around a dust grain in a relatively easy way. This is made possible by the simplifying assumptions. The assumptions do restrict the applicability of the model, but retain its relevance to some real-world plasmas, such as low-temperature plasmas (owing to the cold ion assumption). The model can be used as a basis from which models with less assumptions can be built, albeit at the expense of more complexity.

4.3.1.3 Similarity to Compressible Hydrodynamics

The Navier-Stokes (NS) equation for inviscid compressible fluids quoted in the literature (see, for example, [109]) is

$$\rho\left(\frac{\partial \dot{\boldsymbol{s}}}{\partial t}+\left(\dot{\boldsymbol{s}}\cdot\nabla\right)\dot{\boldsymbol{s}}\right) \quad = \quad \rho f-\nabla p \tag{4.25}$$

where f is the total "volume force" on the fluid particle and p is the pressure.

We compare this with our equation, which is

$$n\left(\frac{\partial\left(\dot{\boldsymbol{s}}\right)}{\partial t}+\left(\dot{\boldsymbol{s}}\cdot\nabla\right)\dot{\boldsymbol{s}}\right)=-c_s^2\nabla n \tag{4.26}$$

and note the similarities. The left hand side is identical, with the particle density, n corresponding to the mass density, ρ. The right hand side has two terms in the NS equation, the pressure term in the Navier -Stokes equation corresponding to the right-hand side term in the fluid model equation.

The first term in the NS equation, the volume force, does not exist in

our model, reflecting that we neglect all volume forces. It is this term that is different to standard formulations (and solutions) of compressible hydrodynamics, which justifies pursuing our own solution and not a commercial compressible fluid dynamics package[1].

The similarities are not surprising. Indeed, we are treating the ions as a fluid, we have not imposed incompressibility and have followed a similar path as in the traditional derivation for Navier-Stokes (e.g. starting with the equations of conservation of momentum and mass). We also make the same assumption of inviscid flow, which simplifies the pressure term. It is these similarities which lead Allen to pursue the control surface approach used in fluid mechanics for studying dust grains in plasmas [1].

We note also the differences, such as the absence of the ion temperature, T_i, in the sound speed in our mode, due to the cold ion assumption. Also, our isothermal assumption is different to the usual adiabatic assumption, which means we avoid the need for the ratio of specific heats, γ.

4.3.2 Equations to Discretise

We now have the equations we need to solve in order to find "potential, plasma velocity and plasma density" around the dust grain. Before we proceed, we need to expand the equations so that they are for the individual components of velocity, using u, v and w for the x, y and z components of velocity respectively.

[1] Other reasons include that a PhD is, in addition to a research endeavour, an educational endeavour as well and that there is more pleasure in deriving a solution to a problem compared to quoting one.

We thus have

$$\frac{\partial(u)}{\partial t} = -\frac{c_s^2}{n}\left(\frac{\partial n}{\partial x}\right) - \left(u\frac{\partial u}{\partial x} + v\frac{\partial u}{\partial y} + w\frac{\partial u}{\partial z}\right) \tag{4.27}$$

$$\frac{\partial(v)}{\partial t} = -\frac{c_s^2}{n}\left(\frac{\partial n}{\partial y}\right) - \left(u\frac{\partial v}{\partial x} + v\frac{\partial v}{\partial y} + w\frac{\partial v}{\partial z}\right) \tag{4.28}$$

$$\frac{\partial(w)}{\partial t} = -\frac{c_s^2}{n}\left(\frac{\partial n}{\partial z}\right) - \left(u\frac{\partial w}{\partial x} + v\frac{\partial w}{\partial y} + w\frac{\partial w}{\partial z}\right) \tag{4.29}$$

$$\frac{\partial(n)}{\partial t} = -n\left(\frac{\partial u}{\partial x} + \frac{\partial v}{\partial y} + \frac{\partial w}{\partial z}\right) - \left(u\frac{\partial n}{\partial x} + v\frac{\partial n}{\partial y} + w\frac{\partial n}{\partial z}\right) \tag{4.30}$$

4.3.3 Normalisation

Before discretisation, we normalise the quantities used. We normalise velocity by the speed of sound, such that

$$u = \mu c_s \tag{4.31}$$

$$v = \beta c_s \tag{4.32}$$

$$w = \omega c_s \tag{4.33}$$

where c_s is the speed of sound in the fluid. We also normalise all distances by the Debye length, such that

$$x = \chi \lambda_{De} \tag{4.34}$$

$$y = \psi \lambda_{De} \tag{4.35}$$

$$z = \zeta \lambda_{De} \tag{4.36}$$

and similarly with the differentials in each direction. The normalisation in distances means the density is also normalised, such that

$$n = \rho \lambda_{De}^3 \tag{4.37}$$

The final normalisation is that of time. The normalisation is chosen for us, by the choice of normalisation for speed and length. To keep the equations

simple, we need to choose

$$t = T\frac{Length\,Normalisation}{Speed\,Normalisation} \tag{4.38}$$

$$= T\frac{\lambda_{De}}{c_s} \tag{4.39}$$

The obvious quantity to normalise time with is the (inverse of) the plasma frequency (ω_p). As we are concentrating on the ion response, we want the ion plasma frequency, ω_{pi}. This is consistent with our case, as

$$t = T\frac{\lambda_{De}}{c_s} \tag{4.40}$$

$$= \frac{T}{\omega_{pi}} \tag{4.41}$$

and, indeed

$$t = \frac{T}{\omega_p}\sqrt{\frac{m_i}{m_e}} \tag{4.42}$$

We therefore have

$$\frac{\partial(\mu)}{\partial T} = -\frac{1}{\rho}\left(\frac{\partial\rho}{\partial\chi}\right) - \left(\mu\frac{\partial\mu}{\partial\chi} + \beta\frac{\partial\mu}{\partial\psi} + \omega\frac{\partial\mu}{\partial\zeta}\right) \tag{4.43}$$

$$\frac{\partial(\beta)}{\partial T} = -\frac{1}{\rho}\left(\frac{\partial\rho}{\partial\psi}\right) - \left(\mu\frac{\partial\beta}{\partial\chi} + \beta\frac{\partial\beta}{\partial\psi} + \omega\frac{\partial\beta}{\partial\zeta}\right) \tag{4.44}$$

$$\frac{\partial(\omega)}{\partial T} = -\frac{1}{\rho}\left(\frac{\partial\rho}{\partial\zeta}\right) - \left(\mu\frac{\partial\omega}{\partial\chi} + \beta\frac{\partial\omega}{\partial\psi} + \omega\frac{\partial\omega}{\partial\zeta}\right) \tag{4.45}$$

$$\frac{\partial(\rho)}{\partial T} = -\rho\left(\frac{\partial\mu}{\partial\chi} + \frac{\partial\beta}{\partial\psi} + \frac{\partial\omega}{\partial\zeta}\right) - \left(\mu\frac{\partial\rho}{\partial\chi} + \beta\frac{\partial\rho}{\partial\psi} + \omega\frac{\partial\rho}{\partial\zeta}\right) \tag{4.46}$$

These are the final equations of the model, which need to be solved. These are the equations that need to be discretised, by whichever discretisation scheme is chosen, and solved by HADES.

5 Discretisation and HADES

5.1 OOP

The choice of programming paradigm for HADES was Object Oriented Programming (OOP). The main reason for this is to allow for a logical breakdown of the problem into smaller parts, which would make building HADES conceptually simpler, while simultaneously allowing for easier maintenance and future extension.

Briefly, OOP attempts to identify the important entities in what is being simulated and base the simulation on describing these entities (the "objects") and their interaction. This means, for example, that we treat the grid on which we save the data for the simulation as an object. We build a "class"[1] for each "object" we are interested; each class describes what the object is, by describing what data the object holds and what actions the object can do. A class for a grid, to continue our earlier example, will create objects that hold data like the number of cells in the grid, the size for each cell and actions like returning a value of a chosen quantity from a specific cell or changing the value of that quantity at a specific cell.

OOP also allows what is termed "data hiding", which means each object in the simulation cannot accidentally change data it should not have access to. This reduces the possibility for mistakes ("data corruption").

OOP allows "inheritance". Inheritance is the ability to create classes that "inherit" from other classes. In HADES, I used inheritance to simplify the grid class. I started by building a grid class with very basic functionality and then I used inheritance to successively build more and more powerful grid classes, which included all the functionality I deemed necessary for HADES. The testing of functionality from parent to successive children classes meant faster development, as a smaller number of methods needed to be tested for each child class.

[1] "class" as in "a class of objects" rather than "a History class"

5.2 Structure

HADES is structured around a main file, which creates the various objects necessary to carry out the calculations required to evolve the system. The objects are created by classes that were built to correspond to the various objects that the whole calculation was broken down into.

5.2.1 Required Objects

There are more than one ways to break down a calculation of this type. I have chosen to break it down as follows.

The first class to be called in HADES is a class that creates an object which takes care of parallelising the code, allowing for the calculation to be done on many processors. This object initialises the Message Passing Interface library (MPI) and holds the parallelisation information, such as the number of processors and the identity of each processor.

The second class to be called in HADES is a class for creating an object which accepts and validates the input parameters for each run. This object holds the choices made for the parameters chosen for each run, such as the plasma density and the plasma flow velocity, among others. It also does a basic validation of the input parameters, such as checking that the grid size requested for simulations that are started with results from past simulations is the same size as the grid size in the past simulations.

The third class called is a class for calculating and storing input quantities derived from the input parameters, such as the normalised version of the input parameters for density.

We can subsequently begin setting up the simulation. We begin with a class for creating a grid. This is the grid on which the approximations for the flow of the fluid are saved. Only one object is created from this class. This is the object for the grid of the simulation. This object can store the dimensions of the grid, the size of the cells in each of the three spatial dimensions, and the value of each quantity we choose to save at each cell position. The object provides "methods" for changing the value of each quantity for each cell, retrieving the value of each quantity at each cell, calculating the gradient of a chosen quantity at each cell, as well as taking care of parallelisation issues, such as the sharing of cell values at the boundaries between the domain handled by different processors.

The grid class also provided the methods for evolving the grid. The decision to incorporate the solver within the grid class was influenced by the ability to use inheritance. The grid class used for evolving the system was essentially a solver class that inherited from the previous grid classes. The decision was also influenced by the fact that the plasma evolves solely under the action of forces contained within it.

The second class called to set up the simulation is the object that divides and allocates the grid to each processor. The parallelisation for HADES has been chosen to be done by dividing up the domain into sub-domains; each sub-domain is handled by a different processor. The class implements one and three dimensional parallelisation.

By this stage, the simulation is set-up with the plasma related parameters, so we can introduce the dust grain(s). The class for creating dust grain objects is therefore called next. At the moment, the class can create any number of spherical dust grains.

We then use the class for creating the object which will be responsible for saving the results of the code - the "reporter" object.

5.3 Work Flow and Algorithms

5.3.1 Fluid Evolution

I will first give a one-paragraph summary of how HADES evolves the fluid, and then I will clarify in more detail.

HADES breaks down the domain into a cuboid honeycomb (i.e. it fills up the space with cuboids without leaving any gaps - see figure 5.1). Each cuboid, or cell, is fixed in space, and represents the spatial discretisation we have had to do, due to out inability to follow the fluid at all places. The required fluid quantities are saved for the centre of each cell. These are the current and previous densities, and the current and previous fluid velocities in each direction.

The numerical method used (Lax-Friedrichs) only needs these quantities to evolve the velocities and density, which, in turn, are the quantities needed by us. These quantities are, in fact two of the three quantities we are aiming to find. The third, the potential, will need to be found by an appropriate

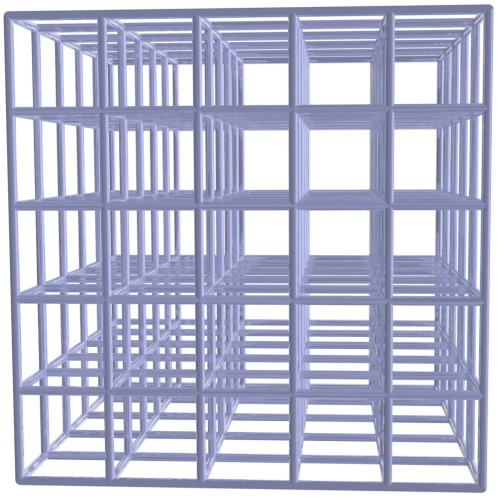

Figure 5.1: A cube honeycomb.

interpretation of the density[2].

Here is an expanded explanation.

5.3.1.1 Initialisation

Having divided the domain up into our cuboid cells, each cell is assigned a density and a fluid velocity in each direction. These are quantities that have been calculated for the centre of the cell, using the user defined initial conditions (see figure 5.2).

The initialisation involves converting all quantities to simulation quantities applicable to each cell. For example, density is converted from m^{-3} to λ_D^{-3}, speed is measured in Mach units and distances in λ_D (where λ_D is the Debye length, defined as $\lambda_D = \sqrt{\frac{\epsilon_0 k_B T_e}{n_0 e^2}}$, ϵ_0, permittivity of free space, k_B, Boltzmann's constant, T_e, electron temperature, n_0, electron density, e, elementary charge).

5.3.1.2 Evolution Loop

HADES begins each calculation step by updating the "previous" fluid quantities with the "current" fluid quantities. In other words, what was $n+1$ in

[2]Quasi-neutrality means the electron density can be found when we know the ion density. We can then use the Boltzmann relationship to find the potential.

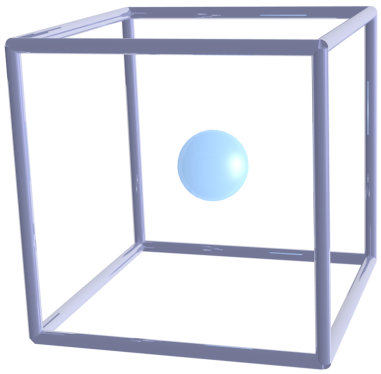

Figure 5.2: The quantities calculated are for the centre of each cell (light blue sphere).

the previous calculation, is saved as n, making space for the new $n+1$. In practice, this is done by swapping the current and previous fluid quantities before the calculation loop. The area where the "previous" quantities are stored will thus contain the n time data. The area holding the "current" data (what will be $n+1$) contains the $n-1$ data, which we can freely write over.

HADES then loops from cell to cell, using the previous fluid quantities to calculate and save the current fluid quantities.

5.3.1.3 Dust

In HADES we have the option to place an arbitrary number of dust grains at arbitrary locations. The current version of HADES only includes a module for spherical dust grains, but modules for other shapes can easily be used instead. The "placement" of dust means that the cells in the domain which would be within the dust are kept at a fixed, pre-determined, state. What this means is that the quantities stored for these cells are kept constant. The primary quantity to determine the behaviour of the fluid around the dust is the density of the cells that are "within" the dust.

5.3.1.4 Output

HADES can save to file for subsequent analysis any of the quantities involved in the calculations.

5.4 Discretisation

HADES can only deal with discretised equations and can only be as good as the discretisation scheme used. Here we discuss the discretisation used.

We use i, j, k as superscripts acting as space indices (in the x, y and z direction respectively) and l as a subscript acting as a time index for all discretisation schemes[3]. Where a generic space index is required (i.e. where i, j, k need to be substituted) we use h. For example, the density of the cell at the current position in all directions would be $\rho_l^{i,j,k}$ and the density of the cell to the right in the x-direction would be $\rho_l^{i+1,j,k}$.

5.4.1 Lax-Friedrichs Scheme

5.4.1.1 Scheme Summary

The method judged to be a good compromise between simplicity and suitability to the problem was the Lax-Friedrichs method. We therefore have

$$\frac{\dot{\mathbf{s}}_{l+1}^h - \frac{1}{2}\left(\dot{\mathbf{s}}_l^{h+1} + \dot{\mathbf{s}}_l^{h-1}\right)}{\Delta T} = -\frac{1}{\rho_l^h}\frac{\left(\rho_l^{h+1} - \rho_l^{h-1}\right)}{2\Delta \boldsymbol{r}} - \dot{\mathbf{s}} \cdot \frac{\left(\dot{\mathbf{s}}_l^{h+1} - \dot{\mathbf{s}}_l^{h-1}\right)}{2\Delta \boldsymbol{r}} \tag{5.1}$$

[3] The discretisation attempt started with lofty ambitions of what the numerical scheme to be used would be like. The scope of this work forces me to use a basic discretisation scheme and reserve the deployment of the as-of-yet unfinished more sophisticated discretisation schemes to future work.

which means that we have

$$\dot{\mathbf{s}}_{l+1}^{h} = \frac{1}{2}\left(\dot{\mathbf{s}}_{l}^{h+1} + \dot{\mathbf{s}}_{l}^{h-1}\right) - \Delta T\left(\frac{1}{\rho_{l}^{h}}\frac{\left(\rho_{l}^{h+1} - \rho_{l}^{h-1}\right)}{2\Delta \boldsymbol{r}} + \dot{\mathbf{s}} \cdot \frac{\left(\dot{\mathbf{s}}_{l}^{h+1} - \dot{\mathbf{s}}_{l}^{h-1}\right)}{2\Delta \boldsymbol{r}}\right) \tag{5.2}$$

Lax's method requires that the Courant-Friedrichs-Lewy (Courant) condition be met. In general, this states that

$$|u|\,\frac{\Delta t}{\Delta x} \leqslant 1 \tag{5.3}$$

and likewise in each direction.

Similarly, for the density, we have

$$\frac{\rho_{l+1}^{h} - \frac{1}{2}\left(\rho_{l}^{h+1} + \rho_{l}^{h-1}\right)}{\Delta T} = -\rho_{l}^{h}\frac{1}{2\Delta \boldsymbol{r}} \cdot \left(\dot{\mathbf{s}}_{l+1}^{h+1} - \dot{\mathbf{s}}_{l+1}^{h-1}\right) - \dot{\boldsymbol{s}}_{l+1}^{h} \cdot \frac{\rho_{l}^{h+1} - \rho_{l}^{h-1}}{2\Delta \boldsymbol{r}} \tag{5.4}$$

where we note the use of the forward in time $\dot{\boldsymbol{s}}_{l+1}^{h}$ on the right-hand side of the equation. This is not part of the standard Lax-Friedrichs method, making this a variation of the standard implementation.

5.4.1.2 Lax-Friedrichs Suitability

The Lax-Friedrichs method has a second-order accuracy in space, but only first-order accuracy in time. It is also fairly dissipative and is normally used more as a building block for more elaborate methods. It is however stable, if the Courant-Friedrichs-Lewy condition is met, and can therefore be used for preliminary results. In building HADES, I needed a stable yet simple method to test the overall program, which is why the second method to implement (after Euler, which was used for the very early testing of the code) was the Lax-Friedrichs method. As it turned out, due to time considerations, Lax-Friedrichs is the only method suitable for the problem at hand that is, at the time of writing, fully implemented. The results reported are therefore produced using this method, which means we need to keep in mind that dissipation is present in the results.

The testing and evolution road-map for HADES includes an implementation of Lax-Wendroff before proceeding with Godunov type methods, such as the piecewise parabolic method (PPM), and finishing with the originally intended method, which is being developed for HADES (and which, at the time of writing, is very unstable).

5.4.1.3 Discretised Equations Used

The equations are separated in each direction to conduct the simulation, so I will demonstrate in full the discretisation done in the code. For clarity, I will omit prefixes that are for the current position, such that $n_l^{i+1,j,k} \rightarrow n_l^{i+1}$.

We will deviate from the Lax scheme in one respect, namely we will use the average of all six adjacent cells to replace $\dot{\boldsymbol{s}}_l^h$ in the time derivative. Specifically, and using density as an example, instead of using

$$\frac{\rho_{l+1} - \frac{1}{2}\left(\rho_l^{k+1} + \rho_l^{k-1}\right)}{\Delta T} = ... \tag{5.5}$$

we will use

$$\frac{\rho_{l+1} - \frac{1}{6}\left(\rho_l^{i+1} + \rho_l^{i-1} + \rho_l^{j+1} + \rho_l^{j-1} + \rho_l^{k+1} + \rho_l^{k-1}\right)}{\Delta T} = ... \tag{5.6}$$

We have, in the x-direction

$$\begin{aligned}\frac{\mu_{l+1} - \frac{1}{6}\left(\mu_l^{i+1} + \mu_l^{i-1} + \mu_l^{j+1} + \mu_l^{j-1} + \mu_l^{k+1} + \mu_l^{k-1}\right)}{\Delta T} \quad = \\ -\frac{1}{\rho_l}\left(\frac{\rho_l^{i+1} - \rho_l^{i-1}}{2\Delta\chi}\right) - \\ \left(\mu_l \frac{\mu_l^{i+1} - \mu_l^{i-1}}{2\Delta\chi} + \beta_l \frac{\mu_l^{j+1} - \mu_l^{j-1}}{2\Delta\psi} + \omega_l \frac{\mu_l^{k+1} - \mu_l^{k-1}}{2\Delta\zeta}\right)\end{aligned} \tag{5.7}$$

Similarly, in the y-direction

$$\frac{\beta_{l+1} - \frac{1}{6}\left(\beta_l^{i+1} + \beta_l^{i-1} + \beta_l^{j+1} + \beta_l^{j-1} + \beta_l^{k+1} + \beta_l^{k-1}\right)}{\Delta T} = -\frac{1}{\rho_l}\left(\frac{\rho_l^{j+1} - \rho_l^{j-1}}{2\Delta\psi}\right) - \left(\mu_l \frac{\beta_l^{i+1} - \beta_l^{i-1}}{2\Delta\chi} + \beta_l \frac{\beta_l^{j+1} - \beta_l^{j-1}}{2\Delta\psi} + \omega_l \frac{\beta_l^{k+1} - \beta_l^{k-1}}{2\Delta\zeta}\right) \tag{5.8}$$

and in the z-direction

$$\frac{\omega_{l+1} - \frac{1}{6}\left(\omega_l^{i+1} + \omega_l^{i-1} + \omega_l^{j+1} + \omega_l^{j-1} + \omega_l^{k+1} + \omega_l^{k-1}\right)}{\Delta T} = -\frac{1}{\rho_l}\left(\frac{\rho_l^{k+1} - \rho_l^{k-1}}{2\Delta\zeta}\right) - \left(\mu_l \frac{\omega_l^{i+1} - \omega_l^{i-1}}{2\Delta\chi} + \beta_l \frac{\omega_l^{j+1} - \omega_l^{j-1}}{2\Delta\psi} + \omega_l \frac{\omega_l^{k+1} - \omega_l^{k-1}}{2\Delta\zeta}\right) \tag{5.9}$$

We finish with the equation for density

$$\frac{\rho_{l+1} - \frac{1}{6}\left(\rho_l^{i+1} + \rho_l^{i-1} + \rho_l^{j+1} + \rho_l^{j-1} + \rho_l^{k+1} + \rho_l^{k-1}\right)}{\Delta T} = -\rho_l\left(\frac{\mu_{l+1}^{i+1} - \mu_{l+1}^{i-1}}{2\Delta\chi} + \frac{\beta_{l+1}^{j+1} - \beta_{l+1}^{j-1}}{2\Delta\psi} + \frac{\omega_{l+1}^{k+1} - \omega_{l+1}^{k-1}}{2\Delta\zeta}\right) - \left(\mu_{l+1} \frac{\rho_l^{i+1} - \rho_l^{i-1}}{2\Delta\chi} + \beta_{l+1} \frac{\rho_l^{j+1} - \rho_l^{j-1}}{2\Delta\psi} + \omega_{l+1} \frac{\rho_l^{k+1} - \rho_l^{k-1}}{2\Delta\zeta}\right) \tag{5.10}$$

These are the final versions of the equations for solving the equations we want using the Lax-Friedrichs method. We would now need HADES to solve them in three-dimensions if it wasn't for another issue that needs discussing.

5.5 Boundary Conditions, or The Strength of the Sink

It has been established that the quantities we are interested in, the density of the plasma around the dust grain and the fluid velocity, and their evolution are determined by the density and its gradient, the fluid flow and its gradient, and the speed of sound. We can set up HADES with all cells in the domain set at the background values for density and fluid velocity. This raises the question, however, of what to do at the boundaries of the domain and the boundary between any dust grain and the plasma.

The boundary to the domain is conceptually the easy one of the two to choose. We are modelling one (or more) dust grain in an infinite plasma. The boundaries should be the horizon to that plasma. We therefore set our ghost cells[4] to be at the background values and force them to stay there. This can potentially create problems if the gradient becomes very steep between the final cells of the domain and the ghost cells. It turned out not to be a problem in our simulations, possibly because Lax-Friedrichs is highly dissipative.

The boundary between the dust grain and the plasma (strictly speaking, between the sheath edge and the plasma) is more problematic. Conceptually, any ion reaching the dust grain (or the sheath edge) is absorbed ("disappears") and no ions enter the plasma from the dust grain. This can be achieved by setting the density inside the dust grain at a suitably lower value than the value of the density in the cells touching the dust grain. The question is, then, what is the correct value? The lower the value chosen, the stronger the pull on the plasma fluid into the dust grain. We would like the model to produce the potential at the sheath edge as an output, rather than using the result from theory as an input.

My initial feeling is that the choice of density inside the dust grain should be zero[5]. The cells surrounding the dust grain should, in other words, be "facing" a vacuum. The reasoning is as follows. The potential on the dust grain should depend on its size, the geometry of the problem (spherical in our case) and on the plasma background values and not on the make-up of the

[4] These are the cells forming a shell around the domain. They are used for calculating what goes in and out of the domain and calculating the values for the cells at the edge of the domain, but they are not used for the final results.

[5] Similar to a penalisation method.

dust grain. In other words, the boundary between the domain and the ghost cells and the dust radius. The density inside the dust grain, then, should be as low as possible, but not low enough that it could lead to unphysical results in the domain. An obvious unphysical result when it comes to density is a negative value. I would therefore be hesitant to have a negative value inside the dust grain. The density should be as low as possible, to allow the background plasma values and the geometry to determine the shape of the density. Otherwise, we would be limiting the density to higher values artificially.

Having said this, it is the intent to explore the effect of changing the value of density inside the dust grain in future work. Most of the results in this work have been produced at the first step of this exploration, with the density set at about a quarter of the background density. For convenience, figures 5.3a and 5.3b are included here; they show, for 2 different flow speeds, the difference between setting the density inside the dust grain at two different values, zero density, and about half background density. Figure 5.4 is a comparison of the density around the dust grain when normalised to a maximum of 1 and a minimum of 0.46 (corresponding to the 46% dust grain density). It can be seen that the shapes of the graphs are very similar for zero flow. It can also be seen that there is a qualitative difference for the case of non-zero flow. For a dust density of 0% of background, there is a reduction in density upstream of the dust grain. For the case of a dust grain with density at 46% of background density, we can see that the density immediatelly upstream to the dust grain increases!

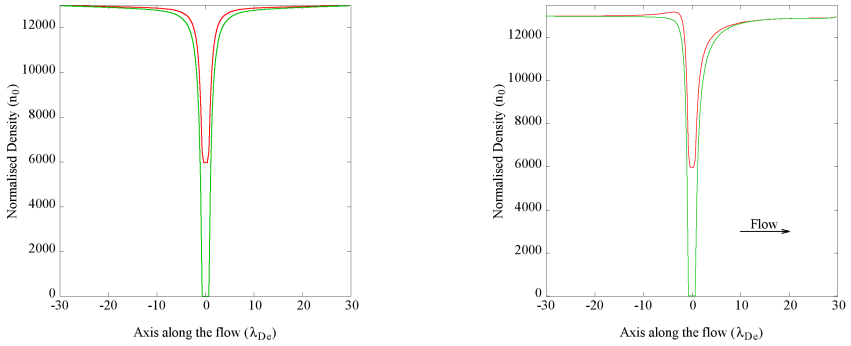

(a) Zero flow.

(b) Flow at Mach 0.8.

Figure 5.3: Effect of changing the effective dust density on the density of the surrounding plasma.

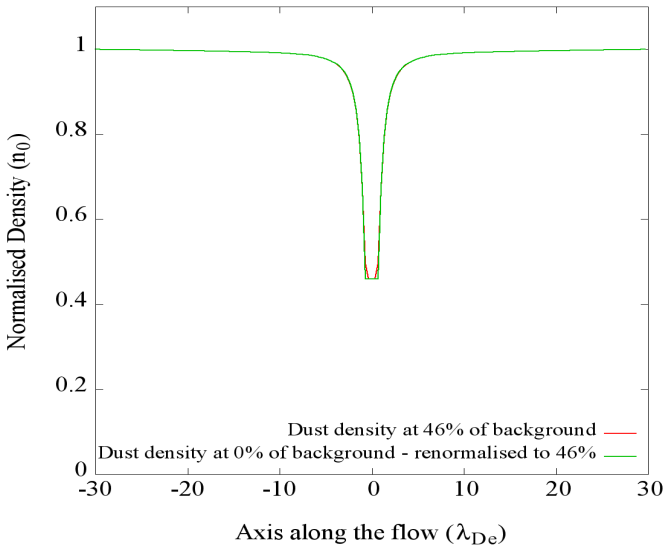

Figure 5.4: Effect of changing the effective dust density on the density of the surrounding plasma for zero flow - demonstration of the similarity of the effect.

Clearly the choice of what density to use as the internal dust density, for the purpose of controlling the strength of the sink that is the dust grain, is something that needs to be investigated further.

6 Fluid Results

I present here what can be considered as preliminary results for the fluid method followed, in studying large dust grains in plasmas. Preliminary because the numerical method used, Lax-Friedrichs, is fairly dissipative, which means there may be details which are smoothed out artificially. These results will be compared with the Lax-Wendroff implementation that will be the next step in the evolution of HADES (and with PPM and other methods that may be implemented).

6.1 Testing

Before professing any sort of confidence on the results of a numerical code, the code needs to be extensively tested to ensure it gives reasonable results. The code needs to, for example, be tested so that the resolution (spatial and temporal) chosen does not impact negatively on the accuracy of the solution to an unacceptable degree. The code also needs to be tested to ensure the solution has converged and is no longer changing (for the steady-state solution). Finally, a code should be tested against known results, to ensure it gives a close enough answer.

Testing is a sizeable part of the development of a scientific code. It is an important task and it is a time-consuming task, as it involves several runs, at various resolutions. Given the time constraints for this report, the testing done for the code was limited. This is partly the reason why the results presented here are clearly identified as "preliminary".

One example of testing done was to investigate the effect of increasing the resolution of the code to the flow velocity. The resolution should have a minimal effect on the flow velocity, as the flow velocity should be a function solely of the physics in the problem studied. At resolutions that are too low, the accuracy suffers, however, so the flow speed will change. The series of simulations ran for this investigation were meant to identify what "too

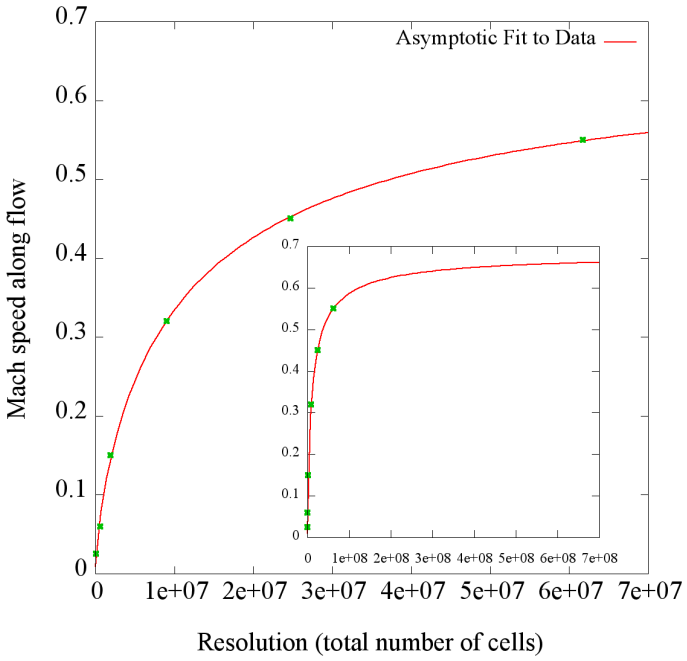

Figure 6.1: Maximum speed achieved for a non-flowing plasma around a dust grain at different domain resolutions.

low" is. At the time of writing this, the value of resolution required for a change in resolution to have a small effect is surprisingly high. Figure 6.1 shows the highest fluid speed achieved for a non-flowing plasma around a dust grain of radius 1 λ_{De} and set at a density of 0% of background for the same simulation ran at different resolutions.

The graph indicates, quite unexpectedly, that a very large resolution is required for the maximum flow speed to reach a value that will be independent of step changes in resolution. This was an unpleasant surprise, as the largest resolution used for graph 6.1 took more than 47 hours of computations, using 72 processors. The direction of interest is the direction of flow, which will always be chosen to be the z-direction. It is in this direction that we want high resolution, but, unfortunately, the resolution in the other directions does affect the results in the z-direction, as shown in figure 6.2.

We note that despite the effect of resolution on the value of the maximum speed, the qualitative nature of the results is not affected, as shown for example, by comparing figures 6.3a and 6.3b.

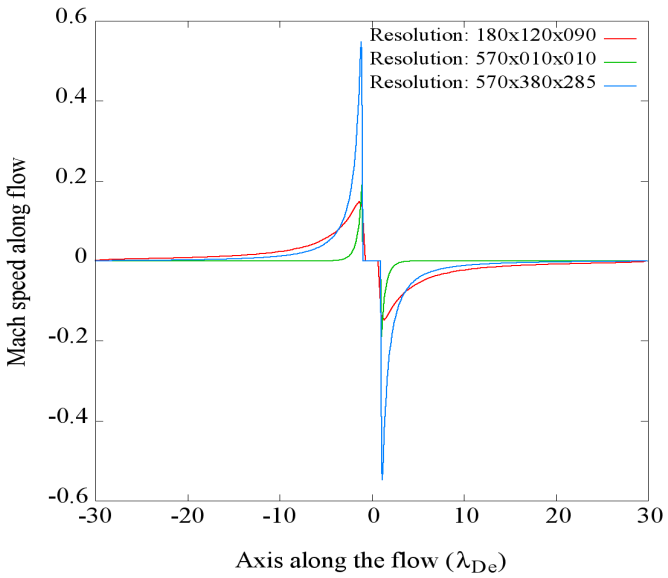

Figure 6.2: Effect of changing the resolution on the value of the speed of the fluid. Resolution is in cells in each direction, z-x-y.

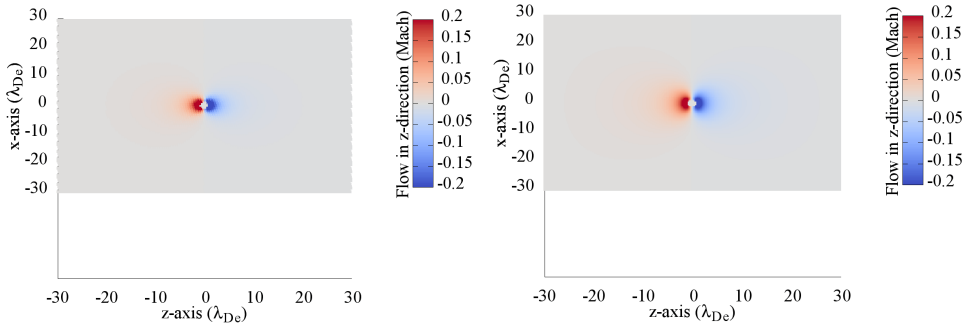

(a) Resolution 570x380x285 cells.

(b) Resolution 300x200x150 cells.

Figure 6.3: Fluid speed in the z direction for two different resolutions.

We will therefore use medium resolution runs for the preliminary results, with a view of comparing with higher reolution simulations in the future.

6.2 Pertinent Parameters

We identify the following parameters as being of interest: Fluid flow, and plasma density. These are present in the equations used. The dust grain radius is the main scale length of interest in the simulation, along with the Debye length. Similar problems in hydrodynamics, however, become self-similar, where the scale is determined by the object around which the flow is passing and different sized-objects perturb the flow identically when lengths are scaled to their size.

We are interested in looking at three fluid flow regimes; we want to look at the case of no flow, the case of subsonic flow and the case of supersonic flow. We thus use Mach 0.0, 0.4, 0.8, 1.0, 1.5, 2.0, 5.0 and 10.0 in our parameter scans.

We are interested in plasma densities, ρ in a wide range, so we use $\rho = 10^5\mathrm{m}^{-3}$ and $\rho = 10^{15}\mathrm{m}^{-3}$ for the preliminary simulations.

6.3 Results

The simulations produced results for the density and flow velocity in each direction for each cell of the domain. We can look at a z-x slice, with z being along the horizontal axis and x on the vertical axis, at $y = 0$, as in figures 6.4a and 6.4b. These are useful for showing a qualitative picture of what the density looks like around a dust grain. We can see the effect of flow on the density around the dust grain. For a non-flowing plasma, the density change is spherically symmetric around the dust grain, going up to the background value within about 10-15 Debye lengths. Conversely, for a strongly flowing plasma, at supersonic flow, we have a very strong asymmetry, with the density going up to background very near the dust grain on the upstream side, but increasing more slowly on the downstream side. This is, of course, what we would expect from supersonic flow, with information about the dust grain being unable to travel upstream. A sub-sonic flow, shown in figure 6.5, shows that there is an asymmetry, as expected, but information about the presence of the dust grain does manage to travel upstream.

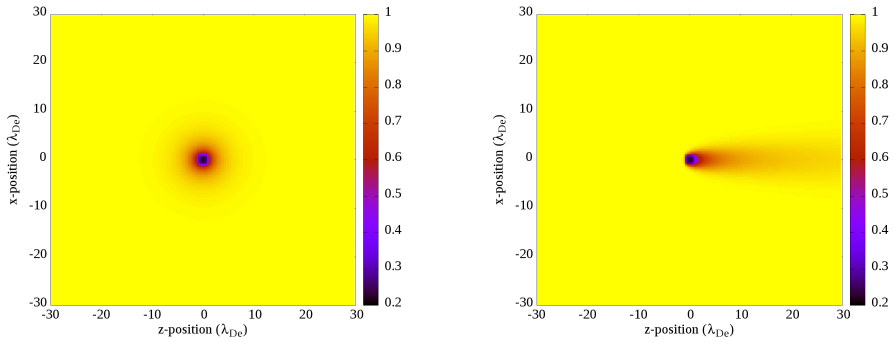

(a) $v_f = Mach\,0$ (b) $v_f = Mach\,10$

Figure 6.4: Comparison, for different flow speeds, of the normalised density (n_0) as a function of position for a dust grain of $r_d = 1\,\lambda_{De}$ and density $n_0 = 10^5\,\mathrm{m}^{-3}$. The figure is a z-x plane at $y = 0$.

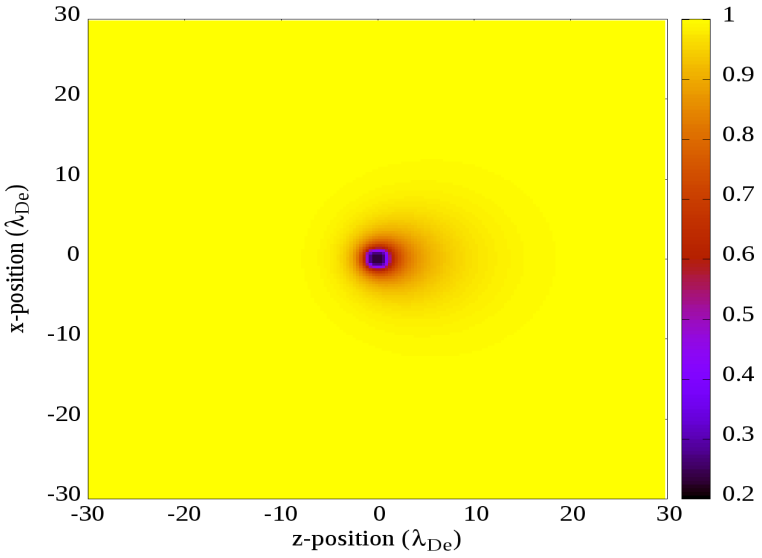

Figure 6.5: Normalised density (n_0) as a function of position for a dust grain of $r_d = 1\lambda_{De}$, in a plasma of flow $v_f = Mach\,0.8$ and density $n_0 = 10^5\,\mathrm{m}^{-3}$. The figure is a z-x plane at $y = 0$.

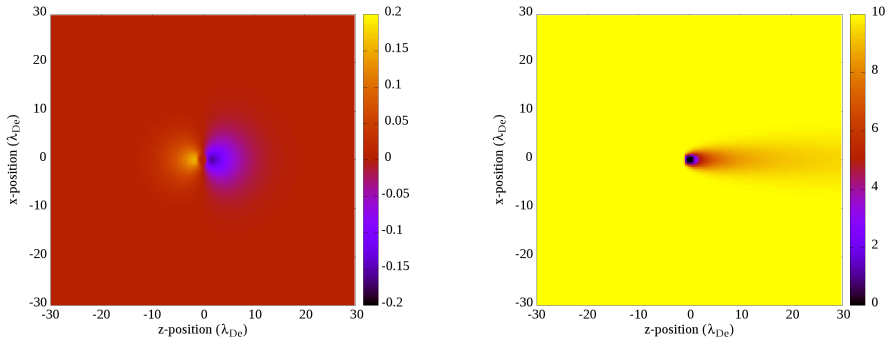

(a) $v_f = Mach\,0$ (b) $v_f = Mach\,10$

Figure 6.6: Effect of fluid flow on the normalised flow in the z-direction (Mach) as a function of position for a dust grain of $r_d = 1\lambda_{De}$ and density $n_0 = 10^5\,\mathrm{m}^{-3}$.

Similar figures can be used for the fluid flow, as in figures 6.6a, 6.6b, 6.7a and 6.7b. We can see that for zero flow, the fluid velocity is, indistinguishably, towards the dust grain in both the x and the z directions. For supersonic flow, the upstream fluid is unaffected by the dust grain and the fluid downstream is moving away from the dust grain at a lower velocity than the flow velocity. It is interesting to note that the fluid picks up a velocity in the x-direction as it goes past the dust grain.

It is perhaps more instructive to look at the values of different quantities along the z-axis, which gives a two-dimensional plot. We can use such plot to make easier comparisons for each parameter. We begin by looking at the effect of fluid flow.

Figures 6.8a to 6.8f show the density along the z-axis (the direction of flow is from negative z to positive z) for Mach 0.0, 0.4, 0.8, 1.0, 1.5, 2.0, 5.0 and 10.0. The graphs look as expected, with higher flow speeds leading to stronger asymmetry. Even at no flow, however, the information about the presence of the dust grain quickly becomes very weak, indicating a strong shielding from the plasma. Conversely, at very high flows, the upstream effect diminishes faster, while the downstream density is affected at much larger distances. Again, this is as expected from normal gas dynamics and other work on plasmas.

The effect of plasma density seems to be non-existent. This is shown in

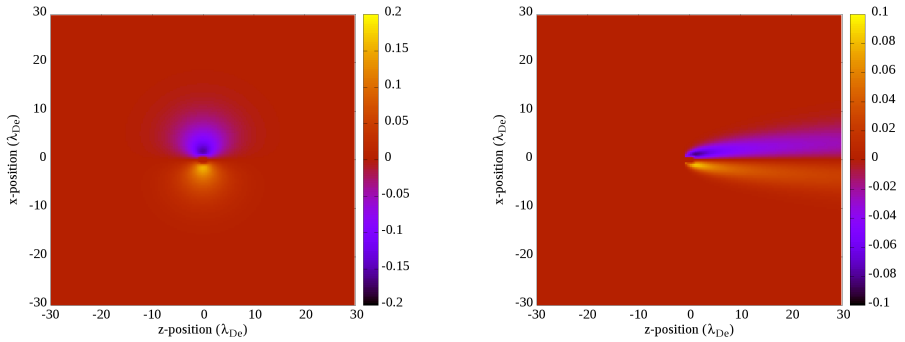

(a) $v_f = Mach\,0$ (b) $v_f = Mach\,10$

Figure 6.7: Effect of fluid flow on the normalised fluid flow in the x-direction (Mach) as a function of position for a dust grain of $r_d = 1\lambda_{De}$, in a plasma of density $n_0 = 10^5\,\mathrm{m}^{-3}$

figures 6.9a and 6.9b for a flow velocity of Mach 5. This is because of the normalisation used, as the unit of length used, the Debye length, scales with density.

6.4 Evaluation

The results up to this point are only results of density around a dust grain. This is because most of the work done was in building up the ability to produce these results and to validate them using existing work. Once there is confidence in the code, the next stage would be to use it, with the appropriate modifications to calculate the charging of the dust grain and the drag force on it, as well as calculating the potential around it. These modifications will be small in scope; indeed, given the assumption of Boltzmann electrons, finding the potential is trivial, as it will simply entail rescaling the density graphs to units of potential. We can see, for example, an area of positive potential downstream from the dust grain, but we do not see a negative area, which has been seen in other work and is assumed to indicate ion focusing. In other words, this work does not corroborate the existence of an ion focusing region.

It will be interesting to compare the momentum imparted on the dust grain by fluid that is absorbed by it and the momentum lost by the fluid

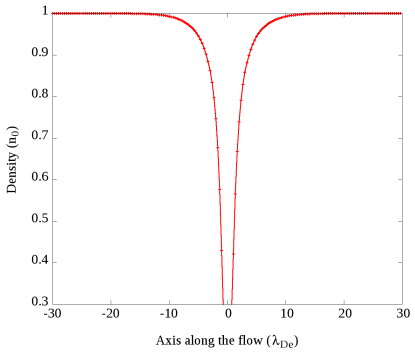

(a) Mach 0.

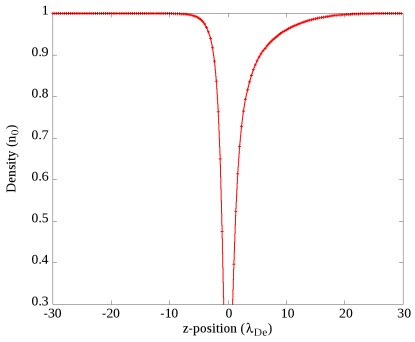

(b) Mach 1.0.

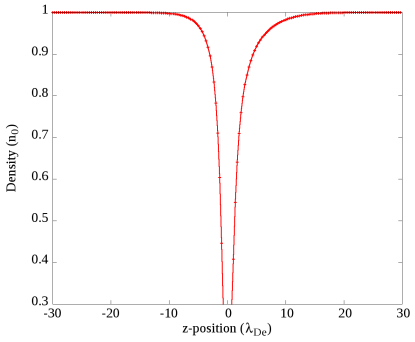

(c) Mach 0.4.

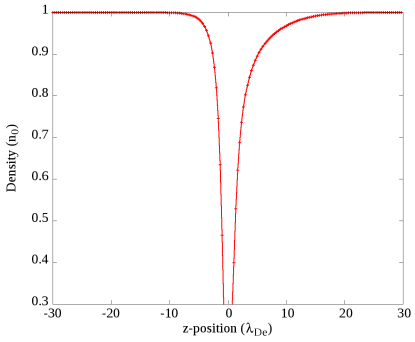

(d) Mach 0.8.

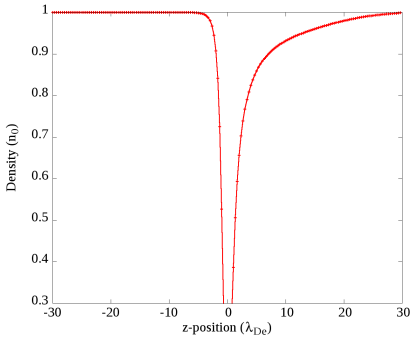

(e) Mach 2.0.

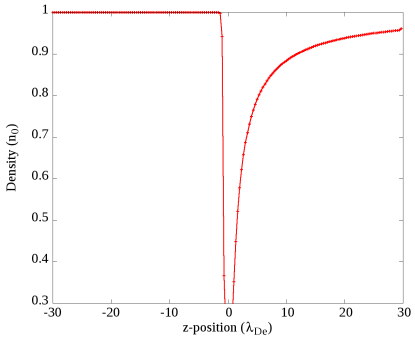

(f) Mach 10.0.

Figure 6.8: Effect of flow on normalised density (n_0) as a function of position for a dust grain of $r_d = 1\lambda_{De}$, in a plasma of density $n_0 = 10^5\,\mathrm{m}^{-3}$.

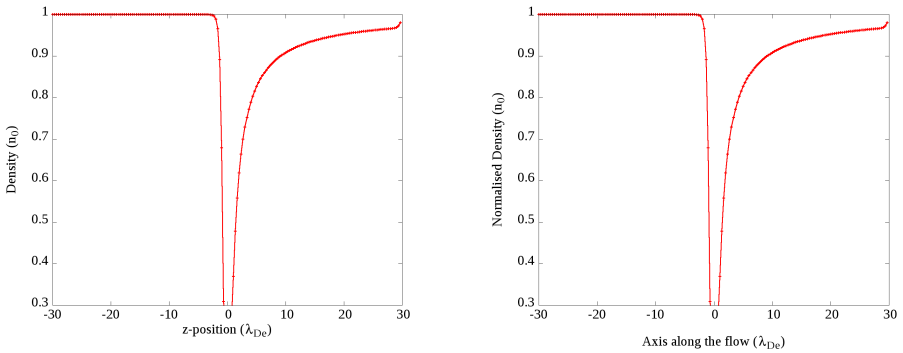

(a) $n_0 = 10^5\,\mathrm{m}^{-3}$ (b) $n_0 = 10^{15}\,\mathrm{m}^{-3}$.

Figure 6.9: Effect of background plasma density on normalised density (n_0) as a function of position for a dust grain of $r_d = 1\lambda_{De}$, in a plasma flowing at Mach 5.

over all the domain. Given the Control Surface Approach work (subsection 2.2.2.3), the drag force would be found by using the momentum lost by the fluid over all the domain. Any difference between the momentum lost because of fluid absorbed by the dust grain and the overall momentum lost by the fluid over all the domain would indicate a loss due to pressure, which would be due to the electric field (which we model as pressure). Based on the density graphs shown here, I expect there will be a difference; this is based on the reduced density and the perturbed fluid flow values downstream of the dust grain.

7 Small Dust Grains

"It is a familiar and significant saying that a problem well-put is half-solved."

John Dewey [110]

Given the stated aim of this work (see section 1.3), we need to choose a suitable method for finding the "potential, plasma velocity and plasma density" around a small dust grain. Kinetic theory is well suited for small dust grains, since we can linearise, given that the effect of a small dust grain is expected to be small. We therefore follow the work done by Filippov et al [2]. We are interested in a moving dust grain, whereas Filippov et al, in both of his 2007 papers [2, 111], used this method (henceforth "the point-sink model") for stationary dust grains. Other authors following Filippov et al's method (for example Khrapak et al [112]), also used this method for stationary dust grains. In a tokamak, we expect dust grains to be ejected from plasma facing components into a flowing plasma. This means we need to adapt the point-sink model to take into account flow.

The aim was to use analytic results as much as possible. It quickly transpired that some of the integrals involved in the process were either unwieldy or impossible for analytic treatment. This necessitated the use of numerical integration for the final results. Contrary to, or perhaps in line with, what John Dewey said, the solution of this problem, after it was "put," presented a reasonable amount of mathematical manipulation. As the mathematics were an integral part[1] of the solution, they take a sizeable part of this chapter.

The work in this chapter is part of a paper-in-preparation with Professors De Angelis and Allen, and Dr. Coppins.

[1] A mildly amusing pun.

7.1 A Moving Dust Grain

In the point-sink model, the dust grain is represented as a sink. Assigning a velocity to the sink is not straightforward. Instead, it is easier to transform to the frame of reference of the dust grain. In this frame of reference, the dust grain is stationary, at the origin, and the plasma is flowing. We can, without loss of generality, orient our axes, such that the flow is along one of these axes. Again w.l.o.g., we can choose this axis to be the z-axis. This means that we need to adjust the distribution function used so it takes into account the flow component in the z-axis.

We can simplify the treatment further, by assuming that the flow is high enough that the thermal component of the plasma, in the z-direction, is negligible compared to the flow. This allows us to model the z-component of the distribution as mono-energetic.

By extension, the flow in the other directions is also negligible compared to the flow speed, so the speed of the ions is dominated by the flow.

Finally, given the cylindrical symmetry of the problem, we can choose, without loss of generality, one of the axes perpendicular to the flow to do our calculations on.

For brevity, this model shall be referred to as the De Angelis point-sink with flow (after professor De Angelis who first suggested pursuing this method, and is also one of the co-authors of the paper-in-preparation), and abbreviated as DAPF.

7.2 The Assumptions

Having established the extra assumptions we will be making, beyond the ones Filippov et al made, we state, here, all the relevant assumptions, before we proceed with the development of the model.

1. The perturbation on the ion species caused by the dust grain is small
    a) This means that the distribution function, f_0, has two parts, namely the unperturbed distribution, F, and the perturbation, f, such that
    $$f_0(\boldsymbol{r}, \boldsymbol{v}) = F(\boldsymbol{v}) + f(\boldsymbol{r}, \boldsymbol{v}) \tag{7.1}$$
2. A small dust grain, i.e. a dust grain with radius r_d such that $r_d \ll \lambda_{D_e}$.

3. A flow speed, U, which is larger than the ion thermal speed, v_{T_i}, i.e. $U > v_{T_i}$.

4. Unperturbed ions are assumed to have a Boltzmann distribution, with the exception of the ion distribution function component in the direction of flow.

   a) Electrons have a much smaller mass than the ions, so their speed is correspondingly larger.

   b) The speed of the ions is assumed to be dominated by the flow in the z direction. In other words

$$\begin{aligned} v &= \sqrt{v_x^2 + v_y^2 + v_z^2} && (7.2) \\ &\approx \sqrt{v_\perp^2 + U^2} && (7.3) \\ &\approx U && (7.4) \end{aligned}$$

5. Electrons are assumed to obey Boltzmann's relation, i.e.

$$n = n_0 e^{-\frac{e\phi}{k_B T_e}} \tag{7.5}$$

   where n is the density, n_0 is the background density, e is the elementary charge, ϕ is the potential, k_B is Boltzmann's constant and T_e is the electron temperature.

6. We can model our small dust grain as a point particle, which can be represented by a delta function. However, we do allow for a finite cross-section when it comes to ion collection.

7. There is cylindrical symmetry parallel to the direction of flow.

8. We can ignore collisions.

9. The above assumptions allow for linearisation of the relevant equations.

10. For convenience, the calculations in this chapter will be done for a hydrogen plasma. The method used can be extended to other plasmas.

    a) This means the background ion density, n_i and the background electron density, n_e are equal: $n_i = n_e = n_0$.

The point-sink model means we have a point dust particle at the origin, with a finite cross-section for collection of ions. This appears contradictory, but it is simply a way of incorporating ion capture in the point-sink model.

7.2.1 The Model

7.2.1.1 Initial Equations

Let us translate the assumptions into the relevant equations. We begin with the distribution functions.

Boltzmann electrons means we can use the Boltzmann relation for electrons,

$$n_e(\boldsymbol{r}) = n_0 e^{\frac{e\Phi}{k_B T_e}} \tag{7.6}$$

where n is the density at $\boldsymbol{r}$, n_0 is the background density (at "infinity", or when $\phi = 0$), Φ is the potential, and e, k_B, T_e are the electron charge, Boltzmann's constant and the electron temperature respectively. This can be linearised because the perturbation is small $\left(\Phi \ll \frac{k_B T_e}{e}\right)$ such that

$$\frac{\delta n_e}{n_0} = \frac{e\Phi}{k_B T_e} \tag{7.7}$$

The unperturbed distribution function of the ions in the x and y directions, can be assumed to be Maxwellian. Hence

$$F_\perp = \frac{e^{-\left(\mathrm{v_x^2}+\mathrm{v_y^2}\right)/2\mathrm{v_{T_i}^2}}}{(2\pi)\, v_{T_i}^2} \tag{7.8}$$

The unperturbed part of the distribution in the z-direction is

$$F_\parallel = \delta(v_z - U) \tag{7.9}$$

where v_z is the velocity in the z direction, U is the flow speed and δ is the Dirac delta function. The full distribution is thus

$$F = n_0 \frac{e^{-\left(\mathrm{v_x^2}+\mathrm{v_y^2}\right)/2\mathrm{v_{T_i}^2}}}{(2\pi)\, v_{T_i}^2} \delta(v_z - U) \tag{7.10}$$

We will need the coupled Poisson's equation, which we state here

$$\nabla^2\Phi = -\frac{e}{\epsilon_0}\left(\delta n_i\left(\boldsymbol{r}\right) - \delta n_e\left(\boldsymbol{r}\right) - Z_d\delta\left(\boldsymbol{r}\right)\right) \tag{7.11}$$

where ϵ_0 is the electric constant, $\delta\left(\boldsymbol{r}\right)$ is the Dirac delta function and Z_d is the charge on the dust grain in electron charges (so that the charge on the dust grain, Q_d is $Q_d = -eZ_d$).

We will also need the point-sink equation, which we linearise

$$\left(\boldsymbol{v}\cdot\nabla\right)f\left(\boldsymbol{r},\boldsymbol{v}\right) = \frac{e}{m_i}\nabla\Phi\left(\boldsymbol{r}\right)\cdot\frac{\mathrm{dF}}{\mathrm{d}\boldsymbol{v}} - \boldsymbol{v}\sigma\left(\boldsymbol{v}\right)\delta\left(\boldsymbol{r}\right)F \tag{7.12}$$

where $\sigma\left(\boldsymbol{v}\right)$ is the capture cross-section of the dust grain.

We now need to solve for potential. This, following the example of Filippov et al, is more easily done using the Fourier transform; we define the Fourier transform and its inverse as follows

$$f_\kappa = \int_{-\infty}^{+\infty} f_r e^{-\imath\boldsymbol{\kappa}\cdot\boldsymbol{r}}\mathrm{d}\boldsymbol{r} \tag{7.13}$$

$$f_r = \int_{-\infty}^{+\infty} f_k e^{\imath\boldsymbol{\kappa}\cdot\boldsymbol{r}}\frac{\mathrm{d}\boldsymbol{\kappa}}{\left(2\pi\right)^3} \tag{7.14}$$

The Poisson equation thus becomes:

$$\kappa^2\Phi_\kappa = \frac{e}{\epsilon_0}\left(\delta n_\kappa^i - \delta n_\kappa^e - Z_d\right) \tag{7.15}$$

where the subscript κ indicates the Fourier transformed quantity and the ion and electron subscripts have been moved to superscripts.

Similarly, the point-sink equation becomes

$$\imath\kappa\cdot\boldsymbol{v}f_\kappa\left(\boldsymbol{v}\right) = \frac{e}{m_i}\imath\kappa\cdot\frac{\mathrm{dF}}{\mathrm{d}\boldsymbol{v}}\Phi_\kappa - v\sigma F \tag{7.16}$$

where $\imath = \sqrt{-1}$.

The linearised expression for electrons becomes

$$\frac{\delta n_\kappa^e}{n_0} = \tau\frac{e\Phi_\kappa}{k_B T_i} \tag{7.17}$$

7.2.1.2 Solving for ϕ_κ - Fourier Space

Now that we have stated our assumptions and relevant equations, we can proceed to solve for the potential in Fourier space, ϕ_κ.

We begin with equation 7.16

$$f_\kappa = \frac{\frac{e}{m_i}\imath\kappa \cdot \frac{\mathrm{dF}}{\mathrm{d}\boldsymbol{v}}\Phi_\kappa - \imath v\sigma F}{\imath\kappa \cdot \boldsymbol{v}} \tag{7.18}$$

It is evident that we have the possibility of division by zero - a pole in the domain. We therefore use the Landau contour to integrate around the pole[2].

$$f_\kappa = \frac{\frac{e}{m_i}\kappa \cdot \frac{\mathrm{dF}}{\mathrm{d}\boldsymbol{v}}\Phi_\kappa + \imath v\sigma F}{\kappa \cdot \boldsymbol{v} - \imath 0} \tag{7.20}$$

We now choose to make use of our cylindrical symmetry assumption. We can choose a plane along an axis perpendicular to the flow, such as the z-x plane, which will contain all the information about the flow. We choose the x-axis, which then makes integration over y trivial.

We thus have

$$\boldsymbol{\kappa} \cdot \boldsymbol{v} = \kappa_x v_x + \kappa_z v_z \tag{7.21}$$

and

$$\boldsymbol{\kappa} \cdot \frac{\mathrm{dF}}{\mathrm{d}\boldsymbol{v}} = \kappa_x \frac{\mathrm{dF}}{\mathrm{dv_x}} + \kappa_z \frac{\mathrm{dF}}{\mathrm{dv_z}} \tag{7.22}$$

We can now calculate the density, which we will subsequently enter into the coupled Poisson equation, to get the potential.

To do so, we integrate over the domain

$$\delta n_\kappa^i = \int_{-\infty}^{\infty} \mathrm{dv_z} \int_{-\infty}^{\infty} \mathrm{dv_x} \int_{-\infty}^{\infty} \mathrm{dv_y} f_\kappa \tag{7.23}$$

[2]This is less trivial than it may appear. It involves considering the time-dependent perturbation, such that

$$\left(\frac{\partial}{\partial \mathrm{t}} + \boldsymbol{v} \cdot \nabla\right) f(\boldsymbol{r}, \boldsymbol{v}, t) = \frac{e}{m_i} \nabla\Phi(\boldsymbol{r}, t) \cdot \frac{\mathrm{dF}}{\mathrm{d}\boldsymbol{v}} - \boldsymbol{v}\sigma(\boldsymbol{v})\,\delta(\boldsymbol{r_0} - \boldsymbol{r}(t))\,F \tag{7.19}$$

This is then Fourier transformed, assuming $\boldsymbol{r}(t) = \boldsymbol{v_0}t$. The $\imath 0$ is added to satisfy causality and then we assume a stationary limit, for which $\omega \to 0$.

We integrate over $\mathrm{dv_y}$ first

$$\int_{-\infty}^{\infty} \mathrm{dv_y} f_\kappa = \int_{-\infty}^{\infty} \mathrm{dv_y} \frac{\frac{e}{m_i}\kappa \cdot \frac{\mathrm{dF}}{\mathrm{d}\boldsymbol{v}}\Phi_\kappa + \imath v\sigma F}{\kappa \cdot \boldsymbol{v} - \imath 0} \tag{7.24}$$

where the integration only applies to F where we have v_y

$$\begin{aligned}
\int_{-\infty}^{\infty} \mathrm{dv_y} F &= \int_{-\infty}^{\infty} \mathrm{dv_y} \\
&\quad n_0 \frac{e^{-\left(\mathrm{v_x^2}+\mathrm{v_y^2}\right)/2\mathrm{v_{T_i}^2}}}{(2\pi)\, v_{T_i}^2} \delta\left(v_z - U\right) && (7.25)\\
&= n_0 \frac{\delta\left(v_z - U\right)}{\sqrt{2\pi} v_{T_i}} e^{-\left(\mathrm{v_x^2}\right)/2\mathrm{v_{T_i}^2}} && (7.26)\\
&= F_y && (7.27)
\end{aligned}$$

Which leaves us with

$$f_{\kappa y} = \frac{\frac{e}{m_i}\kappa \cdot \frac{\mathrm{dF_y}}{\mathrm{d}\boldsymbol{v}}\Phi_\kappa + \imath v\sigma F_y}{\kappa \cdot \boldsymbol{v} - \imath 0} \tag{7.28}$$

Normalisation The analysis that follows is made easier by normalising the relevant quantities.

All speeds are normalised to the ion thermal speed. This makes it easy to check that our assumption that $U > v_{T_i}$ is true. We therefore have

$$\begin{aligned}
u &= \frac{U}{\sqrt{2} v_{T_i}} && (7.29)\\
g &= \frac{v_x}{\sqrt{2} v_{T_i}} && (7.30)\\
g_\parallel &= \frac{v_z}{\sqrt{2} v_{T_i}} && (7.31)
\end{aligned}$$

We also have

$$\kappa = \frac{k}{\lambda_i} \tag{7.32}$$

We follow the normal definition for Mach speed, $M = \frac{v}{c_s}$, where c_s $\left(= \sqrt{\frac{k_B T_e}{m_i}}\right)$ is the speed of sound.

Corresponding to our choice for the normalisation of speed, we normalise

distances to the ion Debye length, $\lambda_i = \sqrt{\frac{\epsilon_0 k_B T_i}{n_0 Z_i^2 e^2}}$. The cross-section of the dust grain, for example, can be normalised such that

$$\sigma_0 = \frac{\sigma(v)}{\lambda_i^2} \tag{7.33}$$

We also choose to normalise potential as follows

$$\phi = \frac{e\Phi}{k_B T_i} \tag{7.34}$$

We also introduce the ratio $\tau = \frac{T_i}{T_e}$.
Also, note that

$$\int_{-\infty}^{\infty} \mathrm{dv_x} = \int_{-\infty}^{\infty} \mathrm{dg}\sqrt{2} v_{T_i} \tag{7.35}$$

$$\int_{-\infty}^{\infty} \mathrm{dv_z} = \int_{-\infty}^{\infty} \mathrm{dg_\parallel}\sqrt{2} v_{T_i} \tag{7.36}$$

$$\overline{F}_y = n_0 \frac{\delta(g_\parallel - u)}{2\sqrt{\pi} v_{T_i}^2} e^{-g^2} \tag{7.37}$$

$$f_{ky} = \frac{\phi_k \left(\frac{k_z}{2} \frac{\mathrm{d\overline{F}_y}}{\mathrm{dy_\parallel}} - g k_x \overline{F}_y \right) + \imath u \sigma_0 \lambda_i^3 \overline{F}_y}{k_x g + k_z g_\parallel - \imath 0} \tag{7.38}$$

Transforming to Fourier Space For the $g_\parallel$ integral, which is the normalised v_z integral, we need to calculate

$$\int_{-\infty}^{\infty} \mathrm{dg_\parallel} \frac{\delta(g_\parallel - u)}{k_x g + k_z g_\parallel - \imath 0} = \frac{1}{k_x g + k_z u - \imath 0} \tag{7.39}$$

$$\int_{-\infty}^{\infty} \mathrm{dg_\parallel} \frac{\frac{\mathrm{d}}{\mathrm{dy_\parallel}} \delta(g_\parallel - u)}{k_x g + k_z g_\parallel - \imath 0} = \frac{k_z}{(k_x g + k_z u - \imath 0)^2} \tag{7.40}$$

Which means

$$\int_{-\infty}^{\infty} \mathrm{dg_\parallel} f_{ky} = \frac{\phi_k \left(-g k_x n_0 \frac{e^{-g^2}}{\sqrt{2\pi} v_{T_i}} \right) + \imath u \sigma_0 \lambda_i^3 n_0 \frac{e^{-g^2}}{\sqrt{2\pi} v_{T_i}}}{k_x g + k_z u - \imath 0} + \frac{\phi_k \frac{k_z^2}{2} n_0 \frac{e^{-g^2}}{\sqrt{2\pi} v_{T_i}}}{(k_x g + k_z u - \imath 0)^2} \tag{7.41}$$

$$= f_{kyg_\parallel} \tag{7.42}$$

We now introduce the quantity $\xi_0 = \frac{k_z u}{k_x}$ so that

$$f_{kyg_{\|}} = \frac{\phi_k \left(-k_x n_0 \frac{g e^{-g^2}}{\sqrt{2\pi} v_{T_i}} \right) + \imath u \sigma_0 \lambda_i^3 n_0 \frac{e^{-g^2}}{\sqrt{2\pi} v_{T_i}}}{k_x \left(g + \xi_0 - \imath 0 \right)} + \frac{\phi_k \frac{k_z^2}{2} n_0 \frac{e^{-g^2}}{\sqrt{2\pi} v_{T_i}}}{k_x^2 \left(g + \xi_0 - \imath 0 \right)^2} \tag{7.43}$$

For the final integral, over g, we need

$$\int_{-\infty}^{\infty} \mathrm{d}g \frac{e^{-g^2}}{(g + \xi_0 - \imath 0)} = \pi \imath e^{-\xi_0^2} - 2\sqrt{\pi} D_f(\xi_0) \tag{7.44}$$

$$= I_0 \tag{7.45}$$

$$\int_{-\infty}^{\infty} \mathrm{d}g \frac{g e^{-g^2}}{(g + \xi_0 - \imath 0)} = \sqrt{\pi} - \xi_0 I_0 \tag{7.46}$$

$$\int_{-\infty}^{\infty} \mathrm{d}g \frac{e^{-g^2}}{(g + \xi_0 - \imath 0)^2} = 2\xi_0 I_0 + 2\sqrt{\pi} \tag{7.47}$$

where $D_f(x) \left(= e^{-x^2} \int_0^x e^{t^2} \mathrm{d}t \right)$ is the Dawson function.

We therefore have

$$\int_{-\infty}^{\infty} \mathrm{d}g f_{kyg_{\|}} = n_0 \left[\phi_k \left(\xi_0 \frac{I_0}{\sqrt{\pi}} \left(1 + \frac{\xi_0^2}{u^2} \right) + \frac{\xi_0^2}{u^2} - 1 \right) + \frac{\imath u \lambda_i^3 \sigma_0}{k_x} \frac{I_0}{\sqrt{\pi}} \right]$$
$$= \delta n_k^i \tag{7.48}$$

which we re-write as

$$\frac{\delta n_k^i}{n_0} = \phi_k \left(\xi_0 \frac{I_0}{\sqrt{\pi}} \left(1 + \frac{\xi_0^2}{u^2} \right) + \frac{\xi_0^2}{u^2} - 1 \right) + \frac{\imath u \lambda_i^3 \sigma_0}{k_x} \frac{I_0}{\sqrt{\pi}} \tag{7.49}$$

We can now substitute the density for the ions and the electrons in Poisson's equation

$$k^2 \phi_k = \phi_k \left(\xi_0 \frac{I_0}{\sqrt{\pi}} \left(1 + \frac{\xi_0^2}{u^2} \right) + \frac{\xi_0^2}{u^2} - 1 \right) + \frac{\imath u \lambda_i^3 \sigma_0}{k_x} \frac{I_0}{\sqrt{\pi}} - \tau \phi_k - \frac{Z_d}{n_0}$$
$$\phi_k = \frac{\lambda_i^3}{k^2 \epsilon_k} \left(\frac{\imath u \sigma_0}{k_x} \frac{I_0}{\sqrt{\pi}} - \frac{Z_d}{N_i} \right) \tag{7.50}$$

where

$$\epsilon_k = 1 + \frac{k_0^2 - \imath\epsilon_i}{k^2} \tag{7.51}$$

$$k_0^2 = 1 + \tau - \frac{\xi_0^2}{u^2} + 2\left(1 + \frac{\xi_0^2}{u^2}\right)\xi_0 D_f(\xi_0) \tag{7.52}$$

$$\epsilon_i = \sqrt{\pi}\left(1 + \frac{\xi_0^2}{u^2}\right)\xi_0 e^{-\xi_0^2} \tag{7.53}$$

Equation 7.50 is the potential in Fourier space. We now need to convert back to "configuration" space.

7.2.1.3 Solving for the Potential in Configuration Space, ϕ_r

The potential in configuration space is

$$\phi_r = \int_{-\infty}^{+\infty} \phi_k e^{\imath\left(\frac{k_y y}{\lambda_i} + \frac{k_x x}{\lambda_i} + \frac{k_z z}{\lambda_i}\right)} \frac{\mathrm{dk}}{\lambda_i^3 (2\pi)^3} \tag{7.54}$$

We expect a real value for the potential, hence we aim to calculate the real part of the integral. We therefore define $\phi_k = \phi_k^r + \imath\phi_k^\imath$, where ϕ_k^r and $\phi_k^\imath$ are the real and imaginary parts of ϕ_k respectively.

$$\phi_k^r = \frac{\lambda_i^3}{\left(k^2 + k_0^2\right)^2 + \epsilon_i^2} \left[\frac{u\sigma_0}{k_x}\left(2D_f(\xi_0)\epsilon_i - \sqrt{\pi}e^{-\xi_0^2}\left(k^2 + k_0^2\right)\right) - \frac{Z_d}{N_i}\left(k^2 + k_0^2\right)\right] \tag{7.55}$$

$$\phi_k^\imath = -\frac{\lambda_i^3}{\left(k^2 + k_0^2\right)^2 + \epsilon_i^2} \left[\frac{u\sigma_0}{k_x}\left(\sqrt{\pi}e^{-\xi_0^2}\epsilon_i + 2D_f(\xi_0)\left(k^2 + k_0^2\right)\right) + \frac{Z_d}{N_i}\epsilon_i\right] \tag{7.56}$$

We also use Euler's formula, such that

$$e^{\imath\left(\frac{k_x x}{\lambda_i} + \frac{k_z z}{\lambda_i}\right)} = \cos\left(\frac{k_x x}{\lambda_i} + \frac{k_z z}{\lambda_i}\right) + \imath\sin\left(\frac{k_x x}{\lambda_i} + \frac{k_z z}{\lambda_i}\right) \tag{7.57}$$

We therefore have

$$\begin{aligned}\phi_r &= \frac{1}{\lambda_i^3 (2\pi)^3} \int_{-\infty}^{+\infty} \mathrm{dk} \\ &\quad \left[\cos\left(\frac{k_x x}{\lambda_i} + \frac{k_z z}{\lambda_i}\right) + \imath \sin\left(\frac{k_x x}{\lambda_i} + \frac{k_z z}{\lambda_i}\right)\right] \\ &\quad [\phi_k^r + \imath \phi_k^i] \end{aligned} \tag{7.58}$$

$$\begin{aligned}\Re\{\phi_r\} &= \frac{1}{\lambda_i^3 (2\pi)^3} \int_{-\infty}^{+\infty} \mathrm{dk} \\ &\quad \left[\cos\left(\frac{k_x x}{\lambda_i} + \frac{k_z z}{\lambda_i}\right) \phi_k^r - \sin\left(\frac{k_x x}{\lambda_i} + \frac{k_z z}{\lambda_i}\right) \phi_k^i\right] \end{aligned} \tag{7.59}$$

For ease of calculation, we split the integral, so that

$$\Re\{\phi_r\} = \Re\{\phi_r\}_1 + \Re\{\phi_r\}_2 \tag{7.60}$$

$$\begin{aligned}\Re\{\phi_r\}_1 &= \frac{1}{\lambda_i^3 (2\pi)^3} \int_{-\infty}^{+\infty} \mathrm{dk} \\ &\quad \cos\left(\frac{k_x x}{\lambda_i} + \frac{k_z z}{\lambda_i}\right) \phi_k^r \end{aligned} \tag{7.61}$$

$$\begin{aligned}\Re\{\phi_r\}_2 &= \frac{1}{\lambda_i^3 (2\pi)^3} \int_{-\infty}^{+\infty} \mathrm{dk} \\ &\quad \left(-\sin\left(\frac{k_x x}{\lambda_i} + \frac{k_z z}{\lambda_i}\right) \phi_k^i\right) \end{aligned} \tag{7.62}$$

The first integral is

$$\begin{aligned}\Re\{\phi_r\}_1 &= \frac{1}{(2\pi)^3} \int_{-\infty}^{+\infty} \mathrm{dk_z} \int_{-\infty}^{+\infty} \mathrm{dk_x} \int_{-\infty}^{+\infty} \mathrm{dk_y} \\ &\quad \frac{\cos\left(\frac{k_x x}{\lambda_i} + \frac{k_z z}{\lambda_i}\right)}{\left(k^2 + k_0^2\right)^2 + \epsilon_i^2} \\ &\quad \left[\frac{u\sigma_0}{k_x}\left(2D_f(\xi_0)\epsilon_i - \sqrt{\pi} e^{-\xi_0^2}\left(k^2 + k_0^2\right)\right) - \frac{Z_d}{N_i}\left(k^2 + k_0^2\right)\right] \end{aligned} \tag{7.63}$$

Integrating over k_y is trivial, in the absence of any dependence on k_y, leaving a $2\pi\delta(y)$, term. This just means the results are for the z-x plane,

which is the plane we chose in the beginning.

$$\begin{aligned}\Re\left\{\phi_r\right\}_1 &= \frac{1}{(2\pi)^2}\int_{-\infty}^{+\infty}\mathrm{dk_z}\int_{-\infty}^{+\infty}\mathrm{dk_x} \\ &\frac{\cos\left(\frac{k_x x}{\lambda_i}+\frac{k_z z}{\lambda_i}\right)}{\left(k^2+k_0^2\right)^2+\epsilon_i^2} \\ &\left[\frac{u\sigma_0}{k_x}\left(2D_f\left(\xi_0\right)\epsilon_i-\sqrt{\pi}e^{-\xi_0^2}\left(k^2+k_0^2\right)\right)-\frac{Z_d}{N_i}\left(k^2+k_0^2\right)\right]\end{aligned} \tag{7.64}$$

Expanding, we end up with fourteen independent integrands. After eliminating integrals that are odd in k_x or k_z, we are left with:

$$\begin{aligned}\Re\left\{\phi_r\right\}_1 &= -\frac{Z_d}{N_i}\frac{1}{(2\pi)^2}\int_{-\infty}^{+\infty}\mathrm{dk_z}\int_{-\infty}^{+\infty}\mathrm{dk_x} \\ &k_z^2\cos\left(\frac{k_z z}{\lambda_i}\right)\frac{\cos\left(\frac{k_x x}{\lambda_i}\right)}{\left(k_z^2+k_x^2+k_0^2\right)^2+\epsilon_i^2}+ \\ &\cos\left(\frac{k_z z}{\lambda_i}\right)\frac{k_x^2\cos\left(\frac{k_x x}{\lambda_i}\right)}{\left(k_z^2+k_x^2+k_0^2\right)^2+\epsilon_i^2}+ \\ &\cos\left(\frac{k_z z}{\lambda_i}\right)\frac{k_0^2\cos\left(\frac{k_x x}{\lambda_i}\right)}{\left(k_z^2+k_x^2+k_0^2\right)^2+\epsilon_i^2}\end{aligned} \tag{7.65}$$

We note that this means we need the following integrals for k_x

$$Int_{kx1} = \int_{-\infty}^{+\infty}\mathrm{dk_x}\frac{\cos\left(\frac{k_x x}{\lambda_i}\right)}{\left(k_z^2+k_x^2+k_0^2\right)^2+\epsilon_i^2} \tag{7.66}$$

$$Int_{kx2} = \int_{-\infty}^{+\infty}\mathrm{dk_x}\frac{k_x^2\cos\left(\frac{k_x x}{\lambda_i}\right)}{\left(k_z^2+k_x^2+k_0^2\right)^2+\epsilon_i^2} \tag{7.67}$$

$$Int_{kx3} = \int_{-\infty}^{+\infty}\mathrm{dk_x}\frac{k_0^2\cos\left(\frac{k_x x}{\lambda_i}\right)}{\left(k_z^2+k_x^2+k_0^2\right)^2+\epsilon_i^2} \tag{7.68}$$

The presence of k_0^2 and ϵ_i complicates the integrals. We note two things which come to our aid. Firstly, we note that since (all) the integrands are even functions, we can convert the limits of the integrals in both k_x and k_z

such that

$$\int_{-\infty}^{\infty} \mathrm{dk_{x,z}} f\left(k_x,\, k_z\right) = 2\int_{0}^{\infty} \mathrm{dk_{x,z}} f\left(k_x,\, k_z\right) \tag{7.69}$$

Secondly, the presence of k_x in these two functions is always in ξ_0. We can define the angle θ such that

$$k_x = k\sin\left(\theta\right) \tag{7.70}$$

$$k_z = k\cos\left(\theta\right) \tag{7.71}$$

Which makes

$$\xi_0 = \frac{u}{\tan\left(\theta\right)} \tag{7.72}$$

removing the k-dependence from ξ_0 and , consequently, from k_0^2 and ϵ_i. We therefore have

$$\int_{-\infty}^{+\infty} \mathrm{dk_z} \int_{-\infty}^{+\infty} \mathrm{dk_x} = 2\int_{0}^{\pi/2} \mathrm{d}\theta \int_{0}^{+\infty} \mathrm{dk}k \tag{7.73}$$

and $\Re\left\{\phi_r\right\}_1$ becomes

$$\begin{aligned}\Re\left\{\phi_r\right\}_1 = & -\frac{Z_d}{N_i}\frac{2}{\left(2\pi\right)^2}\int_{0}^{\pi/2}\mathrm{d}\theta\int_{0}^{+\infty}\mathrm{dk}k \\ & \frac{k^2\cos\left(\theta\right)\cos\left(\frac{k\cos(\theta)z}{\lambda_i}\right)\cos\left(\frac{k\sin(\theta)x}{\lambda_i}\right)}{\left(k^2+k_0^2\right)^2+\epsilon_i^2} + \\ & \frac{k^2\sin^2\left(\theta\right)\cos\left(\frac{k\cos(\theta)z}{\lambda_i}\right)\cos\left(\frac{k\sin(\theta)x}{\lambda_i}\right)}{\left(k^2+k_0^2\right)^2+\epsilon_i^2} + \\ & k_0^2\frac{\cos\left(\frac{k\cos(\theta)z}{\lambda_i}\right)\cos\left(\frac{k\sin(\theta)x}{\lambda_i}\right)}{\left(k^2+k_0^2\right)^2+\epsilon_i^2}\end{aligned} \tag{7.74}$$

which means we need the following k-integrals:

$$Int_{k1} = \int_{0}^{+\infty}\mathrm{dk}\frac{k^3\cos\left(k\cos\left(\theta\right)\zeta\right)\cos\left(k\sin\left(\theta\right)\chi\right)}{\left(k^2+k_0^2\right)^2+\epsilon_i^2} \tag{7.75}$$

$$= I_3^{cc} \tag{7.76}$$

$$Int_{k2} = \int_{0}^{+\infty}\mathrm{dk}\frac{k\cos\left(k\cos\left(\theta\right)\zeta\right)\cos\left(k\sin\left(\theta\right)\chi\right)}{\left(k^2+k_0^2\right)^2+\epsilon_i^2} \tag{7.77}$$

$$= I_1^{cc} \tag{7.78}$$

where $\zeta = \frac{z}{\lambda_i}$ and $\chi = \frac{x}{\lambda_i}$ are the spatial coordinates in ion Debye lengths.

We therefore have

$$\Re\left\{\phi_r\right\}_1 = -\frac{Z_d}{N_i}\frac{2}{(2\pi)^2}\int_0^{\pi/2} \mathrm{d}\theta \left[I_3^{cc}\left(1+\sin^2(\theta)\right) + k_0^2 I_1^{cc}\right] \quad (7.79)$$

We now return to find $\Re\left\{\phi_r\right\}_2$

$$\begin{aligned}\Re\left\{\phi_r\right\}_2 = & \frac{1}{(2\pi)^2}\int_{-\infty}^{+\infty}\mathrm{dk_z}\int_{-\infty}^{+\infty}\mathrm{dk_x} \\ & \left(\sin(k_x\chi)\cos(k_z\zeta)+\cos(k_x\chi)\sin(k_z\zeta)\right) \\ & \frac{1}{\left(k^2+k_0^2\right)^2+\epsilon_i^2}\left[\frac{u\sigma_0}{k_x}\left(\sqrt{\pi}e^{-\xi_0^2}\epsilon_i + 2D_f(\xi_0)\left(k^2+k_0^2\right)\right) + \frac{Z_d}{N_i}\epsilon_i\right]\end{aligned} \quad (7.80)$$

We eliminate odd functions of $k_x$and k_z and convert to integrals over k and θ

$$\begin{aligned}\Re\left\{\phi_r\right\}_2 = & \frac{2u\sigma_0}{(2\pi)^2}\int_0^{\pi/2}\mathrm{d}\theta\int_{-\infty}^{+\infty}\mathrm{dk} \\ & \sqrt{\pi}\frac{e^{-\xi_0^2}\epsilon_i}{\sin(\theta)}\frac{\cos(k\sin(\theta)\chi)\sin(k\cos(\theta)\zeta)}{\left(k^2+k_0^2\right)^2+\epsilon_i^2} + \\ & 2\frac{D_f(\xi_0)\cos^2(\theta)}{\sin(\theta)}\frac{k^2\cos(k\sin(\theta)\chi)\sin(k\cos(\theta)\zeta)}{\left(k^2+k_0^2\right)^2+\epsilon_i^2} + \\ & 2D_f(\xi_0)\sin(\theta)\frac{k^2\cos(k\sin(\theta)\chi)\sin(k\cos(\theta)\zeta)}{\left(k^2+k_0^2\right)^2+\epsilon_i^2} + \\ & 2\frac{D_f(\xi_0)k_0^2}{\sin(\theta)}\frac{\cos(k\sin(\theta)\chi)\sin(k\cos(\theta)\zeta)}{\left(k^2+k_0^2\right)^2+\epsilon_i^2}\end{aligned} \quad (7.81)$$

which means we need the following k-integrals

$$Int_{k3} = \int_0^{+\infty}\mathrm{dk}\frac{\cos(k\sin(\theta)\chi)\sin(k\cos(\theta)\zeta)}{\left(k^2+k_0^2\right)^2+\epsilon_i^2} \quad (7.82)$$

$$= I_0^{cs} \quad (7.83)$$

$$Int_{k4} = \int_0^{+\infty}\mathrm{dk}\frac{k^2\cos(k\sin(\theta)\chi)\sin(k\cos(\theta)\zeta)}{\left(k^2+k_0^2\right)^2+\epsilon_i^2} \quad (7.84)$$

$$= I_2^{cs} \quad (7.85)$$

We therefore have

$$\begin{aligned}\Re\{\phi_r\}_2 &= \frac{u\sigma_0}{2\pi^2}\int_0^{\pi/2} \mathrm{d}\theta \frac{1}{\sin(\theta)} \\ &\left[\sqrt{\pi}e^{-\xi_0^2}\epsilon_i I_0^{cs} + 2D_f(\xi_0)\left(\cos^2(\theta) I_2^{cs} + \sin^2(\theta) I_2^{cs} + k_0^2 I_0^{cs}\right)\right]\end{aligned} \tag{7.86}$$

The overall function is, thus

$$\begin{aligned}\Re\{\phi_r\} &= \frac{1}{2\pi^2}\int_0^{\pi/2} \mathrm{d}\theta \\ &\left[-\frac{Z_d}{N_i}\left(I_3^{cc}\left(1+\sin^2(\theta)\right) + k_0^2 I_1^{cc}\right) + \right. \\ &\left.\frac{u\sigma_0}{\sin(\theta)}\left(\sqrt{\pi}e^{-\xi_0^2}\epsilon_i I_0^{cs} + 2D_f(\xi_0)\left(I_2^{cs} + k_0^2 I_0^{cs}\right)\right)\right]\end{aligned} \tag{7.87}$$

7.2.2 Inputs

7.2.2.1 Required Quantities

The equation for the potential has a a number of inputs that need to be specified.

We need to specify the dust cross section. Various models can be used, such as OML. It has been shown that for high flow velocities the cross section essentially reduces to the geometrical cross section of the dust radius (see [15]).

$$\sigma(v) = \pi R^2 \tag{7.88}$$

which means specifying R also specifies the dust cross section.

The most prominent input required is the charge on the dust grain, Z_d. Again, various models can be used; for our work, we chose to use the vacuum capacitance, such that

$$Z_d = -4\pi\epsilon_0 R\frac{k_B T_e}{e^2}\ln(M\sqrt{\mu}) \tag{7.89}$$

where ϵ_0, R, k_B, T_e, M and μ are the electric constant, the dust radius, Boltzmann's constant, the electron temperature, the Mach speed and the

electron to ion mass ratio respectively. Of these, ϵ_0, k_B, and μ are fixed (we are choosing to concentrate on hydrogen plasmas for now), but we can choose R, T_e, and M.

We also need to specify

$$\begin{aligned} N_i &= n_0 \lambda_i^3 \\ &= \left(\frac{\epsilon_0 k_B \tau T_e}{(n_0)^{1/3} e^2} \right)^{3/2} \end{aligned} \tag{7.90}$$

where n_0, the plasma density, and τ, the ion-to-electron temperature ratio, can be chosen.

7.2.2.2 Chosen Values

We are limited in our choice of values for the required quantities by the assumptions of our model.

We are assuming a small dust grain, so the choice of R is limited to values (much) smaller than the Debye length.

We are also limited in our choice of flow, as we are assuming a flow higher than the ion thermal velocity, i.e. $U > \sqrt{\frac{k_B T_i}{m_i}}$.

We are free to choose τ, T_e, and n_0. As this is the first time this method is used, we would like to compare it against other methods; more specifically, we would like to compare it with PIC codes, which capture the relevant physics without having to make the same number of approximations analytic methods do. This will determine the choice of parameters for the results that will be compared.

One example is a (2D) PIC code by Miloch et al [13], which, in the paper referenced, used an electron-to-ion-temperature ratio (inverse τ) of 100 and 80 (among others) an electron temperature of 0.18 eV and a density of $10^{15}\mathrm{m}^{-3}$. The smallest dust radius Miloch et al also use is 0.625 λ_e, which is at the upper limit of validity for our model.

Miloch, Kroll and Block [14] use a 3D PIC code ("Dust in Plasma 3D" or "DiP3D") in a more recent paper to report, among other results, the potential around a dust grain. They use the following parameters:

- $R = \lambda_D$

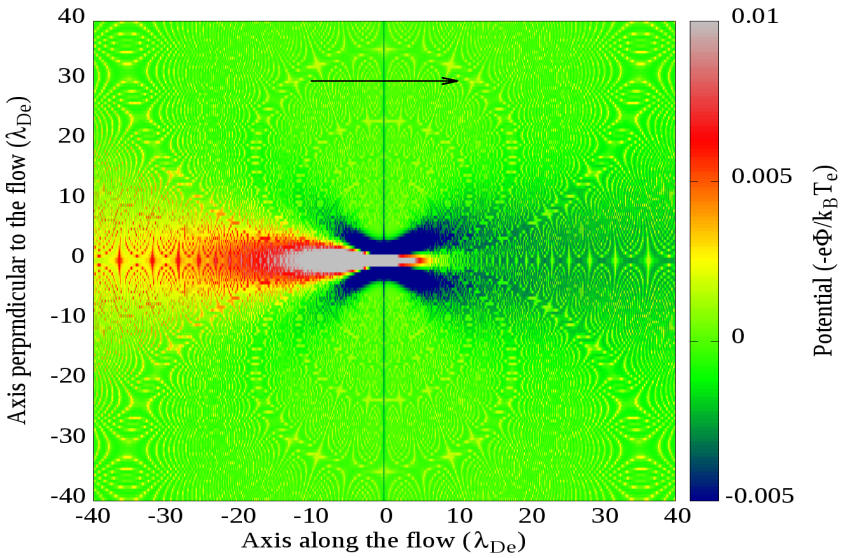

Figure 7.1: DAPF prediction for the potential around a dust grain of radius $0.5\lambda_D$, in a plasma of density $10^5\mathrm{m}^{-3}$ with a flow speed of 1.5 M, $T_e = 1\,\mathrm{eV}$ and $\tau = 1$.

- $v_f = 1.2\,\mathrm{M}$
- $\frac{1}{\tau} = 100$
- $T_e = 3\,\mathrm{eV}$
- $n_0 = 10^{13}\mathrm{m}^{-3}$

7.2.3 Results

We first have a look at the potential around the dust grain for various cases, to see what the model predicts and analyse the results. We will subsequently compare the results of the model with work done using PIC simulations. Note that the direction of flow is shown by an arrow on each figure.

7.2.3.1 Preliminary Analysis

Figure 7.1 shows the potential around a dust grain for a plasma of density $10^5\mathrm{m}^{-3}$, $\tau = 1$, dust grain radius of $0.5\lambda_{De}$, and a flow speed of Mach 1.5.

We notice four structures of interest.

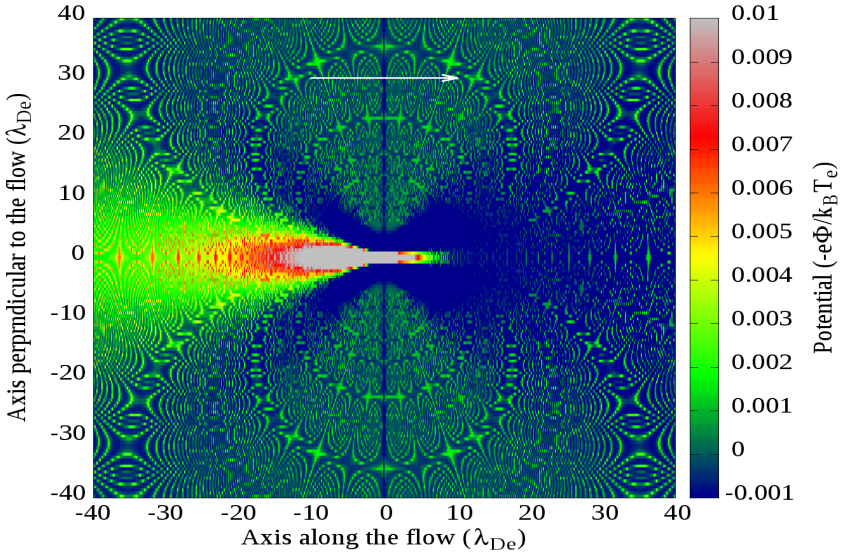

Figure 7.2: DAPF prediction for the potential around a dust grain of radius $0.5\lambda_D$, in a plasma of density $10^5 \mathrm{m}^{-3}$ with a flow speed of 1.5 M, $T_e = 1\,\mathrm{eV}$ and $\tau = 1$, highlighting the upstream structure and ion focusing.

First we notice what looks like a Mach cone; this is a structure which needs further investigation to verify it is the same structure Willis [15, 113] sees in his simulations, namely a weak discontinuity.

Secondly, we notice what would appear to be ion focusing behind the dust grain. This is a structure seen by other authors, including Willis [113], Miloch et al [13] and Maiorov et al [114].

The third structure we notice is upstream. This is an unexpected structure, which does not appear to have been seen by other authors; it certainly has not been commented on by other authors, perhaps because they do not see it in their simulations (figure 4b of [15] may be showing upstream structure). The ion focusing and the upstream structure can be seen more clearly in figure 7.2.

The fourth structure we notice is a ring structure, perpendicular to the direction of flow. Again, this is not a structure that can be seen in work by other authors, nor is it mentioned by other authors. It can be seen more clearly in figure 7.3.

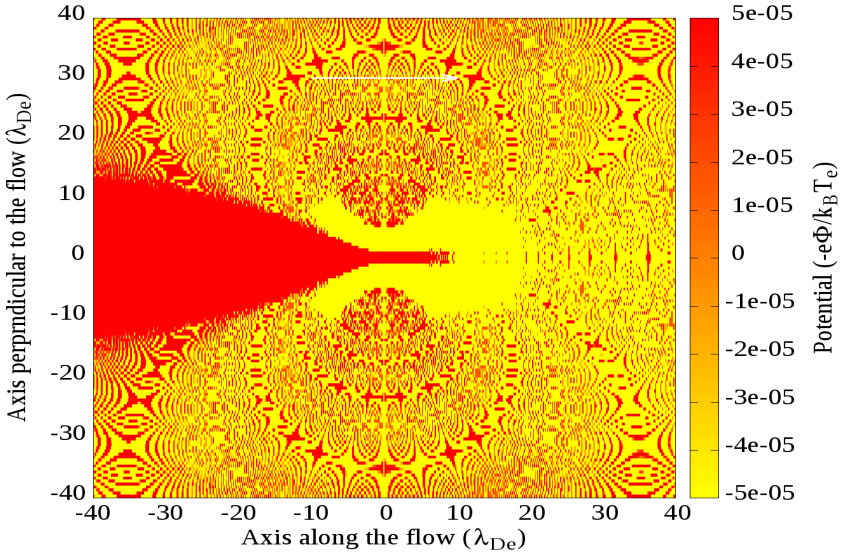

Figure 7.3: DAPF prediction for the potential around a dust grain of radius $0.5\lambda_D$, in a plasma of density $10^5 \mathrm{m}^{-3}$ with a flow speed of 1.5 M, $T_e = 1\,\mathrm{eV}$ and $\tau = 1$, highlighting the ring structure.

Let's look at each structure separately.

"Mach Cone" Willis et al [113] report that the weak discontinuity formed matches the angle of a Mach cone, with the angle, θ_M being approximately

$$\theta_M = \sin^{-1}\left(\frac{c_{s,hot}}{v_d}\right) \tag{7.91}$$

where $c_s = \sqrt{\frac{k_B(T_e+\gamma T_i)}{m_i}}$, with $\gamma \approx 3$ and v_d is the flow velocity. For the values we used for figure 7.1, we cannot use this expression, as arcsine is defined only for values $-1 \leqslant x \leqslant 1$. Using the normal Mach cone angle for gases, we get

$$\theta_M = \sin^{-1}\left(\frac{1}{M}\right) \tag{7.92}$$

$$= 0.73^r \tag{7.93}$$

We can measure the angle of the cone using a contour plot, noting where the weak discontinuity is, as will be evident by the density of the contours.

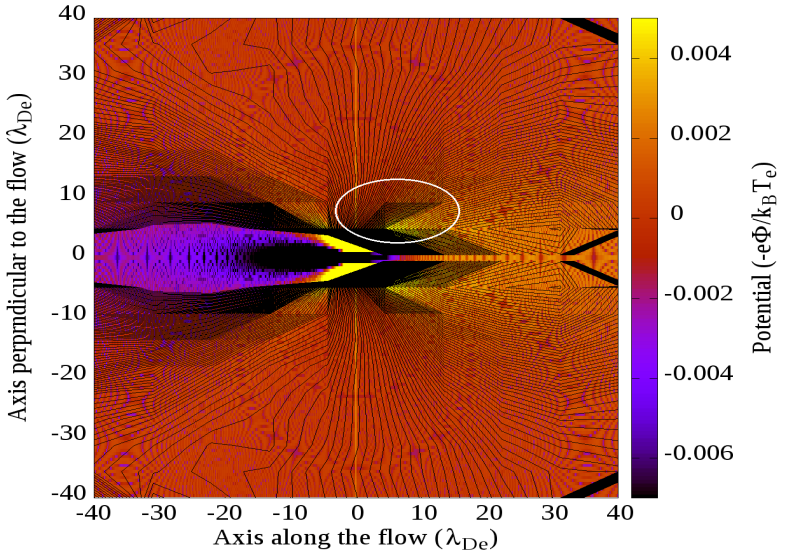

Figure 7.4: A contour plot of potential to highlight the presence of the weak discontinuity and aid in finding the angle of the cone.

This is shown in figure 7.4. The increased density of contours, circled in white, presumably indicates the weak discontinuity region. The front of it would then indicate the angle of the "Mach cone". For this graph, it was measured as 0.81 radians, which compares with the 0.73 radians calculated.

Given the density of the contours, it can be said that there is a weak discontinuity, in the shape of the cone, at an angle that is close to the angle predicted for normal gases.

Ion Focusing Several authors, such as Maiorov et al [114], report an ion focusing region and explain it by invoking the trajectories of the ions near a negatively charged dust grain. The explanations invoke images similar to figure 2.13, which show ion trajectories focused behind the dust grain. We observe such a region in the results from DAPF (see figure 7.5). We note that this effect is stronger for larger dust grains. This is encouraging, as we are not tracking ions, following trajectories, or monitoring the evolution of local charge in time in DAPF; rather, the ion focusing region is calculated in the steady state in DAPF.

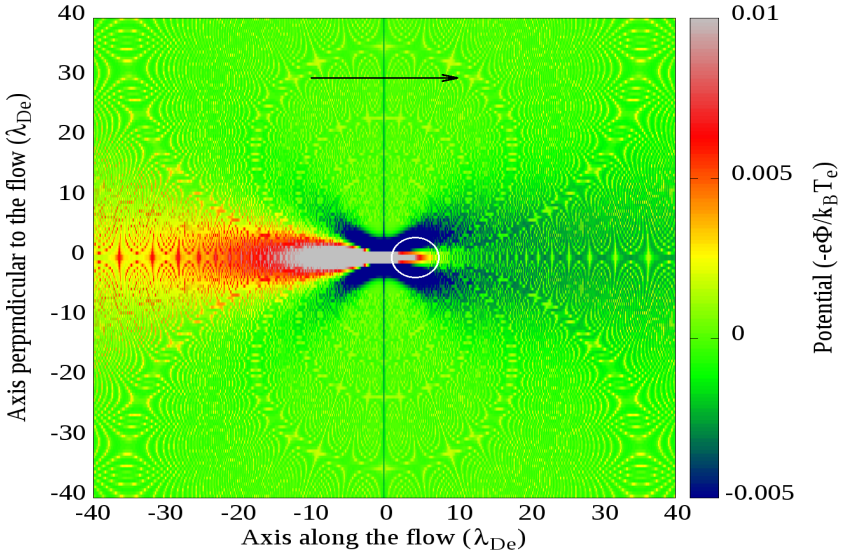

Figure 7.5: DAPF potential around a dust grain of radius $0.5\lambda_D$, plasma density $10^{15}\mathrm{m}^{-3}$, $\tau = 1$, and $v_f = 1.5\,\mathrm{M}$. The positive potential behind the dust grain is circled in white.

Upstream Structure Authors such as Willis et al (in [113]) and [14] include figures in their work that appear to show upstream structures. As the focus of their work is something else, they do not investigate this upstream structure. Upstream effects are not expected for supersonic flow in gases, and a lot of people in the field expect a similar absence of upstream effects in supersonic flow in plasmas. We observe an upstream structure; furthermore, we do not believe this to be an error in the model. Information in a plasma is not solely transferred by sound waves, hence the sound speed does not need to be the upper limit for the speed at which information can travel in a plasma[3].

The upstream structure from DAPF can be seen in figure 7.6.

[3] A lot of models looking at the effect of the dust on the potential in the surrounding plasma assume that the electron distribution function at the sheath edge is Maxwellian, as the part of the distribution shielded by the dust grain is expected to be replaced by the electrons reflected by the negative dust grain. This, however, ignores the relative motion of the dust grain and the plasma (i.e. it approximates zero flow) and the effects this will have on the collision between the dust grain and the electrons.

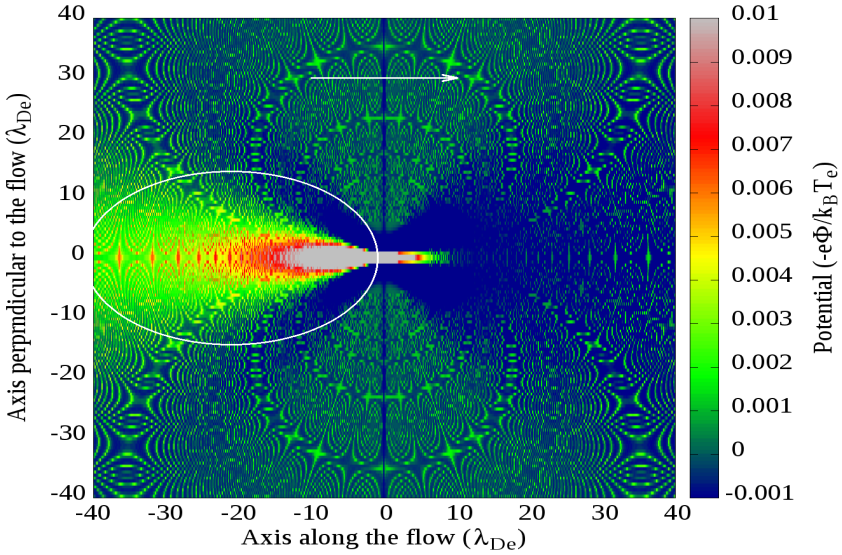

Figure 7.6: DAPF calculated potential around a dust grain of radius $0.5\lambda_D$, in a plasma of density $10^{15}\mathrm{m}^{-3}$, electron temperature 1 eV, $\tau = 1$. The upstream structure is circled.

Ring Structure The ring structure is another unexpected result from the code. The shape is reminiscent of the electric field lines of a dipole. The plasma is polarised in the vicinity of the dust grain, as in "a streaming plasma, a dust grain develops an electric dipole moment" [13], but these ring structures have not been observed in other work. It is important to note that at low potential resolution these structures are not discernible (see figure 7.7 and compare with figure 7.3). Authors whose results are based on simulations (PIC or otherwise) would struggle to get the resolution afforded by a kinetic code. It remains to be verified whether these ring structures are actual predictions of the model, or whether they are a product of the numerical integration required for the results.

7.2.3.2 Parameter Scan

Before we compare the results of DAPF with other models, let us investigate how the results of DAPF vary with each parameter, namely ion-to-electron temperature ratio, τ, density, n_0, electron temperature, T_e, dust radius, R, and flow velocity, v_f.

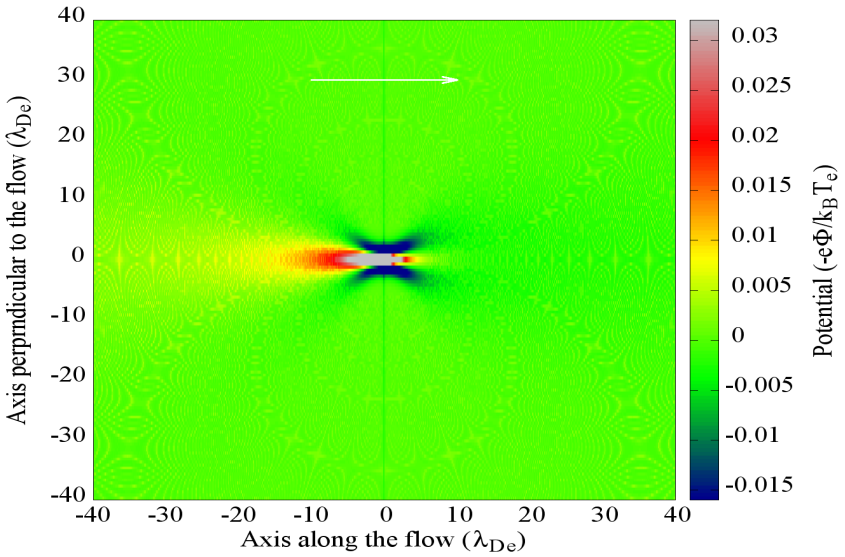

Figure 7.7: DAPF calculated potential around a dust grain of radius $0.5\lambda_D$, in a plasma of density $10^5 \mathrm{m}^{-3}$, electron temperature 1 eV, $\tau = 1$. The ring structure is not discernible, due to the lower resolution in potential.

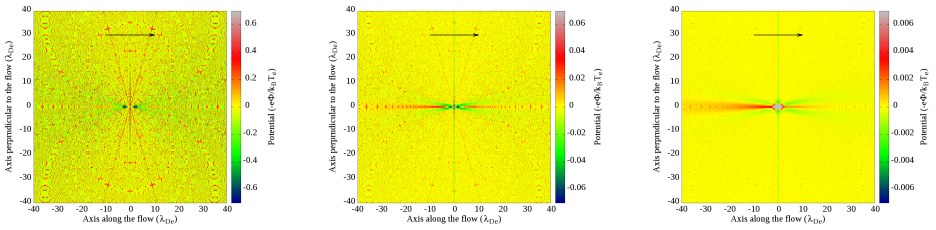

(a) $\tau = 0.01$. (b) $\tau = 0.1$. (c) $\tau = 1$.

Figure 7.8: Prediction of DAPF on the effect of τ on the the potential around a dust grain of radius $0.1\lambda_D$ immersed in a plasma of density $10^{15}\,\mathrm{m}^{-3}$, electron temperature 1 eV, flowing at *Mach* 5 - note the change in the colour scale.

Ion-to-Electron Temperature Ratio, τ Figures 7.8a, 7.8b and 7.8c show the potential prediction of DAPF around a dust grain of radius $0.1\lambda_D$ immersed in a plasma of density $10^{15}\mathrm{m}^{-3}$, electron temperature 1 eV, flowing at *Mach* 5 for three different values of τ (note the change of scale for the potential). It can be seen that τ does affect the value of the potential around the dust grain, with larger τ making the effect of the dust grain on its surrounding plasma smaller. Is this reasonable? One effect of τ is a change in the relative size of the ion and electron Debye lengths. The dust grain size is set using the ion Debye length, but the plots are scaled using the electron Debye length. The change may only be apparent, due to the relative difference between the radius of the dust grain and the size of the plot.

Density, n_0 Figures 7.9a, 7.9b and 7.9c show the potential prediction of DAPF around a dust grain of radius $0.5\lambda_D$ immersed in a plasma of $\tau = 1$, electron temperature 1 eV, flowing at *Mach* 1.5 for three different values of n_0. It can be seen that the plasma density does not affect the effect of the dust grain on the potential of the surrounding plasma. It does need to be noted, that the plasma density affects the size of the Debye length, so the images are not comparable in absolute terms - the dust grain is a different absolute size in each, as is the size of the plasma shown in the figures.

Electron Temperature, T_e Figures 7.10a, 7.10b and 7.10c show the potential prediction of DAPF around a dust grain of radius $0.1\lambda_D$ immersed

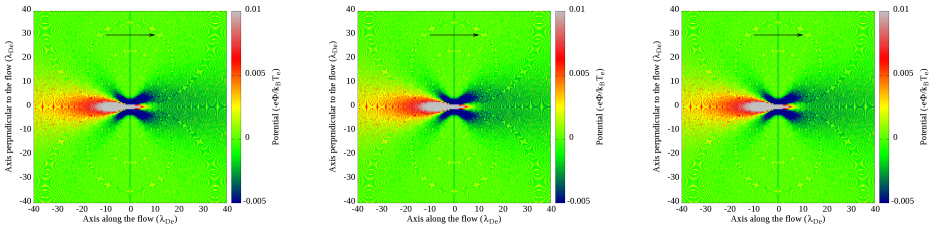

(a) $10^5\,\mathrm{m}^{-3}$ (b) $10^{10}\,\mathrm{m}^{-3}$ (c) $10^{15}\,\mathrm{m}^{-3}$

Figure 7.9: Prediction of DAPF for the effect of background density on the potential around a dust grain of radius $0.5\lambda_D$ immersed in a plasma of electron temperature 1 eV, flowing at Mach 1.5 when $\tau = 1$.

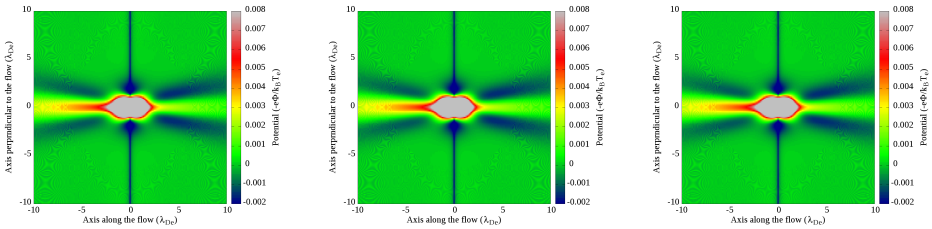

(a) $T_e = 2\,\mathrm{eV}$. (b) $T_e = 10\,\mathrm{eV}$. (c) $T_e = 100\,\mathrm{eV}$.

Figure 7.10: Prediction of DAPF for the effect of electron temperature on the potential around a dust grain of radius $0.1\lambda_D$ immersed in a plasma of density $10^{15}\,\mathrm{m}^{-3}$, flowing at Mach 5.0 when $\tau = 1$.

in a plasma of $\tau = 1$, plasma density $10^{15}\mathrm{m}^{-3}$, flowing at $Mach$ 5 for three different values of T_e. It can be seen that electron temperature does not affect the effect of the dust grain on the potential of the surrounding plasma. It does need to be noted, that the electron temperature affects the size of the Debye length, so the images are not comparable in absolute terms - the dust grain is a different absolute size in each, as is the size of the plasma shown in the figures.

Dust Radius, R Figures 7.11a, 7.11b, and 7.11c, show the potential prediction of DAPF around a dust grain immersed in a plasma of $\tau = 1$, electron temperature 1 eV, density $10^{15}\mathrm{m}^{-3}$, flowing at $Mach$ 5 for three different values of R. It can be seen that the radius of the dust grain has a significant

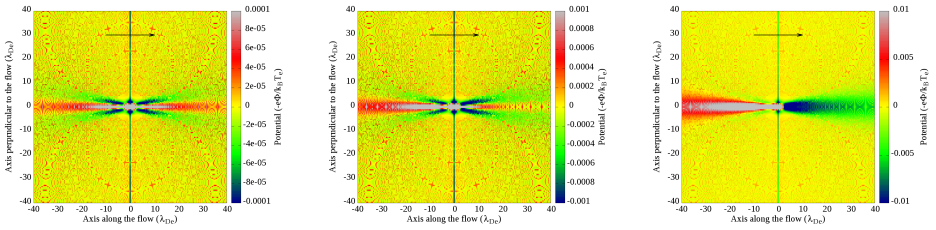

(a) $0.01\lambda_{De}$ (b) $0.1\lambda_{De}$ (c) $0.5\lambda_{De}$

Figure 7.11: Prediction of DAPF for the effect of dust radius on the potential around a dust grain immersed in a plasma of density $10^{15}\,\mathrm{m}^{-3}$, electron temperature 1 eV, flowing at Mach 5.0 when $\tau = 1$.

effect on the summetry of the potential on each side of the $z = 0$ plane. This is not unexpected, as a larger dust grain has a larger cross-section to collect ions, changing the particle distribution from the negative z to the positive z positions. It is worth noting the appearance of the potential for the largest dust grain shown here, to compare with the results of the model for large dust grains. At $R = 0.5\lambda_{De}$, this dust grain size is pushing the boundaries of the applicability of DAPF and is the closest we can get to the range of dust sizes that HADES can model.

Flow Velocity, v_f Figures 7.12a, and 7.12b, show the potential prediction of DAPF around a dust grain immersed in a plasma of $\tau = 1$, electron temperature 1 eV, density $10^{15}\mathrm{m}^{-3}$, flowing at $Mach$ 5 for two different values of v_f. It can be seen that the flow speed has a significant effect on the shape of the perturbation in potential around the dust grain, elongating the effects of the dust grain along the direction of flow.

7.2.3.3 Comparison

We begin comparing by looking at the results of Miloch et al [13]. I remind the reader that Miloch et al use $\tau = 0.01$, $T_e = 0.18\,\mathrm{eV}$, $n_0 = 10^{15}\mathrm{m}^{-3}$, $R = 0.625\lambda_D$ and $v_f = 2.5\,\mathrm{M}$.

They give 2 graphs of potential that can be used for a qualitative comparison, one for a conducting dust grain and one for an insulating dust grain. We note that they normalise their results against the floating potential, defined

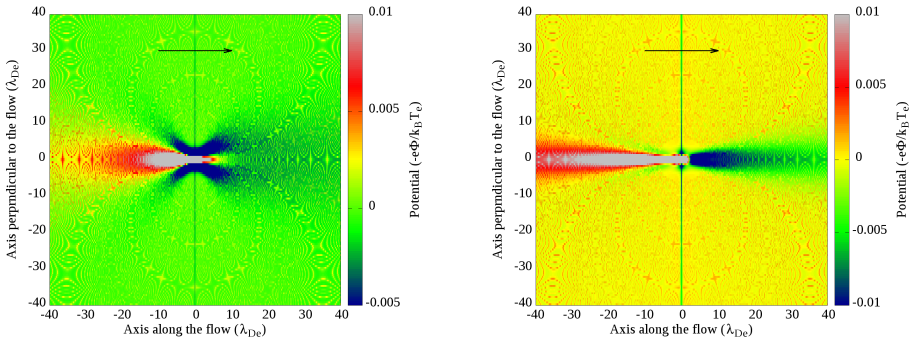

(a) Mach 1.5 (b) Mach 5

Figure 7.12: Prediction of DAPF for the effect of flow velocity on the potential around a dust grain of radius $0.5\lambda_{De}$, immersed in a plasma of density $10^{15}\,\mathrm{m}^{-3}$, electron temperature 1 eV, when $\tau = 1$.

as [115]

$$\phi_f = -\frac{k_B T_e}{2e}\left(1 + \ln\left(\frac{M}{2\pi m}\right)\right) \tag{7.94}$$

where $\frac{M}{m}$ is the ion to electron mass ratio and for which Miloch et al use the value of 120[4]. Given that they use $T_e = 0.18\,\mathrm{eV}$, the floating potential they use is $-0.36\,\mathrm{eV}$.

A comparison between the results from DAPF, normalised the same way as Miloch et al, and the results of Miloch et al [13] is shown in figure 7.13.

The similarities between the two sets of results are not overwhelming, but both models show downstream structures. The structure in our model may more clearly be seen in figure 7.14.

A stark difference is the strength of the upstream features. In Miloch et al, the upstream features seem to significantly less pronounced than the downstream features. It is hard to see this, as Miloch et al choose to not include features far upstream. A larger region around the dust grain is shown in the graphs produced for this work (see figure 7.15).

In the more recent paper, Miloch, Kroll and Block [14] look at a smaller dust grain in a warmer plasma. Using the same parameters and normalisation as in this paper, we compare the results from DAPF and the PIC code

[4]Miloch et al choose a low mass ratio to make the computations required tractable. This highlights a relative weakness of the PIC method, compared to an analytic formulation.

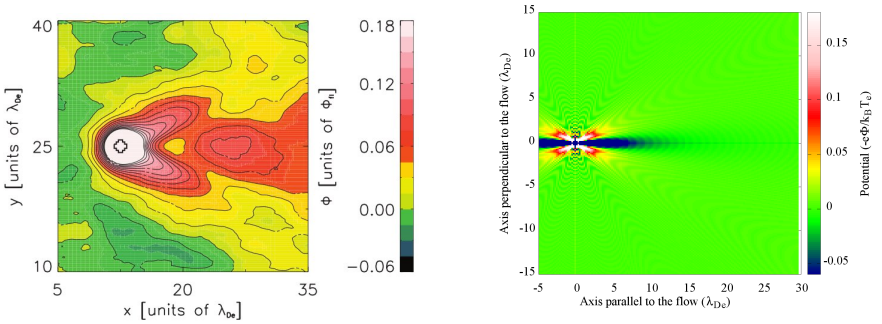

(a) Figure 13 of Miloch et al: "Potential variation for a plasma with ion flow velocity $v_d = 2.5$ in units of Cs around an insulating dust..." [13]

(b) Potential result of the model, using the same parameters and normalisations as Miloch et al, with the exception of τ ($\tau = 0.1$ and not 0.01).

Figure 7.13: Comparison between the results of our model and Miloch et al [13]. Miloch et al place the dust grain at (10, 25), whereas we place the dust grain at (0, 0).

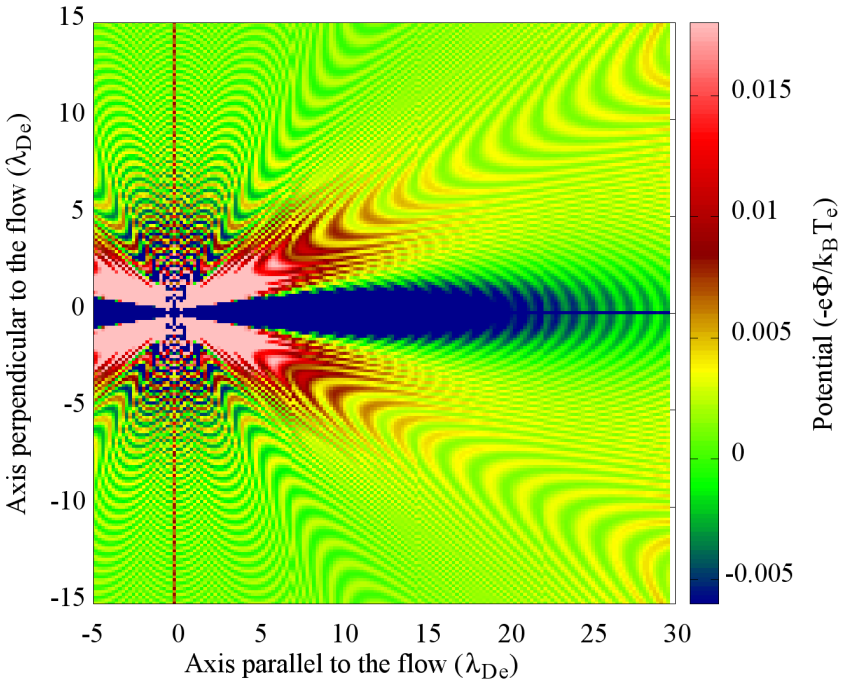

Figure 7.14: DAPF results with the same parameters as in figure 13 of Miloch et al, with the exception of τ ($\tau = 0.1$ and not 0.01). [13].

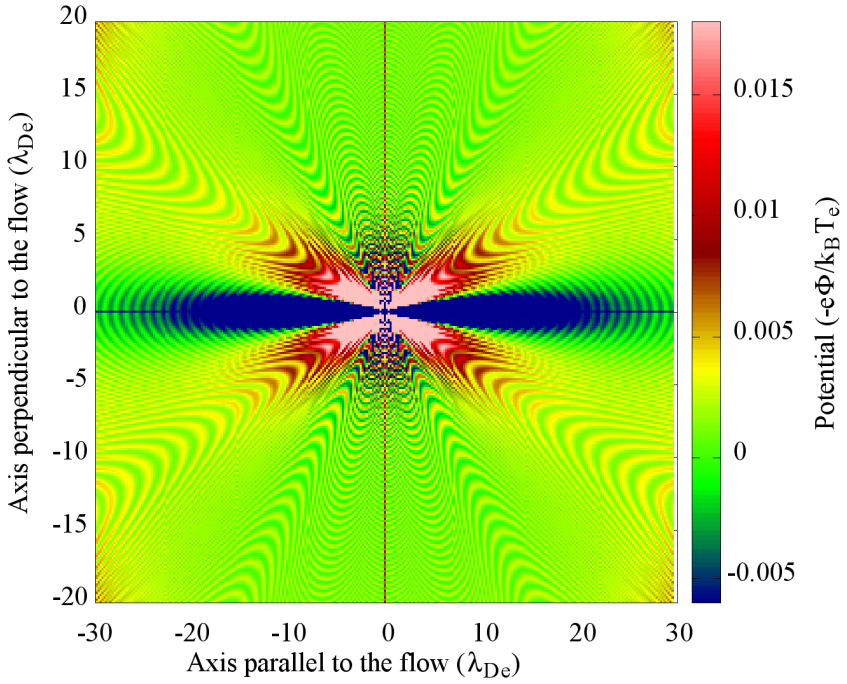

Figure 7.15: Graph showing the presence of upstream effects on the plasma.

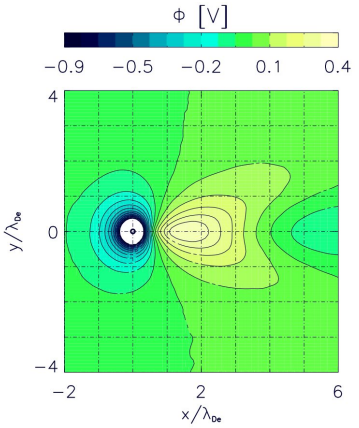

(a) Figure 4 of Miloch, Kroll and Block [14]: "The potential distribution in x-y plane for a single dust grain for the ion drift speed $v_d = 1.2C_s$"

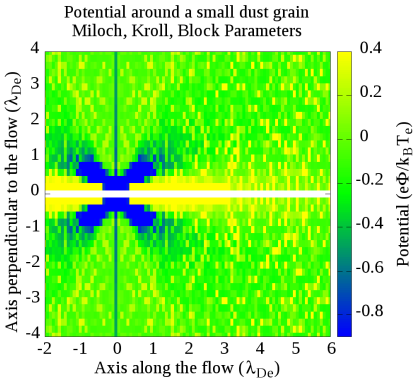

(b) Potential result of the model, using the same parameters and normalisations as Miloch, Kroll and Block [14].

Figure 7.16: Comparison between the results of our model and Miloch, Kroll and Block [14].

(figure 7.16).

It would perhaps be more instructive to have a look at the potential along a line parallel to the z-axis, such as in figure 7.17. We can compare, qualitatively, this graph with Maiorov's result (figure 4 in [114]).

This form becomes even more useful for showing the effect of small dust grains. In the heat-map format, even the effect of dust grains that aren't that small seems to be symmetric in the positive and negative z-direction (figure 7.18a). A closer look, however, (figure 7.18b) shows that there is indeed an asymmetry in the potential because of the dust grain.

7.2.3.4 Evaluation

Our aim was to be able to calculate the potential, ion density and ion velocity around the dust grain. We have succeeded in establishing an expression for potential which successfully replicates important characteristics of the potential around a dust grain in a flowing plasma. The expression successfully replicates the Mach-cone like weak discontinuity originating at the dust grain.

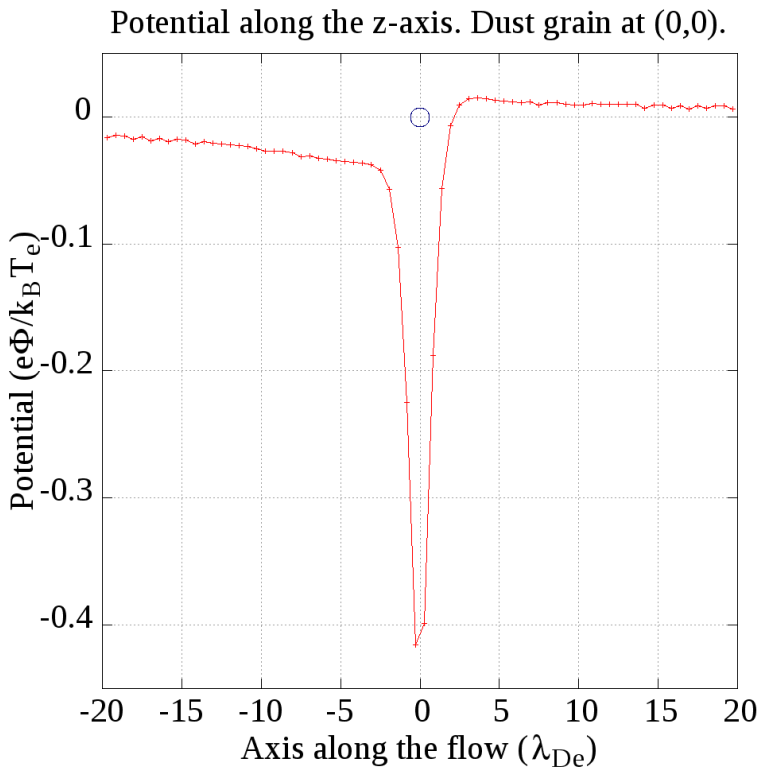

Figure 7.17: Potential along the z-axis for a plasma of density $10^{15}\mathrm{m}^{-3}$, $T_e = 1\,\mathrm{eV}$, $\tau = 1$ and dust radius of $0.5\lambda_D$.

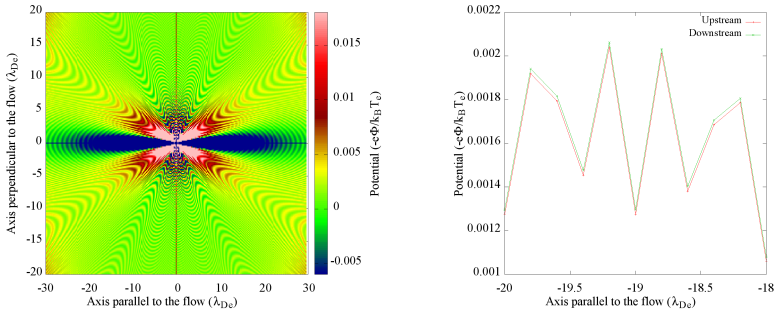

(a) Heat map plot of the potential around a dust grain ($0.625\lambda_D$) in a flowing plasma.

(b) Detail of the plot of potential along the z-axis, in a flowing plasma with a dust grain ($0.625\lambda_D$) at (0, 0).

Figure 7.18: Potential in a flowing plasma with a dust grain at the origin. The asymmetry in the potential is visible.

8 Conclusion

In this chapter, I summarise the findings of the work, give a brief appraisal and discuss future work stemming from these findings.

The chapter will deal with the findings for each part of the work first, beginning with the results for small dust grains. We will continue with the results for large dust grains and then a comparison of the two. We will end with the appraisal of the work and the future work that needs to be carried out.

8.1 Framing the Discussion

It is accepted wisdom that information cannot travel upstream in supersonic flow. This may be the case in normal fluids, where neutral particles are involved, but that is not necessarily the case in plasmas, where charged particles and electric fields determine macroscopic behaviour.

The literature is rich with authors using the fluid analogy to assume normal fluid behaviour for plasmas. Discussions on the presence of a cone-shaped disturbance originating at the dust grain in flowing plasmas, for example, are often framed in terms of Mach cones. Willis [15, 113] distinguishes between the cone-shaped weak discontinuity in flowing plasmas and Mach cones in neutral fluids, making use of the Bohm criterion to determine a cone angle identical to that of Mach cones (a similarity owed to $c_s = v_{Bohm}$).

This accepted wisdom has led to the absence of upstream structures in supersonic flow to be the expected behaviour and the presence of such phenomena to be in need of explaining. Given the presence of charged particles and electric fields in plasmas, the conversation should, perhaps, be reversed. Upstream propagation of information in supersonically flowing plasmas would then be expected and the lack of such propagation would need an explanation. The results for small dust grains presented in this work would thus be

what would be expected and the results for large dust grains would need an explanation.

8.2 Results for a Small Dust Grain

We have investigated the potential, density and flow around a small dust grain, using a kinetic model. The model was an extension of the model used by other researchers (Filippov et al [111]), which treated the dust grain as a point particle, yet included a cross section for collection. The extension allowed for incorporating fluid flow, a new feature unavailable to previous point-sink models.

The results of our solutions revealed a new and, in conventional thinking, unexpected feature, namely upstream perturbations, *even for supersonic flows*. This goes against conventional wisdom, which states that information in a fluid cannot travel faster than the speed of sound. Such features are taken to highlight the differences between plasmas and liquids/gases, and not a possible problem with the model. If there is a problem with the model, it may be that behaviour very near the dust grain, lost to our model due to linearisation which is not valid near the dust grain, is more important than previously thought. A non-linearised solution would be very difficult to pursue analytically.

8.2.1 Comparisons

Miloch, Kroll and Block [14] used a particle-in-cell code to study the interaction between two adjacent dust grains in a plasma. In doing so they produced results for the potential around a single dust grain. Comparing their results for potential to our results for potential, qualitatively, we see that the model we use gives similar results. Specifically, figure 7.17 compares with figure 4b of [14], for example. It is interesting to note that their results indicate the presence of upstream effects for supersonic flows (Mach 1.2 in figure 4a of [14]), but their graphs only extend to 2 Debye lengths upstream from the dust grain. Comparisons with other papers (such as Miloch et al[13]) are difficult because of the lack of focus on the upstream effects of the dust grains simulated.

8.2.2 Appraisal

This work begun with the aim of developing a simple model for the prediction of the effect of a small dust grain on its surrounding plasma. The intent was to use such model to conceptually understand the importance of various parameters on this effect and to be able to predict this effect quickly enough for the model to incorporated in larger codes, like DTOKS. The model has produced unexpected results, however, which create more questions than need addressing. Is the upstream effect real? Do we need to reframe the way we understand the propagation of information upstream from a dust grain in a supersonically flowing plasma? If so, what is the mechanism responsible for it and why have other authors not commented on it? We believe it may be real and definitely worth investigating further.

Part of the aim for this work was to be able to predict the density and the fluid flow as well as the potential. The equations for this have been developed, but at the time of writing they have not been implemented in a program to produce results, which is why they have not been included. They will be included in the paper-in-preparation by the time it is submitted.

8.2.3 Extensions

There are several possible extensions to this work, but the first thing that needs to be investigated is the veracity of the predictions for upstream effects. A possible way of doing this is to include some non-linearities in the model, relaxing the requirement for analytic-only work. This would fit with the shift in focus of the work, from the conceptual understanding of the relevant parameters to investigating a new effect.

Subsequent work will also include using the model to incorporate collisions with neutrals and investigating how they affect the charging of the dust grain and its effect on the surrounding plasma.

8.3 Fluid Code Results

We investigate the possibility of studying large dust grains in plasmas using cold-ion hydrodynamics. Beginning with two conservation equations, for mass and momentum, and with some simplifying assumptions suitable for large dust grains, we end up with equations for ions in a plasma which are

(un)surprisingly similar to the (inviscid) compressible Navier-Stokes equations. The differences prevent the straight-forward use of commercial packages to solve the equations, which led to the development of an in-house software package, HADES, to solve these equations for a range of parameter values.

I was constrained by time and computational resources, so the domain sized was kept small, which meant the dust grain size was also kept small, compared to what would be preferred. This is not considered to be a problem. The problem is self-similar. As long as we assume the dust grain radius to obey $r_d \gg \lambda_{De}$, then the axes units can be thought of as dust radii, with corresponding changes required to the normalisation of time and speed. This will be an improvement that will be part of future work.

8.3.1 Comparisons

Willis [15] investigated the potential around a dust grain in his PhD thesis, using a PIC code. The code (SCEPTIC - see [116]) uses the Boltzmann relation for electrons, but models ions as particles. Willis also concentrates on low ion temperatures and large dust grains (see [113]). Willis's results show a cone which becomes more pronounced as the ion temperature is lowered. We reproduce his figure 6.5 for convenience (figure 8.1). The results from the fluid code do not reproduce the hollow cone. Instead, we observe an oval structure growing from the dust grain as the system is evolved with time (figure 8.2). This structure is not hollow. The fact that we are using a very dissipative numerical method could be the reason, and this will be investigated in future iterations of HADES, when better numerical methods (such as Lax-Wendorff and PPM) have been implemented.

8.3.2 Validity

Do we trust the results from HADES? Given the intent to investigate the results further, with different numerical methods, I cannot say that the results are final. I do believe that the results do capture the basic behaviour of the model, namely a behaviour matching that of non-plasma fluids. A full check would involve a comparison of the potential profile around the dust grain with the potential predicted by other authors. It would be of use to use HADES to predict the floating potential of a dust grain and compare

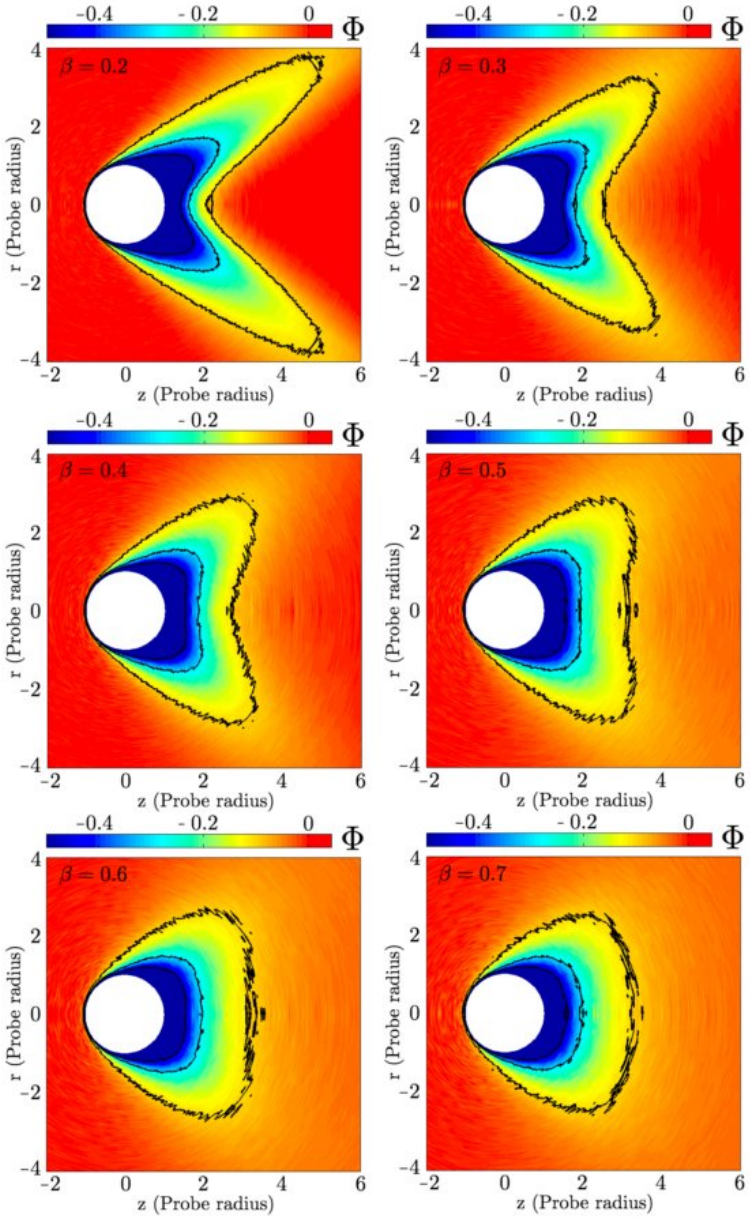

Figure 6.5.: The transition from double to single cone for $\beta = 0.2$ to $\beta = 0.7$. The flow velocity is $1.75\sqrt{kT_e/m_i}$ and the grain radius is $\rho = 80$. $\Phi = -e\phi/kT_e$.

Figure 8.1: SCEPTIC results for a range of ion-electron temperature ratios, produced by Willis [15].

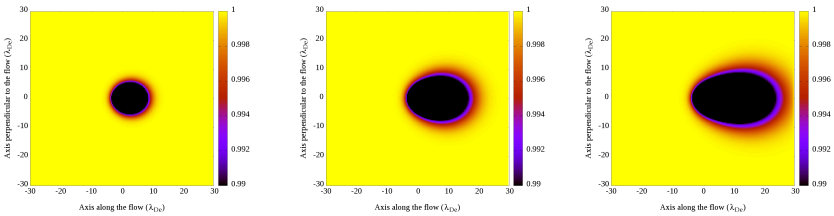

(a) Density at $T = 2$. (b) Density at $T = 6$. (c) Density at $T = 10$.

Figure 8.2: Evolution of density perturbation with time for v_f = Mach 2, $r_d = 1\lambda_{De}$, $n_0 = 10^5 \mathrm{m}^{-3}$.

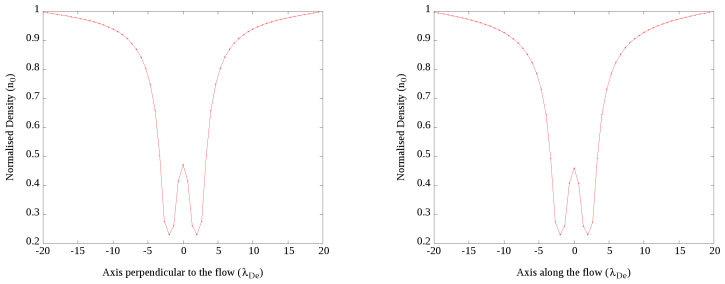

(a) No flow. (b) Flow of $Mach\,5$.

Figure 8.3: The density around two dust grains of $r_d = 1\lambda_{De}$, $n_0 = 10^{15}\mathrm{m}^{-3}$ for no flow and flow of Mach 5.

it with the methods described earlier in this work, such as OML, ABR and other numerical work, such as PIC codes.

8.3.3 Future Work

The work on large dust grains is not finished. A better numerical method needs to be implemented, with the results compared against other work. The code will thus be able, using its current set-up to calculate the density and fluid flow around a dust grain in plasma. Subsequently, the density can be converted to potential, using the Boltzmann relation. This will be the milestone of all three declared targets being met.

This could be followed by investigating ways of establishing what the prediction of HADES is for the floating potential of large dust grains.

Another use of the code is investigating the behaviour of multiple dust grains in the plasma. An example is shown in figure 8.3.

8.4 Final word

This work presents work done in investigating the density and flow around very small and very large dust grains. The two extremes can be compared, to establish any similarities in the results and highlight the differences.

There is still work to be done to meet the initial objectives, after which more questions, raised in the course of the current investigation, need to be addressed and investigated.

Having said this, a lot of ground has been covered already.

A new and novel extension to the point-sink model has been developed, with the code to produce results written and some results produced already. The mathematical model for the density and the fluid flow has also been developed, but not yet implemented to produce results, which is why it has not been included here. This work is expected to evolve to investigate how the addition of neutrals in the calculations affects the quantities of interest. The newly observed effect of upstream effects in supersonic flow also needs to be investigated further.

For large dust grains, the mathematical model has been developed and HADES developed to the point where we get results. The implementation allows for the code to be easily extended, with the implementation of new numerical methods only necessitating new plug-in modules. This will also allow for any extensions to the mathematical model to be easily added, should the investigation take such turn. HADES already allows for the investigation of multiple dust grains, another area where further work is needed.

Bibliography

[1] J. E. Allen. On the drag on an object immersed in a flowing plasma: the control surface approach. *Journal of Plasma Physics*, 73(05):773–783, feb 2007.

[2] AV. Filippov, AG. Zagorodny, AI. Momot, AF. Pal, and AN. Starostin. Charge screening in a plasma with an external ionization source. *Journal of Experimental and Theoretical Physics*, 104(1):147–161, 2007.

[3] Hoffmann R. [Johannes Evangelista Purkinje, half-length portrait, facing front], 1856.

[4] SOHO/EIT (ESA & NASA). Largest Measured Solar Flare, 2003.

[5] GACM Spierings. Wet chemical etching of silicate glasses in hydrofluoric acid based solutions. *Journal of Materials Science*, 28(23):6261–6273, dec 1993.

[6] J. W. Coburn. Plasma etching A discussion of mechanisms. *Journal of Vacuum Science and Technology*, 16(2):391, mar 1979.

[7] H. Thomas, G. Morfill, V. Demmel, J. Goree, B. Feuerbacher, and D. Möhlmann. Plasma Crystal: Coulomb Crystallization in a Dusty Plasma. *Physical Review Letters*, 73(5):652–655, aug 1994.

[8] Hubertus M. Thomas and Gregor E. Morfill. Melting dynamics of a plasma crystal. *Nature*, 379(6568):806–809, feb 1996.

[9] J. P. Sharpe, D. A. Petti, and H. W. Bartels. A review of dust in fusion devices: Implications for safety and operational performance. *Fusion Engineering and Design*, 63-64:153–163, 2002.

[10] K.J. Dietz, T. Ando, A. Antipenkov, S. Chiocchio, G. Federici, G. Janeschitz, E. Martin, and R. Tivey. The ITER divertor. *Proceed-*

ings of 16th International Symposium on Fusion Engineering, 1:73–88, apr 1995.

[11] K Gibson. Edge Plasmas in MCF devices (1st of 3 lectures): Introduction to edge plasma physics, 2010.

[12] J Winter. Dust in fusion devices - experimental evidence, possible sources and consequences. *Plasma Physics and Controlled Fusion*, 40:1201–1210, 1998.

[13] W. J. Miloch, J. Trulsen, and H. L. Pécseli. Numerical studies of ion focusing behind macroscopic obstacles in a supersonic plasma flow. *Physical Review E*, 77(5):056408, may 2008.

[14] W. J. Miloch, M. Kroll, and D. Block. Charging and dynamics of a dust grain in the wake of another grain in flowing plasmas. *Physics of Plasmas*, 17(10):103703+, oct 2010.

[15] CTN Willis. *Dust in stationary and flowing plasmas.* PhD thesis, Imperial College, 2012.

[16] B Karloff. *And the darkness falls,.* World Pub. Co., Cleveland;New York, 1946.

[17] P. J. Hanzlik. The Lure of Medical History. *California and Western Medicince*, 49(2):140–142, 1938.

[18] W Crookes. *On radiant matter, a lecture delivered to the British Association for the Advancement of Science*, volume August 22. [publisher not identified], London, 1879.

[19] L Tonks. The Birth of Plasma. *American Journal of Physics*, 35(9):857, 1967.

[20] I Langmuir. Oscillations in ionized gases. *Physical Review*, 14:627–637, aug 1928.

[21] HM. Mott-Smith. History of "Plasmas". *Nature*, 233:219, 1971.

[22] B Chapman. *Glow Discharge Process Sputtering and plasma etching.* Wiley, 1980.

[23] I Langmuir, CG Found, and AF Dittmer. A New Type of Electric Discharge: The Streamer Discharge. *Science (New York, NY)*, 60(1557):392–394, 1924.

[24] G Gorelik. The Top-Secret Life of Lev Landau. *Scientific American*, 277(2):72–77, aug 1997.

[25] L. Landau. On the vibrations of the electronic plasma. *Journal of Physics*, X(1):25–34, 1946.

[26] JH Malmberg and CB Wharton. Collisionless damping of electrostatic plasma waves. *Physical Review Letters*, 13(6):184–186, aug 1964.

[27] Google Scholar. https://scholar.google.co.uk/schhp?hl=en&as_sdt=1,5, 2015-08-22.

[28] PO Larsen and M von Ins. The rate of growth in scientific publication and the decline in coverage provided by Science Citation Index. *Scientometrics*, 84(3):575–603, sep 2010.

[29] E. Thomas, U. Konopka, D. Artis, B. Lynch, S. Leblanc, S. Adams, R. L. Merlino, and M. Rosenberg. The magnetized dusty plasma experiment (MDPX). *J. Plasma Phys.*, 81(02):1–21, feb 2015.

[30] J Goree and I Hahn. Dusty Plasma Physics Facility for the International Space Station. *Bulletin of the American Physical Society*, Volume 60„ oct 2015.

[31] H M Thomas, G E Morfill, V E Fortov, A V Ivlev, V I Molotkov, A M Lipaev, T Hagl, H Rothermel, S A Khrapak, R K Suetterlin, M Rubin-Zuzic, O F Petrov, V I Tokarev, and S K Krikalev. Complex plasma laboratory PK-3 Plus on the International Space Station. *New Journal of Physics*, 10(3):033036, mar 2008.

[32] Ch Hollenstein, Aa Howling, Ph Guittienne, and I Furno. Industrial plasmas in academia. *Plasma Physics and Controlled Fusion*, 57(1):014010, jan 2015.

[33] M.S Alam, A Roychowdhury, K.K Islam, and A.M.Z Huq. A revisited model for the physical quality of life (PQL) as a function of electrical energy consumption. *Energy*, 23(9):791–801, apr 1998.

[34] N Armaroli and V Balzani. The future of energy supply: challenges and opportunities. *Angew. Chem., Int. Ed.*, 46(Copyright (C) 2013 American Chemical Society (ACS). All Rights Reserved.):52–66, jan 2007.

[35] IPCC (Core Writing Team: R.K. Pachauri and L.A. Meyer). Climate Change 2014: Synthesis Report. Contribution of Working Groups I, II and III to the Fifth Assessment Report of the Intergovernmental Panel on Climate Change ., mar 2014.

[36] D. Turnbull, A. Glaser, and R.J. Goldston. Investigating the value of fusion energy using the Global Change Assessment Model. *Energy Economics*, 51:346–353, sep 2015.

[37] S. Lee and S. H. Saw. Nuclear fusion energy-mankind's giant step forward. *Journal of fusion energy*, 30(5):2–8, feb 2011.

[38] KT Thomas and K Young. A Burning Plasma Diagnostic Initiative for the US Magnetic Fusion Energy Science Program. 2014.

[39] B.A.A Klumov, S.V.B Vladimirov, and G.E.A Morfill. On the role of dust in the cometary plasma. *JETP Letters*, 85(10):478–482, 2007.

[40] S. I. Krasheninnikov, Y. Tomita, R. D. Smirnov, and R. K. Janev. On dust dynamics in tokamak edge plasmas. *Physics of Plasmas*, 11(6):3141–3150, may 2004.

[41] M Bacharis, M Coppins, and John E. Allen. Dust in tokamaks: An overview of the physical model of the dust in tokamaks code. *Physics of Plasmas*, 17(4):042505, 2010.

[42] BM Annaratone, Wolfgang Jacob, C Arnas, and GE Morfill. Critical Review of Complex Plasma (Dusty Plasma) Diagnostics and Manipulation Techniques for the Fusion Community and Others. *IEEE Transactions on Plasma Science*, 37(1):270–280, jan 2009.

[43] H Alfvén. Star formation in a dusty plasma cloud. *Star formation in a dusty plasma cloud., by Alfvén, H.. Tek. Hoegsk., Stockholm, Sweden. Instn. Plasmafys., TRITA-EPP-77-15, 10 p.*, -1, jun 1977.

[44] VM Vasyliunas. Plasma Distribution and FLow. *Physics of the Jovian Magnetosphere*, pages 395–453, 1983.

[45] J T Clarke, J Ajello, G Ballester, L Ben Jaffel, J Connerney, J-C Gérard, G R Gladstone, D Grodent, W Pryor, J Trauger, and J H Waite. Ultraviolet emissions from the magnetic footprints of Io, Ganymede and Europa on Jupiter. *Nature*, 415(6875):997–1000, feb 2002.

[46] C. K. Goertz and G. Morfill. A Model for the Formation of Spokes in Saturn's Ring. *Icarus*, 53(2):219–229, feb 1983.

[47] RL Merlino. Dusty plasmas and applications in space and industry. *Transworld Research Network India Plasma Physics Applied*, 37661(2):73–110, 2006.

[48] B Wu. Photomask plasma etching A review. *Journal of Vacuum Science & Technology B: Microelectronics and Nanometer Structures*, 24(2006):1, jan 2006.

[49] R. G. Poulsen. Plasma etching in integrated circuit manufacture A review. *Journal of Vacuum Science and Technology*, 14(1):266, jan 1977.

[50] H Kobayashi. Behavior of Dust Particles in Plasma Etching Apparatus. *Japanese Journal of Applied Physics*, 50(8):08JE01, aug 2011.

[51] AR Galaly and FF Elakshar. Dust Plasma Effect on the Etching Process of Si[100] by Ultra Low Frequency RF Plasma. *Journal of Modern Physics*, 04(02):215–225, feb 2013.

[52] GE. Morfill and AV. Ivlev. Complex plasmas: An interdisciplinary research field. *Reviews of Modern Physics*, 81(4):1353–1404, oct 2009.

[53] I Cook. Economic , Safety and Environmental Characteristics of Commercial Fusion Power.

[54] J Roth, E. Tsitrone, A. Loarte, Th Loarer, G. Counsell, R. Neu, V. Philipps, S. Brezinsek, M. Lehnen, P. Coad, Ch Grisolia, K. Schmid, K. Krieger, A. Kallenbach, B. Lipschultz, R. Doerner, R. Causey, V. Alimov, W. Shu, O. Ogorodnikova, A. Kirschner, G. Federici, and

A. Kukushkin. Recent analysis of key plasma wall interactions issues for ITER. *Journal of Nuclear Materials*, 390-391(1):1–9, jun 2009.

[55] I Cook, D Maisonnier, and NP Taylor. European fusion power plant studies. *Fusion science and ...*, 47:384–392, 2005.

[56] B.D. Bondarenko. Role played by O A Lavrent'ev in the formulation of the problem and the initiation of research into controlled nuclear fusion in the USSR. *Uspekhi Fizicheskih Nauk*, 171(8):886, aug 2001.

[57] M G Haines. Fifty years of controlled fusion research. *Plasma Physics and Controlled Fusion*, 38(5):643, 1996.

[58] JP Conner, DC Hagerman, and JL Honsaker. *Operational characteristics of the stabilized toroidal pinch machine, Perhapsatron S-4*. 1958.

[59] JA Phillips. Magnetic Fusion. *Los Alamos Science*, 1983.

[60] TH Stix. Highlights in Early Stellarator Research at Princeton. *J Plasma Fusion Res Ser*, 1:3–8, 1998.

[61] H Daido, M Nishiuchi, and AS Pirozhkov. Review of laser-driven ion sources and their applications, 2012.

[62] M Bacharis. *Theoretical Study of Dust in RF Discharges and Tokamak Plasmas*. PhD thesis, Imperial College, 2009.

[63] V Fortov, A Ivlev, S Khrapak, A Khrapak, and G Morfill. Complex (dusty) plasmas: Current status, open issues, perspectives. *Physics Reports*, 421(1-2):1–103, dec 2005.

[64] R Fitzpatrick. Introduction to Plasma Physics: A graduate level course. *University of Texas at Austin, Austin, TX*, 2006.

[65] KU Riemann. The Bohm criterion and sheath formation. *Journal of Physics D: Applied Physics*, 24(4):493–518, apr 1991.

[66] I Langmuir. Positive Ion Currents in the Positive Column of the Mercury Arc. *General Electric Review*, 26, nov 1923.

[67] I. Langmuir. Positive Ion Currents From the Positive Column of Mercury Arcs. *Science*, 58(1502):290–291, oct 1923.

[68] R N Franklin. Where is the sheath edge ? *Journal of Physics D: Applied Physics*, 37(9):1342–1345, may 2004.

[69] I Langmuir. The interaction of electron and positive ion space charges in cathode sheaths. *Physical Review*, 33(6):954–989, 1929.

[70] L. Tonks and I. Langmuir. A General Theory of the Plasma of an Arc. *Physical Review*, 34(6):876, 1929.

[71] D Bohm. The Characteristics of Electrical Discharges in Magnetic Fields. In *edited by A Guthrie and RK Wakerling*, page 77. McGraw-Hill, 1949.

[72] J L B Goree Goree. Charging of particles in a plasma. *Plasma Sources Science and Technology*, 3(3):400, aug 1994.

[73] H. M. Mott-Smith and I Langmuir. The Theory of Collectors in Gaseous Discharges. *Physical Review*, 28(4):727–763, oct 1926.

[74] J. E. Allen, B. M. Annaratone, and U. de ANGELIS. On the orbital motion limited theory for a small body at floating potential in a Maxwellian plasma. *Journal of Plasma Physics*, 63(4):299–309, may 2000.

[75] FF Chen. Langmuir probes in RF plasma: surprising validity of OML theory. *Plasma Sources Science and Technology*, 18(3):035012, aug 2009.

[76] XZ Tang and G Luca Delzanno. Orbital-motion-limited theory of dust charging and plasma response. *Physics of Plasmas*, 21(12):123708, dec 2014.

[77] C. Silva, G. Arnoux, S. Devaux, D. Frigione, M. Groth, J. Horacek, P.J. Lomas, S. Marsen, G. Matthews, L. Meneses, and R.A. Pitts. Characterization of scrape-off layer transport in JET limiter plasmas. *Nuclear Fusion*, 54(8):083022, aug 2014.

[78] G. Arnoux, T. Farley, C. Silva, S. Devaux, M. Firdaouss, D. Frigione, R.J. Goldston, J. Gunn, J. Horacek, S. Jachmich, P.J. Lomas, S. Marsen, G.F. Matthews, R A Pitts, M. Stamp, and P.C. Stangeby.

Scrape-off layer properties of ITER-like limiter start-up plasmas in JET. *Nuclear Fusion*, 53(7):073016, jul 2013.

[79] J. E. Allen, R L F Boyd, and P Reynolds. The Collection of Positive Ions by a Probe Immersed in a Plasma. *Proceedings of the Physical Society. Section B*, 297, 1957.

[80] R. V. Kennedy and J. E. Allen. The floating potential of spherical probes and dust grains. II: Orbital motion theory. *Journal of Plasma Physics*, 69(6):485–506, aug 2003.

[81] A V Ivlev, S K Zhdanov, S A Khrapak, and G E Morfill. Ion drag force in dusty plasmas. *Plasma Physics and Controlled Fusion*, 46(12B):B267–B279, dec 2004.

[82] J D Callen. *Fundamentals of plasma physics*. Springer, 2003.

[83] E. Rutherford. The scattering of α and β particles by matter and the structure of the atom. *Philosophical Magazine*, 92(4):379–398, 2012.

[84] FF. Chen. *Introduction to Plasma Physics and Controlled Fusion*. Springer, 1984.

[85] I H Hutchinson. Collisionless ion drag force on a spherical grain. *Plasma Physics and Controlled Fusion*, 48(2):185–202, feb 2006.

[86] S. A. Khrapak. Momentum Transfer in Complex Plasmas: Results of Binary Collision Approach. *AIP Conference Proceedings*, 799(2005):283–286, 2005.

[87] S. A. Khrapak, A. V. Ivlev, G. E. Morfill, and H. M. Thomas. Ion drag force in complex plasmas. *Physical Review E - Statistical, Nonlinear, and Soft Matter Physics*, 66(4):2–5, oct 2002.

[88] A. V. Ivlev, S. A. Khrapak, S. K. Zhdanov, G. E. Morfill, and G. Joyce. Force on a charged test particle in a collisional flowing plasma. *Physical Review Letters*, 92(May):205007–1, may 2004.

[89] ZW Xu. Cloud-Sea Computing Systems: Towards Thousand-Fold Improvement in Performance per Watt for the Coming Zettabyte Era. *Journal of Computer Science and Technology*, 29(2):177–181, mar 2014.

[90] O Raz, GG de Villota, Teng Li, E Wittebol, and HJS Dorren. The need for low-cost optical transceivers in future data center networks. In *2015 17th International Conference on Transparent Optical Networks (ICTON)*, pages 1–4. IEEE, jul 2015.

[91] British Petroleum. BP Statistical Review of World Energy, June 2015, 2015.

[92] A.J. Christlieb, R. Krasny, and J.P. Verboncoeur. A treecode algorithm for simulating electron dynamics in a Penning Malmberg trap. *Computer Physics Communications*, 164(1-3):306–310, dec 2004.

[93] FH. Harlow and M. W. Evans. A Machine Calculation Method for Hydrodynamic Problems. *Los Alamos Scientific Laboratory*, page 54, 1956.

[94] FH Harlow. PIC and its progeny. *Computer Physics Communications*, 48(1):1–10, 1988.

[95] J Dawson and C Oberman. High-Frequency Conductivity and the Emission and Absorption Coefficients of a Fully Ionized Plasma. *Physics of Fluids*, 5(5):517, dec 1962.

[96] JP Verboncoeur, AB Langdon, and NT Gladd. An object-oriented electromagnetic PIC code. *Computer Physics Communications*, 87(1-2):199–211, 1995.

[97] JC Maxwell. V. Illustrations of the Dynamical Theory of Gases. – Part I . On the Motions and Collisions of Perfectly Elastic Spheres. *Philosophical Magazine Series 4*, 19(124):19–32, 1860.

[98] AA Vlasov. The vibrational properties of an electron gas. *Physics-Uspekhi*, 721, 1968.

[99] H Alfven. Existence of Electromagnetic-Hydrodynamic Waves. *Nature*, 150(3805):405–6, 1942.

[100] FG Verheest. General dispersion relations for linear waves in multicomponent plasmas. *Physica*, 34(1):17–35, 1967.

[101] PK Shukla. Experiments and Theory of Dusty Plasmas. . . . *-American Institute of . . .*, 11(1):10–23, 2011.

[102] EF Toro. *Riemann solvers and numerical methods for fluid dynamics. A practical introduction*. Springer Science and Business Media, 2009.

[103] FL Richardson. *Weather prediction by numerical processes*. Cambridge University Press, 1922.

[104] R. V. Southwell. *Relaxation Methods in Engineering Science - A Treatise on Approximate Computation*. Read Books Design, 1940.

[105] C Hirsch. *Numerical Computation of Internal and External Flows: The Fundamentals of Computational Fluid Dynamics: The Fundamentals of Computational Fluid Dynamics*. Butterworth-Heinemann, 2007.

[106] W Press, S Teukolsky, W Vetterling, and B Flannery. *Numerical recipes 3rd edition: The art of scientific computing*. 2007.

[107] F Glines, M Anderson, and D Neilsen. Scalable relativistic fluid dynamics for heterogeneous computing. *Bulletin of the American Physical Society*, 2015.

[108] A Iserles. *A First Course in the Numerical Analysis of Differential Equations*. Cambridge University Press, 1996.

[109] AI Ruban and JSB Gajjar. *Fluid Dynamics: Part 1: Classical Fluid Dynamics*. OUP Oxford, 2014.

[110] J Dewey. Logic: The theory of inquiry (1938). *The later works*, 1925.

[111] A. V. Filippov, A. G. Zagorodny, A. I. Momot, A. F. Pal, and A. N. Starostin. Interaction of two macroparticles in a nonequilibrium plasma. *Journal of Experimental and Theoretical Physics*, 105(4):831–845, 2007.

[112] S. A. Khrapak, B. A. Klumov, and G. E. Morfill. Electric potential around an absorbing body in plasmas: Effect of ion-neutral collisions. *Physical Review Letters*, 100(22):1–4, jun 2008.

[113] CTN Willis, JE Allen, M Coppins, and M Bacharis. Wakes formed by dust grains in supersonically flowing plasmas. *Physical Review E*, 84(4):046410, oct 2011.

[114] S. Maiorov, S. Vladimirov, and N. Cramer. Plasma kinetics around a dust grain in an ion flow. *Physical Review E*, 63(1):017401, dec 2000.

[115] W J Miloch, H. L. Pécseli, and J. Trulsen. Numerical simulations of the charging of dust particles by contact with hot plasmas. *Nonlinear Processes in Geophysics*, 14(5):575–586, 2007.

[116] I H Hutchinson. Ion collection by a sphere in a flowing plasma: I. Quasineutral. *Plasma Physics and Controlled Fusion*, 44(9):1953–1977, sep 2002.